Materials Today Bio 34 (2025) 102114

Contents lists available at ScienceDirect

Materials Today Bio

journal homepage: www.journals.elsevier.com/materials-today-bio

Conductive polymers in smart wound healing: From bioelectric stimulation to regenerative therapies

Yanhua Jiang [a,1], Yongjian Zhou [a,1], Yu Tian [b], Noushin Nabavi [c], Milad Ashrafizadeh [d], João Conde [e,*], Zhe Li [a,**], Liang Guo [f,***]

[a] Department of Anesthesiology, The First Affiliated Hospital of China Medical University, Shenyang, Liaoning, China
[b] Science Research Center, Huizhou Central People's Hospital, Huizhou, Guangdong, China
[c] Independent Researcher, Victoria, V8V 1P7, British Columbia, Canada
[d] Department of Radiation Oncology, Shandong Provincial Key Laboratory of Radiation Oncology, Shandong Cancer Hospital and Institute, Shandong First Medical University, Shandong Academy of Medical Sciences, Jinan, 250000, Shandong, China
[e] Comprehensive Health Research Centre (CHRC), NOVA Medical School, Faculdade de Ciências Médicas, NMS|FCM, Universidade NOVA de Lisboa, Lisboa, Portugal
[f] Department of Cardiology, The First Affiliated Hospital of China Medical University, Shenyang, Liaoning, China

ARTICLE INFO

Keywords:
Conductive polymers
Wound healing
Electrical stimulation
Smart dressings
Tissue regeneration
Cardiothoracic surgeries

ABSTRACT

Wound healing, particularly in particularly after surgical operations and especially cardiothoracic surgeries, presents a significant global healthcare burden due to prolonged recovery time, recurrent infections, and limited effectiveness of the conventional therapies. The recent advancements in biomaterials have positioned conductive polymers (CPs) as promising components in the design of next-generation wound care technologies. CPs, such as polypyrrole (PPy), polyaniline (PANI) and poly (3,4-ethylenedioxythiophene) (PEDOT), possess unique electrical, chemical and biological properties, making them ideal for integration into multifunctional and responsive wound dressings. The present review focuses on the emerging role of CPs in wound healing, along with their incorporation into various delivery platforms including hydrogels, nanofibers, membranes, microneedle patches and 3D scaffolds. These materials provide a synergistic approach by enabling localized electrical stimulation, enhancing tissue regeneration, and producing antibacterial, antioxidant and anti-inflammatory effects. In particular, it is discussed how CP-based systems can be engineered to respond dynamically to the wound microenvironment such as pH, temperature or enzymatic activity, for accelerating controlled drug release and real-time therapeutic intervention. It also highlights the integration of CPs with complementary technologies such as triboelectric nanogenerators, biosensors and photothermal agents, contributing to smarter, more personalized wound care solutions. Moreover, this review addresses the current challenges, including biocompatibility, degradation kinetics and scalability, with a summary of the directions for the future research to optimize clinical translation. Based on the recent findings across materials science, bioengineering and regenerative medicine, this review illustrates the transformative potential of CPs in advancing effective, non-invasive and patient-specific wound healing strategies.

1. Introduction

The skin, which is the largest organ of the body, serves as an essential barrier protecting the internal tissues from damage, infections, UV radiation and extreme heat or cold. This vital position is susceptible to injury, significantly affecting people and healthcare expenses in the US, which amount to approximately $50 billion for non-healing wounds, over $12 billion for scars, and approximately $7.5 billion for burns. Especially at-risk groups such as diabetics, the elderly and individuals with genetic conditions frequently encounter persistent healing problems, emphasizing the critical demand for improved wound care therapies[1] In addition, for patients after surgical operations, especially

* Corresponding author.
** Corresponding author.
*** Corresponding author.
E-mail addresses: joao.conde@nms.unl.pt (J. Conde), jllizhe@126.com (Z. Li), lguo@cmu.edu.cn (L. Guo).
[1] authors contributed equally to this manuscript.

https://doi.org/10.1016/j.mtbio.2025.102114
Received 18 May 2025; Received in revised form 8 July 2025; Accepted 17 July 2025
Available online 21 July 2025

those after cardiothoracic surgeries, wound healing is even more crucial. If the wound suffers from chronic infection, it can lead to serious complications. To repair a skin injury, the damaged barrier must first be covered with a blood clot. Cells from different skin layers migrate from the to close the gap until the tissue is fully reunited, aiding in the separation of the clot or scab. The various types of skin cells participate in this healing process, directed by a combination of mechanical and chemical signals. A variety of these signals arise from inflammatory cells, which are attracted to the injury site by damage-related signals and through the pathogens they help fight. On the one hand, certain aspects of wound healing, such as angiogenesis, are temporary and can be reversed. On the other hand, certain processes, such as the accumulation of scar collagen, last indefinitely, affecting the long-term results of wound healing [2]. Given the immense clinical and economic burdens of impaired wound healing, there is a pressing need for innovative materials and technologies that can actively support and accelerate tissue repair, prompting the exploration into electrically active solutions such as conductive polymers.

In contrast to the conventional dressings, intelligent wound dressings deploy built-in sensors and cutting-edge materials, such as stimuli-responsive polymers, to continuously observe and respond to alterations in wounds, providing customized care during various healing phases. The process of wound healing consists of multiple stages, each featuring unique physiological characteristics. Also, these dressings are designed to respond appropriately to the environmental shifts during recovery. The various types of advanced wound dressings have been developed to enhance treatment, including biomechanical dressings, stimuli-responsive variants, self-healing formulations for dynamic wounds, self-removable options and monitoring dressings. These dressings aid in monitoring the healing process, reducing infections, mitigating the risks of chronic wounds, and promoting independent tissue regeneration through constant interaction with the wound. Their flexible features provide a practical option for effective and customized wound care [3]. To meet the complicated demands under dynamic wound environments, the integration of responsive, multifunctional materials such as conductive polymers (CPs) in smart dressings holds significant potential for personalized, real-time therapeutic intervention.

CPs are the organic polymers capable of conducting electricity. They are distinct from the traditional insulators because of their conjugated backbone which includes delocalized π-electrons. Their conductivity is significantly enhanced by a method known as doping, usually through oxidation (p-doping), allowing them to reach conductivity levels similar to those of metals. Various doping techniques are accessible, including chemical, electrochemical and photo-induced methods. Additionally, the drawbacks of CPs, such as fragility and insufficient mechanical properties, can be alleviated through the development of composites or mixtures. CPs such as polypyrrole (PPy), polyaniline (PANI) and poly (3,4-ethylenedioxythiophene) (PEDOT) demonstrate excellent biocompatibility, which can be improved through the incorporation of biomolecules. In wound care, CPs are being thoroughly studied for their ability to facilitate electrical stimulation (ES), mimicking the body's natural electrical signals to improve cell movement and tissue repair. CPs in dressings and scaffolds enable a more consistent delivery of ES, and some research suggests they could enhance wound healing even without external stimulation [4]. These unique properties position CPs as ideal candidates for the next-generation wound dressings, capable of merging electrical functionality with biocompatibility to actively drive tissue regeneration. Fig. 1 provides a schematic representation of the application of CPs for wound healing acceleration.

The primary aim of this review is to provide a comprehensive and critical evaluation of the emerging role of CPs in wound healing, with a particular focus on their integration into smart wound dressings and regenerative therapies. Based on the insights obtained from recent

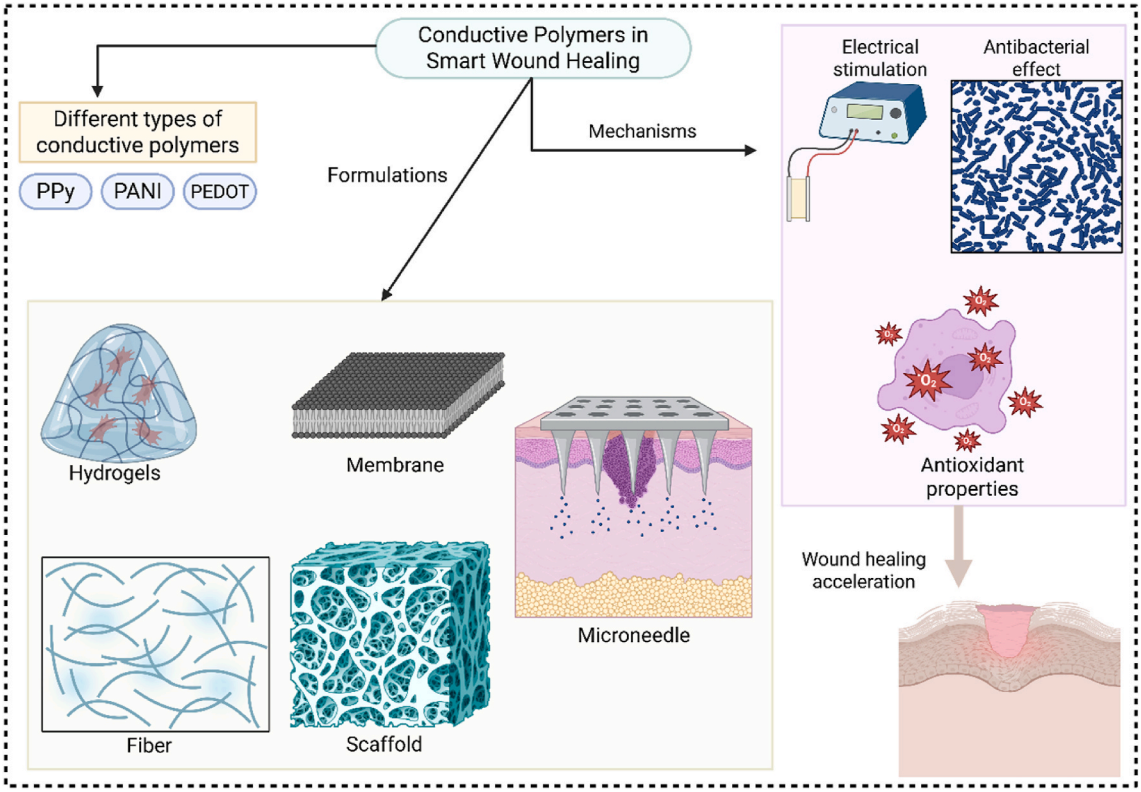

Fig. 1. Overview of CP-based smart wound healing strategies. CPs such as PPy, PANI and PEDOT are integrated into advanced wound dressing platforms. These materials enable localized ES, mimic the bioelectrical environment of skin, and provide multifunctional benefits such as antibacterial activity, antioxidant effects and responsive drug delivery. Through these mechanisms, CP-based systems accelerate tissue regeneration, enhance angiogenesis and reduce inflammation, providing a promising avenue for the personalized, non-invasive treatment of both acute and chronic wounds (Created with biorender.com).

advancements, this review explores how CPs such as PPy, PANI and PEDOT are reshaping wound care by offering electroconductive, biocompatible and multifunctional platforms mimicking the bioelectrical environment of skin. It highlights the capability of these materials to support and amplify natural healing processes through ES, antibacterial activity, antioxidant properties and smart drug delivery mechanisms. Furthermore, this review aims to illuminate the mechanisms by which CP-based hydrogels, nanofibers, membranes, microneedle patches and 3D scaffolds interact with biological systems to accelerate tissue repair, reduce infection and modulate immune responses. By evaluating both preclinical and clinical evidences, this review seeks to identify the current limitations, potential safety concerns and translational challenges while emphasizing the transformative potential of CP-based technologies to enable personalized, non-invasive and responsive wound care solutions in both acute and chronic settings. Finally, this review is intended to guide future research and innovation by bridging the interdisciplinary knowledge acquired from materials science, bioengineering and regenerative medicine.

2. Skin structure

The skin consists of two main layers including the dermis and the overlaying avascular epidermis. The dermis, constituting the majority of the skin, comprises connective tissue components such as collagen, elastin, glycosaminoglycans (collectively known as the extracellular matrix or ECM), fibroblasts, blood vessels, pilosebaceous units, sweat glands, adipose cells, mast cells and infiltrating leukocytes. The epidermis, predominantly composed of keratinocytes (~95 %), also includes melanocytes, Langerhans cells and Merkel cells. It is structured into four separate layers: stratum basale (SB), stratum spinosum (SS), stratum granulosum (SG) and stratum corneum (SC). SB comprises a solitary layer of basal cells anchored to the basement membrane by hemidesmosomes, exhibiting keratins K14 and K5. SS is characterized by spiny cells resulting from many desmosomes and contains lamellar bodies (LBs) that signify the initiation of lipid production and express keratins K1 and K10. SG is distinguished by keratohyalin granules (KHG) composed of profilaggrin, loricrin and keratins, accompanied by enhanced protein and lipid production. Lamellar bodies in sebaceous glands reach maximum density and release lipid contents into the extracellular space, establishing a permeability barrier for the skin. These lipids, in conjunction with hydrolytic enzymes, can be converted into ceramide-enriched bilayers crucial for barrier functionality. The transformation into corneocytes involves keratin condensation, lipid body production and organelle degradation, partially mediated by calcium gradients. The stratum corneum as the topmost layer comprises terminally developed corneocytes embedded in the lipid layers derived from lamellar bodies, developing a "brick-and-mortar" architecture. It comprises 18–21 layers of flattened corneocytes, which differ in hydration and structural characteristics according to their location. Corneodesmosomes maintain cellular cohesiveness in the inner stratum corneum, but their progressive disintegration in the outer stratum corneum promotes desquamation, which is a meticulously regulated shedding process underpinned by structural characteristics and natural moisturizing elements resulting from filaggrin degradation [5]. Alongside the dermis and epidermis, the human skin comprises the hypodermis as its deepest layer. The epidermis functions as the principal physical barrier, consisting of many stratified epithelial layers. Although the majority of body parts have four sub-layers such as SC, SG, SS and SB, thicker regions such as the palms and soles additionally have the stratum lucidum (SL). The SG, SS and SB constitute the viable epidermis, with around 50–100 μm in thickness, whereas the SC and SL are non-viable, with a thickness of about 10–20 μm. Keratinocytes, which represent the predominant cell type, start in the stratum basale and move outward over approximately 14 days, undergoing differentiation, lipid accumulation and cornification to become corneocytes in the stratum corneum, which are finally lost by desquamation within two weeks. Differentiating keratinocytes produce LBs abundant in the lipid precursors and enzymes, which, upon reaching the SG–SC contact, discharge their contents to form a structured extracellular lipid matrix. This lipid matrix, mainly consisting of ceramides (CERs), non-esterified fatty acids (NEFAs) and cholesterol (CHOL), occupies the interstitial space among protein-rich corneocytes, establishing a resilient "bricks and mortar" structure. The stratum corneum has 15 to 25 layers of flattened, enucleated corneocytes embedded within a lipid matrix, with corneodesmosomes maintaining cohesion and a cornified envelope providing mechanical stability. Corneocytes also include natural moisturizing factors (NMFs) that facilitate water retention and protect against desiccation. The SC consists of around 5–15 % lipids, 75–80 % proteins and 5–10 % miscellaneous substances by dry weight. Sebaceous glands, in conjunction with the stratum corneum, generate sebum, a distinctive lipid mixture including wax esters and squalene, which combines with stratum corneum lipids to create surface skin lipids (SSLs). These SSLs fortify the epidermal barrier by diminishing transepidermal water loss and provide protection against microbiological, chemical and physical stresses, thereby maintaining skin health and functionality [6].

Skin wound healing is a complicated and tightly controlled biological process, necessitating a coordinated response from diverse cellular and structural elements throughout all skin layers. The intact epidermis serves as a protective, impermeable barrier and contains epidermal stem cells within structures such as hair follicles, sweat glands and sebaceous glands. It comprises keratinocytes, Merkel cells and melanocytes, as well as immune cells such as Langerhans cells, which can be used to evaluate the microenvironment and orchestrate immune responses via lymphatic communication. Resident CD^{4+} and CD^{8+} memory T cells endure as immunological sentinels, while the underlying dermis, abundant in extracellular matrix, blood arteries and receptors, supplies nutrition and accommodates other immune cells, including macrophages, mast cells, dendritic cells and fibroblasts. The subcutaneous adipose tissue serves as an energy reservoir and a source of growth factors essential for host defense and hair control. In adult animals, standard skin injuries heal through fibrosis and do not regenerate appendages such as hair follicles and adipose tissue. In mice, extensive full-thickness wounds can initiate wound-induced hair neogenesis (WIHN), which is a regeneration mechanism activated by the Wnt signaling, resulting in the production of new hair follicles and associated adipocytes. This phenomenon is contingent upon size and generally manifests in wounds larger than 1.0 cm^2 in juvenile mice or 2.25 cm^2 in adult specimens. During WIHN, neogenic hair follicles transition into the anagen phase, release bone morphogenetic proteins and transform local myofibroblasts into adipocytes. Repigmentation is promoted by the migration of melanocyte stem cells, whilst M2 macrophages provide growth factors increasing hair follicle cycling and development. Mature neutrophils can inhibit this regeneration process. The dynamics of wound healing varies by anatomical site. For example, vaginal skin is significantly different due to the lack of subcutaneous fat, diminished keratinization, persistent wetness and microbial exposure. Notwithstanding these challenges, genital injuries frequently heal with little scarring, mainly because of the abundance of androgen and estrogen receptors in the area. Subsequent to the injury, elevated aromatase activity enhances local estrogen levels, facilitating keratinocyte and fibroblast migration while attenuating inflammation through the downregulation of pro-inflammatory cytokines, providing a hormonally mediated scar-reducing healing profile unique to the specific body regions [7].

3. Wound healing: principals and steps

Angiogenesis is considered as the development of new blood vessels from pre-existing ones and is an essential and delicately regulated process in wound healing. The vascular endothelial growth factor (VEGF) family comprising VEGF-A, VEGF-B, VEGF-C and VEGF-D, along with placental growth factor (PLGF), primarily regulates this process by

binding to the tyrosine kinase receptors VEGFR1/2 and co-receptors NRP-1/2, thereby stimulating endothelial cell activities such as proliferation, migration and survival. In chronic wounds, the lack or dysregulation of angiogenic factors affects signalling pathways including VEGF, epidermal growth factor (EGF), transforming growth factor-beta (TGF-β) and bone morphogenetic protein (BMP), thus preventing healing. Although vital unregulated angiogenesis can result in the excessive scar tissue or keloids, recent advancements highlight the significance of functional nanoparticles including ZnO, Au, Ag, CeO, Cu and Terbium-based nanoparticles, which initiate critical signalling cascades by activating reactive oxygen species (ROS), such as mitogen-activated protein kinase (MAPK), phosphoinositide 3-kinase (PI3K), focal adhesion kinase (FAK), protein kinase B (Akt) and endothelial nitric oxide synthase (eNOS) pathways. Therefore, angiogenesis is promoted throughout different phases of wound healing [8]. During the initial hemorrhagic stage of an injury, blood vessels quickly constrict to promote clot development and stop bleeding [9,10]. This process relies on the interactions between endothelial cells, platelets and the triggering of coagulation cascades, along with platelet-specific hemostatic agents [11,12]. The subendothelial matrix in blood vessels triggers platelet activation by revealing ECM proteins such as collagen and von Willebrand factor. These proteins attach to the receptors, enhancing platelet adhesion. Thrombin activates platelets to alter their shape and discharge granules containing bioactive compounds, leading to a stable aggregation of platelets, fibrin and fibronectin preventing additional blood loss [13]. Additionally, the clot serves as a foundation and transport vehicle for immune cells arriving at the area of injury [14]. Platelets provide growth factors that activate surrounding skin cells, thus significantly contributing to the initiation of the proliferative stage of wound repair [15,16].

Wound healing is a tightly controlled process that involves multiple stages, starting with hemostasis to minimize blood loss via vasoconstriction, platelet clumping and fibrin clot development. Activated platelets release crucial growth factors including platelet-derived growth factor (PDGF), TGF-β and VEGF, enhancing cellular responses through endocrine, paracrine, autocrine or intracrine signalling mechanisms. These cytokines bind to the receptors on target cells, triggering signalling cascades and gene activation to promote inflammation, angiogenesis, fibroblast growth and extracellular matrix remodeling. PDGF draws in neutrophils and macrophages while also acting as a mitogen and chemoattractant for fibroblasts and smooth muscle cells, thereby enhancing collagen synthesis and promoting tissue repair. The precise timing, strength and length of these episodes are crucial for effective wound healing [17]. Wound healing is a multifaceted, progressive process that occurs in four interconnected stages: hemostasis, inflammation, proliferation and maturation, each of which is vital for tissue repair. This process begins with rapid clot formation to stop bleeding, followed by an inflammatory reaction where immune cells remove pathogens and debris while platelets release growth factors to promote healing. In the proliferation stage, angiogenesis and fibroblast activity assist in rebuilding damaged tissue, which leads to the wound contraction, while maturation involves collagen remodeling and apoptosis to strengthen the healed area. This complex sequence depends on various factors, including treatment effectiveness, wound severity and methodology, prompting the investigation into advanced biomaterials such as collagen, fibrin, silk fibroin and keratin, providing structural stability and enhance healing. The diverse features of wounds necessitate further exploration of biological mechanisms to improve therapies, particularly those involving nanomaterials, for the effective and targeted wound care [18].

Wound healing starts with hemostasis, an urgent response that transpires during the initial minutes after injury to prevent hemorrhage and stabilize the affected area. When the skin is disrupted, capillaries contract to minimize blood loss, while platelets, which are small, disc-shaped, anuclear cell fragments, swiftly gather near the wound site, clinging to exposed ECM proteins such as fibronectin and vitronectin. Activated platelets secrete dense and alpha granules that include coagulation components, bioactive chemicals and inflammatory cytokines, such as interleukin (IL)-1α, IL-1β, IL-6, IL-8 and TNF-α. These substances not only facilitate the clot formation but also trigger the inflammatory response by attracting immune cells. IL-8 is a potent chemoattractant for neutrophils, signifying the onset of the early inflammatory phase. Thrombin, a crucial component, enhances platelet activation and clot stability, while regulatory mechanisms including prostaglandins, activated protein C and thrombin inhibition ensure the appropriate cessation of coagulation to avert excessive thrombosis. Platelets actively participate in immunological signalling, leukocytes recruitment and initial host defense. As inflammation progresses, neutrophils act as the initial immune cells to invade the site, releasing inflammatory mediators to eliminate pathogens and necrotic tissue prior to apoptosis. Lysophosphatidylcholine released by dead neutrophils recruits monocytes, which could migrate to the wound and develop into M1 macrophages under the effect of IFN-γ and LPS, thereby enhancing inflammation through further cytokine production. Concurrently, the additional pro-inflammatory signals are produced by mast cells, which refer to the resident immune cells that secrete histamine, tumor necrosis factor (TNF) and IL-4, and by the neuropeptides released via cutaneous neurons. This highlights the interaction between the neurological and immune systems. The shift from inflammation to repair is finally facilitated by the polarization of M1 to M2 macrophages. M2 macrophages release anti-inflammatory cytokines such as IL-10 and growth factors including TGF-β, thus facilitating tissue regeneration and mitigating excessive inflammation. During these phases, the biochemical milieu of the wound would undergo dynamic changes, from clot formation and immune cell recruitment to the resolution of inflammation, which facilitates future tissue growth and repair [19,20].

The proliferation and remodeling stages of wound healing encompass a meticulously orchestrated sequence of biochemical pathways that reinstate tissue integrity, affected by the interaction among many cell types and molecular cues. Approximately four days after injury, the proliferative phase commences, which is characterized by the production of granulation tissue, re-epithelialization, angiogenesis and immunomodulation. Fibroblasts, stimulated by various growth factors such as TGF-β and PDGF, play a pivotal role in this phase by generating ECM components and differentiating into myofibroblasts in response to mechanical stress and increased TGF-β1 concentrations. Myofibroblasts, distinguished by α-SMA expression, synthesize collagen types I and III to facilitate wound contraction. Nevertheless, their prolonged presence, attributable to inadequate apoptosis and diminished matrix metalloproteinase (MMP) activity, may result in scarring. Keratinocytes, stimulated by cytokines including IL-1, IL-6 and TNF-α, along with epidermal and fibroblast growth factors, traverse the wound bed to restore the epidermal barrier. They also participate in the reciprocal communication with fibroblasts and immune cells to modulate proliferation and immunological activation. Endothelial cells, activated by VEGF and PDGF, facilitate neovascularization, therefore providing oxygen and nutrients for tissue repair. As healing advances, the remodeling phase begins, during which type III collagen is destroyed by MMPs and supplanted by stronger, more organized type I collagen, thereby augmenting the tensile strength of the tissue. A decrease in hyaluronic acid and fibronectin levels indicates the cessation of matrix production. The disruption caused to the biochemical equilibrium among growth factors, cytokines and ECM remodeling enzymes, especially due to sustained TGF-β1 signalling and excessive collagen accumulation, increases the possibility of the wound advancing towards fibrotic scarring instead of regenerative repair [21]. Fig. 2 illustrates the process of healing wounds. Table 1 demonstrates the different stages of the wound healing process.

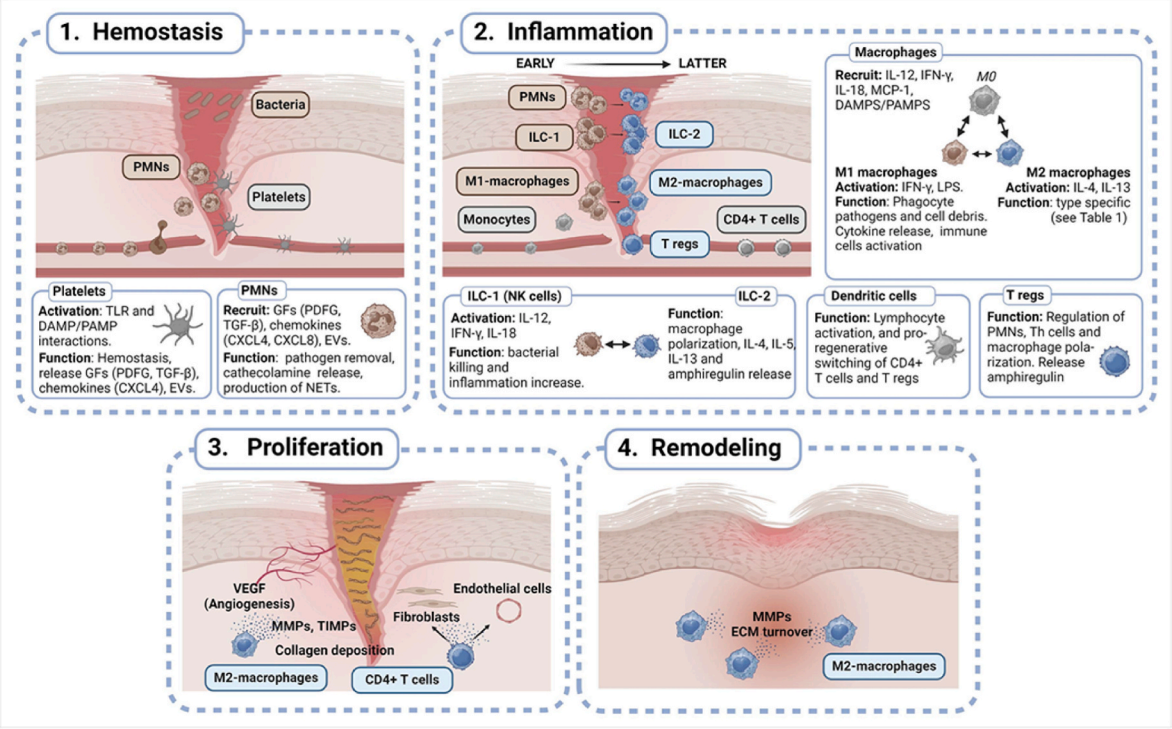

Fig. 2. The various stages of wound recovery. It represents the four interconnected and consecutive stages of wound healing: hemostasis, inflammation, proliferation and remodeling. In the early hemostasis phase, platelets and PMNs are rapidly recruited to the location of injury by damage-associated molecular patterns (DAMPs) and microbial invasion, leading to the clot formation, the secretion of pro-inflammatory mediators including PDGF and TGF-β, and the development of neutrophil extracellular trap (NETs). During the inflammatory phase, the first responders such as PMNs and group 1 ILC-1s are followed by monocytes transformed into M1 macrophages, stimulated by IFN-γ and IL-12 to boost inflammation and assist in pathogen elimination. Afterwards, the immune reaction shifts as M2 macrophages, ILC-2s, CD^{4+} T cells and Tregs emerge to promote the resolution of inflammation and the healing of tissue. Dendritic cells aid in the presentation of antigens and the activation of T cells. The proliferation stage involves angiogenesis, recruitment of fibroblasts, and deposition of ECM, supported by M2 macrophages and CD^{4+} T cells through VEGF and MMP/TIMP signalling, thereby promoting the formation of granulation tissue. Finally, during remodeling, M2 macrophages persist in regulating MMPs and facilitating ECM turnover, which supports tissue maturation and scar development. Due to this coordinated engagement of immune cells and signalling molecules, effective wound healing and tissue repair are ensured. Reprinted with permission from Ref [22].

Table 1
A summary of the different stages of wound healing.

Phase	Timing	Key Cellular Players	Main Events/Activities
Hemostasis	Immediate (minutes to hours)	Platelets, clotting factors	Vasoconstriction Platelet aggregation Fibrin clot formation to stop bleeding
Inflammation	Hours to ~3 days	Neutrophils, macrophages, mast cells	Neutrophil infiltration Removal of debris and pathogens Release of inflammatory cytokines
Proliferation	~3–14 days	Fibroblasts, keratinocytes, endothelial cells	Angiogenesis (new blood vessel formation) Fibroblast proliferation Collagen deposition Formation of granulation tissue
Maturation (Remodeling)	2 weeks to months (can last >1 year)	Fibroblasts, myofibroblasts	Collagen remodeling Scar tissue formation Increase in tensile strength Apoptosis of excess cells

The wound healing process is traditionally divided into four distinct yet overlapping phases, each characterized by specific cellular activities and biological events. Initially, during the hemostasis phase, bleeding is rapidly controlled through the aggregation of platelets and the activation of clotting factors, leading to the formation of a stable fibrin clot. This immediate response is triggered within minutes of injury and is critical for preventing excessive blood loss. Subsequent to hemostasis, the inflammation phase is initiated, typically lasting for several days. During this stage, neutrophils and macrophages are recruited to the wound site, where they are tasked with the removal of invading pathogens, dead cells and debris through various processes such as phagocytosis and cytokine release. Once the wound is cleared, the proliferation phase is started. Fibroblasts, keratinocytes and endothelial cells are mobilized to promote tissue regeneration, granulation tissue formation, angiogenesis and re-epithelialization, thereby restoring the structural framework of the injured tissue. Finally, the maturation or remodeling phase is entered, which can extend for several months. Throughout this prolonged stage, collagen is extensively reorganized and remodelled by fibroblasts and myofibroblasts to enhance the tensile strength of the repaired tissue. Excessive cells are gradually removed through apoptosis, and the scar tissue formation is completed. Through this coordinated sequence of events, tissue integrity and functionality are finally restored following injury. The stages of wound healing and more information about this process can be found in these reviews [23–29].

4. Classification of wounds

4.1. Chronic wounds

Chronic wounds are injuries that do not heal within the standard timeframe of one to three months and do not end up with the normal structure and function of the skin restored. The Wound Healing Society categorizes these lesions into four primary types according to their etiology: pressure ulcers, diabetic ulcers, venous ulcers and arterial ulcers. These injuries signify a health concern that is prevalent but sometimes disregarded, particularly within the global geriatric demographic. Assessing the prevalence of chronic wounds is challenging due to the variety of wound classifications and ambiguous criteria. A 2017 systematic study projected that roughly 5.7 million Americans suffer with chronic wounds, providing an annual cost of almost $20 billion. Aside from the economic challenges, chronic wounds can also significantly diminish quality of life, resulting in pain, restricted mobility, mental turmoil, recurrent hospitalizations and, in certain instances, mortality [30].

In chronic wounds, the inflammatory phase frequently gets extended and dysregulated, preventing the advancement to the tissue healing. This chronic inflammation entails atypical immune responses, characterized by the sustained presence of neutrophils and macrophages under pro-inflammatory conditions, malfunctioning keratinocytes and fibroblasts, along with compromised signaling cascades involving cytokines, microRNAs (miRNAs) and transcription factors. The innate immune system, via pattern recognition receptors on keratinocytes and immune cells, reacts to the injury and infections. However, its dysregulation may impede recovery. The shift of macrophage polarization from M1 to M2 is essential for entry into the proliferative phase, and the disturbances in this process, resulting from modified metabolic conditions, reduced IFN-β levels or compromised SET domain bifurcated histone lysine methyltransferase 2 (SETDB2) expression, are linked to chronicity. Neutrophils, essential for early defense, can become detrimental when they remain active, releasing toxic enzymes and generating NETs, which hinder tissue regeneration. Mast cells and γδ T cells similarly affect repair but may potentially lead to the fibrosis or prevented healing, contingent upon their conditions. Adaptive immune cells, such as regulatory T cells and innate lymphoid cells, also influence healing but demonstrate impaired activity in chronic wounds. Furthermore, the variety and dysfunction of fibroblasts are crucial in chronic wound pathology, with pro-fibrotic and inflammatory fibroblast subtypes being more abundant in diabetic wounds. Infection and hypoxia exacerbate healing, biofilms protect bacteria from therapies and sustain inflammation, and hypoxic environments stimulate hypoxia-inducible factor 1 (HIF1) pathways, which are potential therapeutic targets now under clinical exploration. Therefore, chronic wound healing is regulated by a complex nonlinear interaction of immunological, cellular and molecular components, underscoring the necessity for human-specific study models and tailored therapeutics [31].

Chronic wound healing is a disturbed physiological process characterized by extended inflammation and compromised tissue regeneration, frequently observed in situations such as diabetes, vascular disease and obesity. Wound healing typically comprises four phases, hemostasis, inflammation, proliferation and maturation. However, it is impaired in chronic wounds due to variables such as excessive inflammation, diminished angiogenesis, tissue necrosis and aberrant immune responses. Diabetic foot ulcers, vascular ulcers and pressure ulcers are prevalent, especially among the older population. Chronic wounds are characterized by ongoing immune cell infiltration (neutrophils and macrophages), diminished regulatory cells (dendritic cells and eosinophils) and disrupted signalling cascades including cytokines, chemokines and miRNAs. Some particular immunological dysfunctions, such as the overexpression of MMP-9, uneven cytokine profiles, defective transcription factors (Foxm1 forkhead box M1 (FOXM1), signal transducer and activator of transcription 3 (STAT3)) and disturbed miRNA expression, exacerbate healing by perpetuating inflammation and compromising tissue architecture. This finally results in fibrosis, inadequate vascularization and delayed epithelial regeneration [32].

4.2. Acute wounds

Annually, about 6 million individuals in the United States suffer from acute and chronic wounds, incurring around $25 billion (USD) in healthcare expenses. Uncomplicated acute wounds often adhere to a predictable healing timeframe determined by the nature and severity of the damage. Typical clinical signs of infection in these wounds include erythema, edema, increased temperature and purulent exudate. Conversely, persistent wounds such as diabetic ulcers exhibit hindered healing owing to many aggravating factors. The influencing factors may encompass advanced age, severity of diabetes, inadequate treatment adherence, peripheral neuropathy, compromised immunological function, and/or arterial or venous insufficiency. Despite significant advancements made in wound care over the last few decades, researchers and healthcare professionals persist in exploring novel therapeutic options to prevent and manage infections in both acute and chronic wounds. Systemic antibiotics, taken orally or intravenously, are routinely utilized for the management of acute wound infections. Topical antimicrobials, such as creams, gels and ointments, are commonly employed in the management of persistent wound infections to target deeper infections resulting from bacterial or fungal infiltration of the subcutaneous layers [33]. Acute trauma, a significant global health issue, is one of the four leading causes of death, frequently arising from vehicular accidents, battle injuries or surgical complications, with uncontrolled hemorrhage being the principal factor of early fatality. The body's inherent coagulation mechanisms are sometimes inadequate for rapid hemostasis, particularly in the intricate wounds involving irregular internal organs or arterial hemorrhage. Efficient hemostasis, including platelet and fibrin functions, is crucial for halting hemorrhage and facilitating healing, which highlights the need for effective wound dressings that augment coagulation and tissue regeneration. Acute wounds, often superficial and resulting from abrupt external damage, normally heal within 1–2 weeks but may induce significant pain owing to nerve exposure and need a wet healing environment. Chronic wounds demonstrate compromised healing attributable to a multitude of patient, environmental and wound-specific variables. It plays an essential role in preventing the transition of acute wounds into chronic wounds, as healing is a complicated multi-phase process susceptible to disruption. The risk factors encompass substandard surgical conditions, compromised patient health (malnutrition, comorbidities), wound attributes and insufficient wound treatment, all of which may lead to extended healing time and infections [34].

5. Conductive polymers in wound healing acceleration

5.1. Conductive polymers

5.1.1. Polypyrrole

Inefficient wound healing continues to pose a frequent clinical issue, with no completely effective treatment available. Electrospun nanofibrous bandages provide a hopeful option because they mimic the natural ECM. PPy/polydopamine (PDA)/poly(l-lactide) (PLLA) nanofiber membranes demonstrate exceptional multifunctional characteristics, rendering them extremely appropriate for wound healing applications. The electrospun fibers have a core-shell structure, with PLLA as the core and homogenous PDA and PPy layers as the shell. These surface alterations significantly improve hydrophilicity, antioxidant activity and electrical conductivity, which are crucial for enhancing cell adhesion, regulating wound exudate and enabling endogenous electrical communication. These materials exhibit enhanced water absorption and swelling capability, facilitating a moist wound environment. PDA and PPy have robust ROS-scavenging capabilities, mitigating oxidative stress

in cells. Upon exposure to near-infrared (NIR) irradiation, PPy/PDA/PLLA attains a temperature of around 47 °C, facilitating the photothermal antibacterial activity devoid of antibiotics. This is effective in eradicating *E. coli* and *S. aureus* under both in vitro and in vivo settings. The hemostatic performance is significantly improved by accelerated clot formation, increased platelet adhesion and the presence of Fe^{3+} ions. Although cytocompatibility assays demonstrate high cell viability and low toxicity, histological staining indicates less inflammation and enhanced fibroblast activity. In full-thickness skin wound models, PPy/PDA/PLLA enhances wound closure, facilitates neovascularization and stimulates hair follicle regeneration, supported by a localized thermotherapeutic effect that increases blood flow and promotes tissue healing [35]. Despite the promising properties of the PPy/PDA/PLLA nanofibrous dressing, one notable limitation lies in the byproducts and degradation profile of the PLLA core. As PLLA degrades, it generates lactic acid, which can lead to localized pH reductions and potential inflammatory responses if not properly buffered. Moreover, the long degradation time of PLLA may not align with the dynamic phases of wound healing, potentially hindering tissue remodeling. Future studies should focus on tuning the degradation rate by blending PLLA with faster-degrading polymers or incorporating pH-neutralizing agents. Additionally, thorough in vivo investigations are required to evaluate the systemic effects of prolonged degradation and the bioactivity of degradation byproducts for safety and optimal healing outcomes.

Crosslinking with chitosan (CHIT)-based nanofiber composites, crosslinked with dialdehyde cellulose (DAC) and augmented with colloidal PPy, were formulated and thoroughly studied for their prospective use in wound healing. FT-IR spectroscopy validated the successful oxidation of cellulose to DAC and its subsequent CHIT by Schiff base production, while the further interaction between DAC and PPy further increased structural complexity. The characterization of PPy colloid revealed stable, well-dispersed spherical nanoparticles of 35 nm in size, exhibiting conductive and UV–Vis active characteristics. The integration of DAC significantly improved the tensile strength of CHIT nanofibers (from around 8.6 MPa to around 14.6 MPa), whereas the addition of PPy particles further augmented mechanical stiffness, despite resulting in diminished strain at break due to increasedj rigidity. The use of PPy significantly enhanced swelling behavior, with the CHIT_DAC_PPy 10 % sample exhibiting over 1200 % swelling and 92 % equilibrium water content, making it optimal for absorbing wound exudate. Structural SEM investigation validated substantial fiber expansion following hydration and enhanced chemical stability under acidic conditions due to covalent DAC crosslinking. In a hydrated condition, the conductivity of PPy composites rose to the levels (up to 11.6 mS/cm) comparable to those of human tissue, which is vital for bioelectronic applications. Biological assessments indicated the absence of cytotoxic effects, as fibroblasts proliferated effectively in the presence of the composites while preventing undesirable adhesion advantageous for dressing replacement. Antioxidant experiments revealed a PPy-dependent decrease in ROS under both cell-free and neutrophil-based systems, correlating with PPy concentration. Macrophage response tests indicated reduced production of NO and IL-6, indicating less pro-inflammatory activation. In vitro scratch studies demonstrated improved wound closure, particularly with CHIT_DAC_PPy 10 %, signifying better facilitation of cell migration. Antibacterial tests demonstrated significant efficiency against *S. aureus*, especially in PPy-loaded composites ($A > 6$), but the activity against *E. coli* was negligible [36].

The healing of chronic wounds is frequently obstructed by bacterial infections and diminished trans-epithelial potential. Revolutionary patches that merge ES with antibacterial properties provide a remedy, but different obstacles are encountered, such as the dependence on external power sources and antibiotic resistance. The PPy/polycaprolactone (PCL)-based triboelectric nanogenerator (TENG) patch is a multifunctional self-sustaining wound dressing intended to facilitate the healing of infected wounds via ES, antibacterial properties and improved tissue regeneration. The PPy/PCL membrane, synthesized using the chemical vapor deposition of PPy onto electrospun PCL fibers, is capable of structural integration. At an ideal $FeCl_3$ catalyst concentration of 15 %, the patch exhibits superior electrical conductivity, hydrophilicity and mechanical flexibility , which are essential characteristics for ensuring comfort during skin contact and maintaining moisture equilibrium. The TENG functions in a vertical contact-separation mode, transforming biomechanical energy (ambulation, jogging, respiration) into electrical impulses. Output voltages reach a maximum of 8 V contingent upon activity, and the device maintains stability after 2400 cycles. Nevertheless, the performance deteriorates at high humidity and recuperates upon drying. Antibacterial experiments demonstrate the synergistic eradication of *E. coli* and *S. aureus* by the positive surface charge of PPy and low-voltage ES, which disrupts bacterial membranes via autolysis instead of electroporation or harmful byproducts. In vitro studies demonstrate that the TENG significantly promotes fibroblast proliferation, migration and adhesion, accompanied by the increased production of FAK and growth factors including VEGF, fibroblast growth factor (FGF) and TGF-β via ERK/MAPK pathway. In a diabetic rat model with infected wounds, the TENG group demonstrated enhanced wound closure, increased collagen deposition and angiogenesis, while inhibiting the inflammatory marker IL-6. The TENG patch provides a comprehensive solution to the treatment of chronic, infected wounds by fostering a conducive healing milieu through electrical stimuli and biocompatible materials [37].

PP-CDLut-AMY microneedles (MN) are multifunctional, minimally invasive wound dressings designed to address bacterial biofilm infections, diminish oxidative stress and enhance tissue regeneration by integrated photothermal therapy, antioxidant administration and biofilm degradation. The encapsulation of luteolin (Lut) within cyclodextrin (CD) significantly improved its solubility (~331-fold), stability and antioxidant efficacy. PDA-PPy (PP) nanocomposites exhibited effective NIR-responsive photothermal characteristics, with temperatures exceeding 60 °C after 5 min of exposure to 808 nm laser irradiation. MNs produced using mold casting and freeze–thaw techniques exhibited remarkably high mechanical strength (tip force ~2.18 N), penetration depth (~150 μm) and exceptional swelling capacity (~487 %) for wet wound healing. The integration of CDLut significantly enhanced DPPH radical scavenging (~76 %), whereas PP facilitated strong, consistent photothermal heating. Although α-amylase (AMY) diminished the antioxidant efficacy of Lut to some extent due to molecular interactions, it was crucial in biofilm disintegration, effectively degrading the extracellular polysaccharides of *S. aureus* biofilms (disruption rate ~83 %). In vitro, PP-CDLut-AMY MNs exhibited potent bactericidal activity against *S. aureus* and *E. coli* under NIR light, causing bacterial survival rates to fall below 2 %. SEM and Live/Dead staining validated bacterial membrane rupture, but MNs devoid of PP or light did not demonstrate similar effects. Furthermore, in vivo studies indicated safe cytocompatibility and hemocompatibility, with no evidence of organ damage. In a diabetic mouse wound model infected with *S. aureus* biofilms, only the combination of PP-CDLut-AMY MN and NIR light achieved near-complete wound closure (~97 %) by day 11, significantly surpassing control treatments. Histological investigations demonstrated substantial collagen deposition, increased neovascularization (CD31 upregulation) and significantly reduced inflammation (TNF-α downregulation), highlighting improved skin regeneration. The combined actions of antioxidant release, biofilm degradation by AMY and PP-induced photothermal eradication of bacteria resulted in rapid inflammation resolution and tissue regeneration. Therefore, PP-CDLut-AMY MN offers a secure, intelligent, and effective therapeutic framework for the treatment of chronic, biofilm-infected wounds, especially in difficult scenarios such as diabetic ulcers [38].

Present obstacles in the advancement and clinical application of sophisticated wound dressings arise from the intricate and fluctuating characteristics of the wound healing process, which is especially true for the chronic and infected wounds where elements such as bacterial

biofilms, oxidative stress, compromised vascularization and dysregulated inflammation coexist. Despite the promising multifunctionality of electrospun nanofibrous membranes such as PPy/PDA/PLLA, CHIT-DAC-PPy composites, TENG-based patches and PP-CDLut-AMY microneedles, including antioxidant properties, photothermal antibacterial activity, electrical conductivity and biofilm degradation, their incorporation into clinical practice is impeded by various limitations. Although the PPy/PDA/PLLA dressing has superior photothermal and ROS-scavenging properties, the gradual acidic breakdown of PLLA may induce localized inflammation and impede tissue regeneration. The CHIT-DAC-PPy composites demonstrate remarkable swelling and antioxidant properties. Nevertheless, their restricted antibacterial efficacy (ineffective against *E. coli*) and mechanical stiffness hinder adaptability. The TENG patches have diminished efficacy in humid conditions, which is crucial in wet wound settings, and their dependence on mechanical stimulation may be unreliable in immobile or critically sick patients. MN systems such as PP-CDLut-AMY MNs exhibit remarkable biofilm elimination and tissue regeneration via synergistic pathways. Nonetheless, their efficacy is contingent upon external NIR irradiation, potentially restricting their use in resource-limited environments. Furthermore, the long-term biosafety of CPs, their breakdown byproducts and photothermal agents is inadequately investigated, particularly in vulnerable populations such as diabetics and the elderly. Future research should focus on developing wound dressings with adjustable degradation profiles, incorporating intelligent stimuli-responsive systems that function independently based on physiological signals (pH, temperature, enzyme presence), and improving antibacterial efficacy without any dependence on external stimuli or antibiotics. Furthermore, integrating real-time biosensing with therapeutic administration has the potential to convert passive dressings into active diagnostic-driven systems. It is essential to explore various innovations including biodegradable TENGs, self-regulating antioxidant release, the on-demand medication delivery via responsive microneedles and the multifunctional hydrogels that neutralize pH variations. Moreover, comprehensive in vivo investigations and prolonged biocompatibility evaluations are crucial for comprehending systemic reactions, ensuring patient safety and synchronizing degradation kinetics with the stages of wound healing. The integration of materials science, bioelectronics and regenerative medicine is essential for the development of advanced wound treatments that are customized, self-sustaining, and capable to address the existing challenges in chronic wound management.

Intestinal perforation presents a significant medical issue, frequently resulting in various complications such as tissue adhesion due to traditional surgery. A multifunctional hydrogel, A30, synthesized from gelatin methacryloyl (GelMA) and PPy, was produced, demonstrating improved mechanical strength, hemostatic capability, conductivity and wound healing capabilities. Gelatin was initially methacrylated to produce GelMA with differing substitution levels, and PPy was integrated by polymerization and then crosslinked through Schiff base reactions. The A30 hydrogel had the highest compressive modulus and enhanced cytocompatibility with L929 and HUVEC cells relative to currently available chitosan-based hydrogels. SEM imaging revealed a porous three-dimensional network architecture that facilitated the effective absorption of wound exudate while preserving structural integrity in PBS. The A30 hydrogel exhibited superior hemostatic efficacy in both mouse tail and liver hemorrhage models. Cell migration and angiogenesis were enhanced, as evidenced by the elevated expression of VEGF, HIF, FGF and Ang in HUVEC cells. PC12 neuronal cells exhibited substantial depolarization, evidencing the conductive properties of the hydrogel. To mitigate postoperative tissue adhesion, PEG-NHS was integrated into the hydrogel to manufacture an anti-adhesive variant named AA-A30. The hydrolyzed NHS ester developed a protective surface layer, successfully inhibiting tissue attachment while maintaining the mechanical stability, degradation rate, and cytocompatibility of the hydrogel. No toxicity or immunological reaction was observed in vivo after implantation. In a mouse full-thickness skin wound model, A30 hydrogel significantly expedited wound healing, enhanced granulation tissue and skin appendage development, and elevated the production of VEGF and EGF while inhibiting the inflammatory marker IL-1β. In a cecum perforation model, AA-A30 successfully inhibited tissue adhesion, as evidenced by macroscopic observation and histological examination, with the regulation of inflammatory and fibrinolytic gene expression [39].

A new multifunctional hydrogel system denoted as PDA@AgNPs-PPyGel-Fe was produced and described, including polydopamine-coated silver nanoparticles (PDA@AgNPs), conductive polypyrrole-modified gelatin (PPyGel) and ferric ion (Fe^{3+}) cross-linking. The effective reduction of Ag^{+} to Ag^{0} by PDA was validated using UV–vis spectroscopy, revealing a distinctive surface plasmon resonance (SPR) peak at 420 nm, indicative of spherical silver nanoparticles (10–50 nm). A rapid gelation process produced hydrogels following the addition of Fe^{3+}, while metal–catechol coordination and hydrogen bonding were leveraged to create stable, porous structures suitable for tissue engineering, with pore diameters between 20 and 50 μm. As the concentration of PDA@AgNP rose, the pore size diminished due to intensified cross-linking. All hydrogel versions demonstrated exceptional water absorption (~85 % water content) and swelling characteristics, which are essential for sustaining a moist wound environment. PDA@AgNPs improved strain tolerance and compressive strength (up to 55 kPa), while a higher AgNP concentration enhanced hydrogel conductivity (from 14 to 36 mS/cm), exceeding skin conductivity and facilitating LED illumination. This reaffirms their electrical potential for bioelectronic wound applications. Rheological analysis demonstrated a high storage modulus ($G' > G''$) and a strain-sensitive reversible gel–sol transition, confirming viscoelastic stability and exceptional self-healing capabilities. The hydrogels were capable of complete reassembly within 30 min after damage, significantly quicker than numerous documented hydrogel systems. The antioxidant activity was evidenced by DPPH and ABTS plus radical scavenging tests, with a scavenging efficiency of around 100 % achieved for the maximum concentration of PDA@AgNPs, which is ascribed to the phenolic and catechol groups in PDA. Antibacterial experiments demonstrated significant bactericidal efficacy (>90 % against *E. coli* and *S. aureus*), corresponding with Ag^{+} release and surpassing control PPyGel-Fe hydrogels. Hemolysis ratios were under 5 %, and all samples demonstrated satisfactory coagulation activity (BCI <30 %), affirming superior blood compatibility. Cytocompatibility was confirmed by CCK-8 tests and microscopy, with over 80 % L929 cell vitality and normal morphology demonstrated after 72 h [40].

Wound infections pose a significant health threat, leading to the development of antibacterial dressings for efficient recovery. Multifunctional bioactive films (GC/BP) were designed by incorporating berberine hydrochloride (BH) and PPy into a chitosan (CS) and gelatin (GE) matrix to produce photothermal, conductive, antibacterial and biocompatible wound dressings. The ideal PPy concentration (5 %) was established by reconciling photothermal efficiency with safety, with fast heat production (up to 55.2 °C) and remarkable stability demonstrated. Structural and mechanical studies indicated that the integration of BH and PPY improved the density and flexibility of the film, while preserving adequate tensile strength and reducing stiffness, which makes them applicable under dynamic wound settings. The films had an amorphous structure and robust intermolecular interactions, showing excellent compatibility among the components. Optical tests indicated that BH and PPy diminished transmittance and brightness, particularly PPy owing to their black coloring. All films exhibited elevated water vapor permeability (WVP) and hydrophilicity, which is crucial for exudate control. Thermal investigation by TGA and DSC demonstrated excellent thermal stability with negligible influence from BH or PPY. The GC/BP film exhibited significantly enhanced electrical conductivity (0.3119 μS/cm), which is attributable to the conjugated structure of PPY. Drug release experiments demonstrated a biphasic BH release profile, characterized by an early burst followed by persistent diffusion, according to a first-order kinetic model. The films demonstrated prolonged

antioxidant activity (up to 92.54 % DPPH clearance after 48 h), which is ascribed to GE peptides, the inherent characteristics of BH and the conjugated system of PPY. Hemolysis and cytotoxicity experiments validated biocompatibility, with hemolysis rates below 5 % and no cytotoxicity to L929 fibroblasts. Antibacterial investigations demonstrated the substantial suppression of *S. aureus* (up to 98.6 %) and modest efficacy against *E. coli*, which was significantly enhanced with the addition of PPy due to its positive charge damaging bacterial membranes. Under NIR illumination, the GC/BP films demonstrated enhanced antibacterial efficacy via photothermal therapy, eliminating over 99 % of both bacterial strains. Fluorescence and SEM imaging validated membrane rupture and bacterial mortality. In vivo wound healing models using infected mice exhibited expedited healing in GC/BP + NIR-treated wounds (93.2 % closure in 9 days), diminished inflammation (reduced TNF-α levels), augmented fibrous tissue development and increased vascularization (elevated CD31 expression). Systemic toxicity assessment revealed no organ impairment or weight reduction in the treated animals [41]. Despite the significant advancements exhibited by systems such as PP-CDLut-AMY microneedles, PDA@AgNPs-PPyGel-Fe hydrogels and GC/BP bioactive films, fundamental constraints remain, including the restricted long-term biocompatibility data in human models, the possible cytotoxicity or pro-inflammatory reactions elicited by nanomaterials or photothermal agents at elevated dosages, and the difficulties in reconciling mechanical strength with flexibility under dynamic wound settings. Moreover, although photothermal therapy improves antibacterial effectiveness, it is still necessary to further examine the potential for thermal injury to adjacent healthy tissues from extended or repeated NIR radiation. Disruption of biofilms presents a particularly intricate challenge owing to the durability of bacterial extracellular matrix and the necessity for regulated enzyme release kinetics. The complexity of chronic wounds, especially in diabetic patients, requires the use of materials that can dynamically adapt to fluctuating microenvironments, which is a capability that most existing dressings do not adequately provide. From a translational viewpoint, scalable manufacturing techniques, regulatory approval processes and production cost-effectiveness are still inadequately investigated. Future research should focus on creating "smart" wound dressings that enable real-time sensing and responsive therapeutic administration, including incorporating biosensors for monitoring pH, temperature or bacterial load, coupled with triggered release mechanisms. The design of next-generation microneedles or hydrogels may integrate stimuli-responsive features, like magnetic, enzymatic or pH-sensitive components that adapt to wound conditions. Furthermore, it is crucial to conduct an investigation into biodegradable and immunomodulatory nanomaterials that facilitate tissue regeneration while alleviating chronic inflammation. The improved collaboration between natural bioactive substances (such as polyphenols and peptides) and nanostructured carriers may enhance therapeutic efficacy and reduce toxicity. The application of modern 3D bioprinting and tissue engineering techniques may facilitate the personalization of dressings for individualized wound geometries and pathologies. Moreover, broadening in vivo investigations to encompass big animal models and executing comparison trials with current clinical standards are crucial for the assessment of long-term efficacy and safety. Future research should be carried out by investigating the integration of ES treatments with conductive dressings to enhance tissue healing and nerve regeneration, thereby expanding the scope of wound care.

Bacterial infections significantly impede the healing of wounds. The antibacterial therapies that involve photothermal and photodynamic methods with NIR light in semiconductor nanomedicine are efficient but might encounter issues with band structure alignment. A new nanomaterial, namely PPy-bismuth oxychlorid (BiOCl) intercalated nanosheets, was developed by following a space-confined manufacturing process, where PPy was integrated with BiOCl nanosheets to establish a multifunctional platform for NIR photoresponsive antibacterial treatment and wound healing. BiOCl functioned as an optimal template owing to its two-dimensional architecture, stability and biocompatibility, thus facilitating the in situ intercalation of ultrathin PPy nanosheets (~2 nm). Structural and compositional investigations via TEM, AFM, EDS, FTIR, Raman and XRD validated successful intercalation without compromising the BiOCl lattice, while XPS analysis revealed the robust atomic-level contacts between PPy and BiOCl, promoting efficient charge separation. Optical evaluation demonstrated that the intercalated material exhibited extensive NIR absorption and improved photothermal and photodynamic capabilities, with superior ROS production and photothermal conversion (~50 °C in 10 min). Photocurrent and photoluminescence assessments validated enhanced electron-hole separation in the hybrid nanosheets. The PPy-BiOCl nanosheets demonstrated exceptional bactericidal efficacy (~99 % against *S. aureus* and *E. coli*) through synergistic photodynamic and photothermal therapy actions, with significant reusability exhibited and bacterial membrane rupture verified under near-infrared illumination. In vivo experiments via a *S. aureus*-infected full-thickness wound model demonstrated expedited healing, considerable reduction in bacterial load and inflammation, as well as enhanced collagen deposition, particularly under near-infrared irradiation. Thermal imaging revealed fast and localized heating at wound locations. Biosafety evaluations demonstrated outstanding cytocompatibility with bone marrow stromal cells, little hemolysis (<1 %) and the absence of toxicity in major murine organs after 14 days. The photoresponse was mechanistically ascribed to effective π–π transitions in PPy and band alignment with BiOCl, which augmented ROS production and hot electron dynamics (Fig. 3) [42]. Despite the promising results achieved with PPy-BiOCl intercalated nanosheets for NIR-triggered antibacterial therapy and wound healing, there remain several challenges that need to be addressed for clinical translation and broader biomedical applications. One of the foremost issues is the precise control over the intercalation process and reproducibility at a large scale. Space-confined synthesis techniques, despite being effective in laboratory settings, may pose scalability limitations and require further optimization for industrial-level productions. Additionally, the long-term stability and biodegradability of the nanocomposite in physiological environments remain concerning, especially on account of the chronic wound treatment where repeated application may be necessary. There is also a need to investigate the pharmacokinetics, biodistribution and potential accumulation of nanomaterials in vivo over extended periods to thoroughly understand any latent cytotoxic or immunogenic responses. While the study shows minimal toxicity after 14 days, longer observation windows are essential for safety validation. Another challenge lies in the depth of NIR light penetration, which may be insufficient for treating deep-seated infections or wounds covered by thick tissues, necessitating strategies such as integrating upconversion nanoparticles or multi-modal irradiation techniques. Moreover, although the synergistic photothermal and photodynamic mechanisms are effective, the balance between ROS generation and heat production remains crucial for preventing healthy tissues from potential collateral damage.

5.1.2. Polyaniline

Flexible conductive hydrogel-based E-skin represents a promising option for biotherapeutic and sensing applicatgions. Conductive silk fibroin/polyaniline/silver nanoparticle (SPAg) complexes improve the compatibility of polyaniline in the hydrogel matrix. These complexes are incorporated into a covalently crosslinked polymer network, resulting in poly(acrylamide-co-sulfobetaine methacrylate) hydrogels (PSPAg). The hydrogels demonstrate outstanding biocompatibility, mechanical durability and sensory functions. When linked to smartphones through Bluetooth, the E-skin can precisely monitor human gestures, assisting in wound healing by boosting angiogenesis and collagen synthesis for quicker recovery [43]. Chronic wounds are often worsened by infections, making treatment quite difficult. While antibiotics are frequently used, they can cause bacterial resistance and negative side effects. Although positively charged substances show promise for

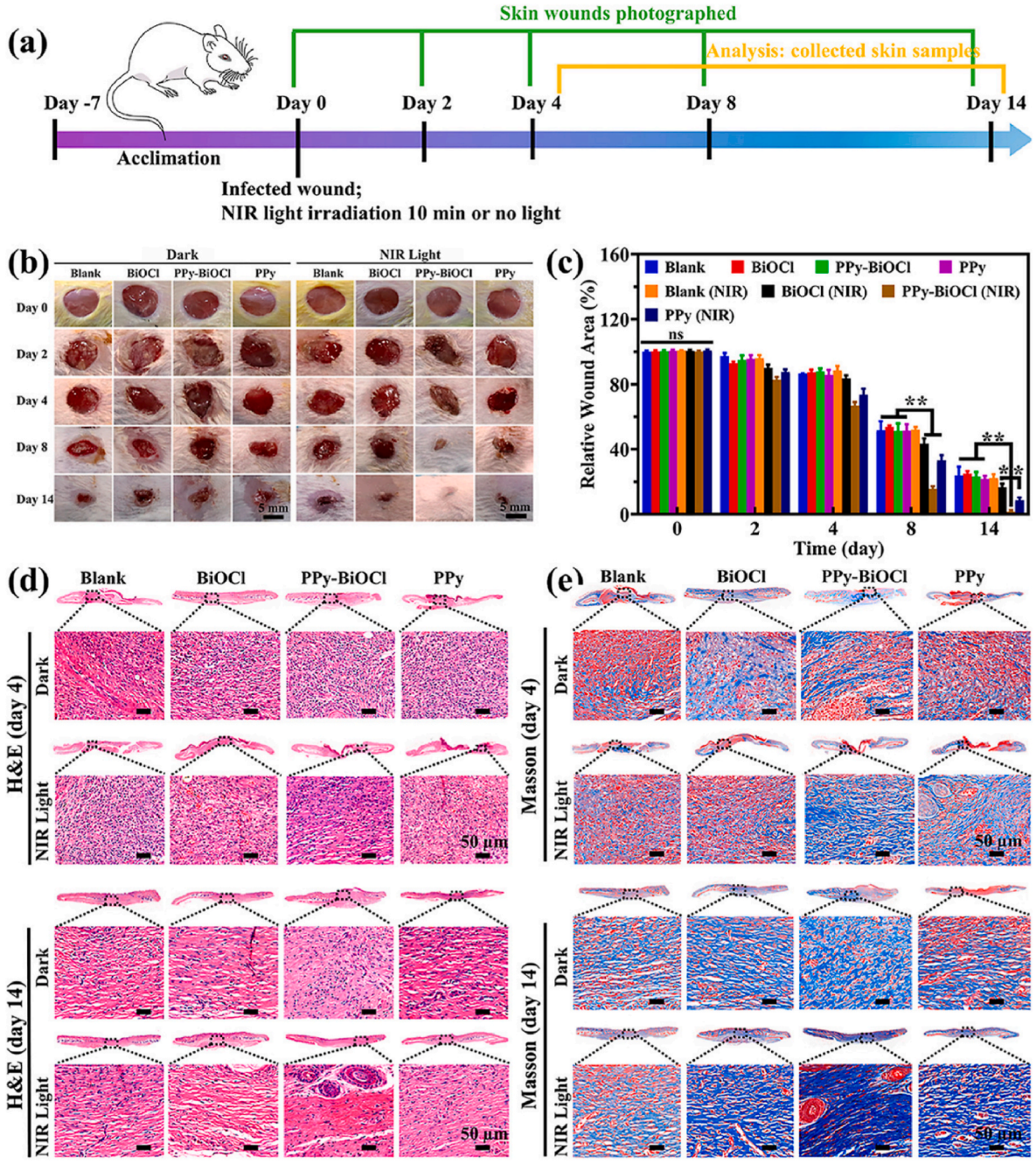

Fig. 3. In vivo evaluation of PPy-BiOCl intercalated nanosheets showing accelerated healing of wound infections. (a) Summary of established murine infection models and the corresponding experimental methods. (b) A murine wound infection model was used to evaluate the healing performance of PPy-BiOCl intercalated nanosheets in darkness and during NIR exposure, accompanied by the corresponding wound images captured at 0, 2, 4, 8, and 14 days. The average wound healing metrics of mice were assessed via Image J, based on the original injured area of the mice. (d) H and E and (e) Masson's trichrome staining of skin specimens in murine wounds at the intervals of 4 and 14 days. Reprinted with permission from Ref [42].

antibacterial uses, their application is often restricted by the toxicity to cells or complicated methods of synthesis. A new polyacrylamide-based hydrogel (PSP hydrogel) integrating polyaniline (PANI) and sulfonated hyaluronic acid (SHA) was produced to improve conductivity, antibacterial efficacy, mechanical strength and wound healing properties. PANI was synthesized through in situ polymerization and optimized via SHA, achieving a sulfonation degree of 17.9 %, which resulted in a conductivity that was about 40 times greater than the SHA-only hydrogel. Despite the hydrophobicity of PANI, the hydrogel maintained a substantial swelling capacity (1373 %), which is crucial for exudate absorption. The hydrogel exhibited a 300 % enhancement in tensile strength and increased elasticity, due to the stiff structure of PANI, hydrogen bonding and a fortified interpenetrating network. The PSP hydrogel demonstrated significant antibacterial efficacy against Gram-positive bacteria, including *S. aureus* and *S. epidermidis*, which is attributable to the preferential interaction of PANI with lipoteichoic acid (LTA) in their cell walls. This interaction resulted in membrane wrinkling and rupture. The hydrogel also obstructed bacterial adhesion and hindered biofilm development. The combination of ES considerably enhanced antibacterial activity, reducing bacterial numbers by more than two orders of magnitude. In the infected wound models, wounds treated with PSP and ES exhibited the most rapid healing, achieving

complete closure by day 14, increased epithelial regeneration, diminished granulation tissue width, augmented collagen deposition (61 %) and significantly elevated neovascularization (as indicated by CD31 staining). This highlights its substantial therapeutic potential for the management of chronic infected wounds [44].

The hydrogels derived from natural systems are outstanding for tissue repair, especially in skin regeneration, but face issues such as low mechanical strength and conductivity. To address these constraints, the advanced polyvinyl alcohol (PVA) hydrogels that integrate $Ti_3C_2T_x$ (MXene) and PANI have been designed for wound healing. MXene enhances hydrogen bonding in PVA, providing NIR-activated antibacterial features, whereas PANI boosts conductivity and interacts chemically with PVA, thereby enhancing the mechanical properties of the hydrogel. The PVA/MXene/PANI hydrogels demonstrate outstanding mechanical strength, electrical conductivity and excellent antibacterial properties, which improves cell proliferation and migration, thus expediting the healing of skin wounds [45].

Antibacterial hydrogel wound dressings are in high demand for facilitating wound healing and avoiding infections. Nonetheless, there remains a considerable problem arising from the development of hydrogels that integrate adjustable antibacterial properties with enough mechanical strength, while circumventing bacterial resistance and possible toxicity. A multifunctional photothermal-responsive hydrogel was produced by incorporating PANI-grafted methacrylated glycol chitosan (PANI-g-MeGC) nanoparticles (Me-PANI NPs) into a polyacrylamide (PAM) matrix and was then extensively studied for wound dressing applications. The PANI-g-MeGC copolymer was effectively synthesized, exhibiting the unique signatures of both PANI and MeGC. The amphiphilic characteristics of this copolymer enabled its self-assembly into stable spherical Me-PANI nanoparticles (about 180–216 nm) under ultrasonic treatment, with the best conditions identified as a 1:4 PANI:MeGC feed ratio and a concentration of 1 mg/mL. These nanoparticles demonstrated significant NIR absorbance and superior photothermal conversion capabilities, swiftly reaching bactericidal temperatures (>50 °C) when exposed to 808 nm laser irradiation. The photothermal impact in vitro completely eradicated *Staphylococcus aureus* and substantially destroyed methicillin-resistant *S. aureus* (MRSA) biofilms, demonstrating strong antibacterial properties. When incorporated into the PAM hydrogel (resulting in NPs@PAM), the material maintained a porous, highly swellable architecture (approximately 1300 % swelling) and demonstrated exceptional mechanical durability, with improved compressive and tensile strength as well as an elongation of up to 400 %, rendering it appropriate for application on mobile or articulated body regions. NIR irradiation of the NPs@PAM hydrogel resulted in regulated surface heating, with optimal photothermal and mechanical characteristics attained at an NP concentration of 10 mg/mL. Antibacterial investigations demonstrated nearly total bacterial elimination following 10 min of near-infrared exposure. Moreover, the hydrogel demonstrated an exceptional performance in water retention under simulated wound circumstances, maintaining over 70 % of its weight over a period of 7 days, even after photothermal activation. Biocompatibility evaluations with NIH3T3 fibroblasts demonstrated elevated cell viability (>80 %) under all circumstances, with no harmful effects observed after NIR irradiation [46].

Despite the remarkable advancements in the development of conductive and multifunctional hydrogels for wound healing and electronic skin (E-skin) applications, there remain several challenges that limit their clinical translation and long-term performance. One significant challenge is to achieve a delicate balance between mechanical robustness, electrical conductivity, biocompatibility and antibacterial efficacy without any compromise on individual function. Many hydrogels, despite being mechanically strong or conductive, fall short of requirements in dynamic physiological environments due to brittleness, cytotoxicity or poor adaptability to skin movements. The incorporation of conductive materials such as PANI and AgNPs has shown promise, but issues such as the intrinsic hydrophobicity of PANI, its limited dispersion and potential toxicity, as well as the risk of nanoparticle-related inflammatory responses, remain pressing concerns. Additionally, chronic wound healing is often hindered by bacterial infections and biofilm formation, which not only delay tissue regeneration but also pose the risk of systemic infections. While positively charged materials and photothermal approaches (NIR-responsive systems) have demonstrated robust antibacterial properties, their safety and consistency in long-term in vivo use still require further investigation. Various ES-responsive hydrogels, such as those leveraging PSP and PANI composites, show enhanced healing via collagen synthesis and angiogenesis. However, the integration of ES devices into wearable platforms remains complex and costly. Moreover, although natural polymer-based hydrogels such as those derived from silk fibroin or chitosan possess superior biocompatibility, they generally lack the mechanical and electrical properties needed for full-thickness wound repair or smart skin electronics. Another ongoing limitation is the potential for bacterial resistance development even with novel antimicrobial mechanisms, highlighting the need to develop non-antibiotic-based strategies. It remains a formidable hurdle to ensure reproducibility, scalability and the regulatory approval of multifunctional hydrogels that exhibit consistent performance in diverse patient populations. Future research should focus on developing the next-generation hydrogel systems that integrate multi-modal functionalities in a hierarchically organized stimuli-responsive matrix. One promising direction is to design the intelligent hydrogels that can respond to multiple physiological cues such as pH, temperature and bacterial load, thus triggering controlled drug release, photothermal activity or ES precisely when needed. Another innovative approach could involve dynamic covalent chemistry and self-healing networks, allowing the hydrogel to autonomously recover after mechanical damage while maintaining long-term adherence and integrity under dynamic strain. Additionally, exploring biodegradable immunomodulatory nanocomposites that not only support healing but also modulate local immune responses may accelerate recovery in infected or chronic wounds. An exciting frontier is the use of biofabrication techniques such as 3D printing and microfluidics to engineer spatially patterned hydrogel scaffolds with region-specific properties, vascularization-promoting zones, antibacterial zones or sensor-embedded sections. The integration of wireless and battery-free electronics into hydrogel matrices is crucial for practical E-skin applications, enabling real-time data transmission for remote health monitoring. Moreover, the hybrid materials combining synthetic polymers with genetically engineered biomacromolecules (recombinant silk or elastin analogs) could offer unprecedented tunability in mechanical and biological performance. Finally, the rigorous in vivo long-term studies across diverse animal models and eventual clinical trials are essential to the validation of safety, efficacy and performance consistency, ultimately paving the way for regulatory approval and clinical integration of these highly versatile and transformative wound healing platforms.

5.1.3. PEDOT

Cell sheet technology offers significant advantages for wound healing by preserving compact cellular structures and the natural ECM, which promotes tissue regeneration and prevents diseases. While autologous and allograft cell sheets show therapeutic effectiveness, traditional cell sheets can suffer from central necrosis due to insufficient oxygen or nutrient delivery. A multifunctional electroactive wound dressing platform was created using the flat and porous membranes covered with conductive PEDOT:PSS. Additionally, its impacts on mechanical characteristics, cellular behavior and wound healing were thoroughly assessed both in vitro and in vivo. The porous membranes, produced by adjusting spin-coating rates, exhibited adjustable porosity and surface roughness, with the P5 membrane (5000 rpm) demonstrating the greatest porosity, roughness and stiffness. The use of PEDOT:PSS improved the mechanical strength and conductivity of the membranes, particularly in porous designs, with six coating cycles deemed ideal. Atomic force microscopy demonstrated that roughness

and Young's modulus increased with coating duration and porosity, thereby enhancing keratinocyte adherence and proliferation. ES at 200 mV significantly improved cellular activity, especially on porous membranes, due to their increased electroactive surface area. Immunofluorescence labeling demonstrated that porous membranes under ES prompted substantial actin rearrangement, enhanced cell junction integrity and the development of confluent keratinocyte sheets, which could be separated using electrical signals and exploiting resistance variations. In vivo, full-thickness skin wounds treated with P5 membranes containing cell sheets under ES exhibited expedited healing, characterized by swift epithelial coverage, diminished inflammation (lower TNF-α levels), augmented angiogenesis (CD31) and significantly enhanced wound closure within 7 days relative to control groups. Immunohistochemical tests validated the increased expression of re-epithelialization and differentiation markers (K14 and K10) with tight junction proteins (Occludin and Claudin-1) in the P5+ES group. Notably, ES, in conjunction with the mechanical signals from the porous material, enhanced cellular activities more efficiently than mechanical or biochemical stimuli independently (Fig. 4) [47].

The current challenges in the development and clinical application of multifunctional electroactive wound dressing platforms, such as those using PEDOT:PSS-coated porous membranes, revolve around optimizing the balance between mechanical integrity, biocompatibility and controlled ES to prevent issues such as central necrosis and poor integration with host tissue. Although the porous design of the P5 membrane and the application of ES significantly enhanced wound healing by promoting cell proliferation, junction integrity and keratinocyte sheet formation, it remains challenging to achieve consistent and scalable fabrication of such porous membranes with uniform electroactive properties. Moreover, there is a need for better control over the spatial and temporal dynamics of ES to tailor cellular responses across different wound types and patient-specific conditions. The immune response modulation, despite showing promise, must also be further studied to ensure long-term biocompatibility and avoid potential adverse reactions due to conductive polymers. Future perspectives in this field include the integration of real-time biosensing capabilities within the dressing materials to dynamically monitor wound microenvironment parameters such as pH, temperature, oxygen levels and inflammatory markers, thus enabling the precision modulation of electrical stimuli. Additionally, combining ES with biochemical cues such as controlled drug or growth factor release from the dressing could lead to the synergistic effects, further accelerating the process of healing. For chronic wounds, especially in diabetic or elderly patients, the adaptive systems that automatically regulate electrical input in response to healing progress could revolutionize treatment outcomes. Furthermore, expanding the platform to support co-culture of multiple cell types (keratinocytes, fibroblasts, endothelial cells) on multi-layered electroactive substrates may be better for mimicking natural skin architecture and improving graft integration. Novel future studies could also investigate biodegradable and self-healing conductive polymers as alternatives to PEDOT:PSS, thus reducing the need for removal and minimizing long-term residue in the body. Exploring 3D bioprinting to fabricate personalized, anatomically matched wound dressings embedded with electroactive elements could bridge the gap between bench research and real-world applications. Finally, comprehensive in vivo studies across various models, including diabetic and immunocompromised conditions, and early-phase clinical trials play an essential role in validating the translational potential of these advanced wound healing technologies. For further comparative analysis of CP-based systems, please refer to Section 9.

5.2. Different platforms in wound healing acceleration

5.2.1. Membranes

Individuals with diabetes frequently encounter several consequences, including the development of chronic sores. Diabetic wounds have a compromised microenvironment characterized by increased ROS and a disproportion between pro-inflammatory and anti-inflammatory cells and molecules, which severely hinders the wound healing and regeneration process. A multifunctional diabetic wound dressing was created, consisting of a doxycycline hydrochloride (DOXH)-loaded electrospun polyurethane (PFKU) membrane coupled with a 3D-printed conductive GelMA-Bio-IL hydrogel, to synergistically promote wound healing via electroactivity and immunomodulation. Characterization demonstrated that the membranes (M and MD) preserved a uniform fibrous shape with a high DOXH loading efficiency of 15 %, while the conductive hydrogel exhibited adequate conductivity of around 0.754 S/m and mechanical compliance. In vitro assays validated the ROS-responsive degradation of PFKU and the augmented release of DOXH in oxidative conditions (H_2O_2), hence endorsing early-stage immunomodulation. The MD-CH coating greatly enhanced endothelial cell motility and produced M2 macrophage polarization, exhibiting low cytotoxicity, as evidenced by cell tests. In vivo, full-thickness diabetic wounds treated with MD-CH dressings demonstrated accelerated closure, increased collagen deposition, enhanced neovascularization (CD31 expression), and superior skin regeneration with a higher number of cutaneous appendages relative to other groups. Histological and molecular investigations validated the superiority of MD-CH in facilitating organized collagen fiber synthesis, enhancing pro-angiogenic factors (VEGF, PDGF), and regulating pro-healing gene expression (Col-I, TGF-β1). Immunohistochemical staining demonstrated a considerable increase in M2 macrophage presence (CD206/CD68) and a decrease in inflammation, while ROS tests and cytokine profiling indicated that the combination of DOXH and the conductive hydrogel most efficiently scavenged ROS and inhibited IL-6, IL-1β, and TNF-α (Fig. 5) [48]. Despite the promising therapeutic outcomes demonstrated by the multifunctional MD-CH dressing, several limitations remain. The long-term biocompatibility and potential systemic effects of the DOXH compound and conductive hydrogel components require further investigation, especially in larger animal models or clinical settings. Additionally, the complexity and cost of fabricating the dual-component system may pose challenges for large-scale production and clinical translation. Future research should focus on optimizing the scalability and manufacturability of the dressing, evaluating long-term safety and efficacy, and exploring the integration of smart, stimuli-responsive systems for real-time monitoring and controlled drug release to further enhance personalized diabetic wound care.

5.2.2. (Nano)fibers

5.2.2.1. Development of platforms. Electrospun nanofibrous scaffolds consisting of HCl-doped poly(aniline-co-3-aminobenzoic acid) (3ABAPANI), a conductive copolymer of aniline and 3-aminobenzoic acid mixed with polylactic acid (PLA) were created and analyzed for possible use in tissue engineering and wound healing. The resultant 3ABAPANI-PLA nanofibers exhibited unique honeycomb-like network architectures characterized by high porosity and improved conductivity (up to 8.1 mS cm^{-1}), markedly surpassing that of pure PLA fibers. With the rise in the proportion of 3ABAPANI, fiber diameters diminished, mechanical strength enhanced (up to 30 MPa), and surface hydrophobicity augmented (contact angle rose from 72.8° to 93.5°), all of which affirm its appropriateness for ES in biological contexts. In vitro evaluations with COS-1 fibroblast cells demonstrated improved biocompatibility, characterized by planar shape, elongated pseudopodia, and markedly increased proliferation on 3ABAPANI-PLA surfaces in comparison to PLA or glass. Cell viability exceeded 99 %, and microscopy verified superior adhesion and proliferation. The nanofibers not only supported mammalian cell function but also shown significant antibacterial efficacy, decreasing viable *Staphylococcus aureus* to 31 % in contrast to over 95 % on control surfaces. These nanofibrous materials serve as a dual-function scaffold, facilitating cell development while preventing bacterial colonization, without the need of cytotoxic chemicals such as silver

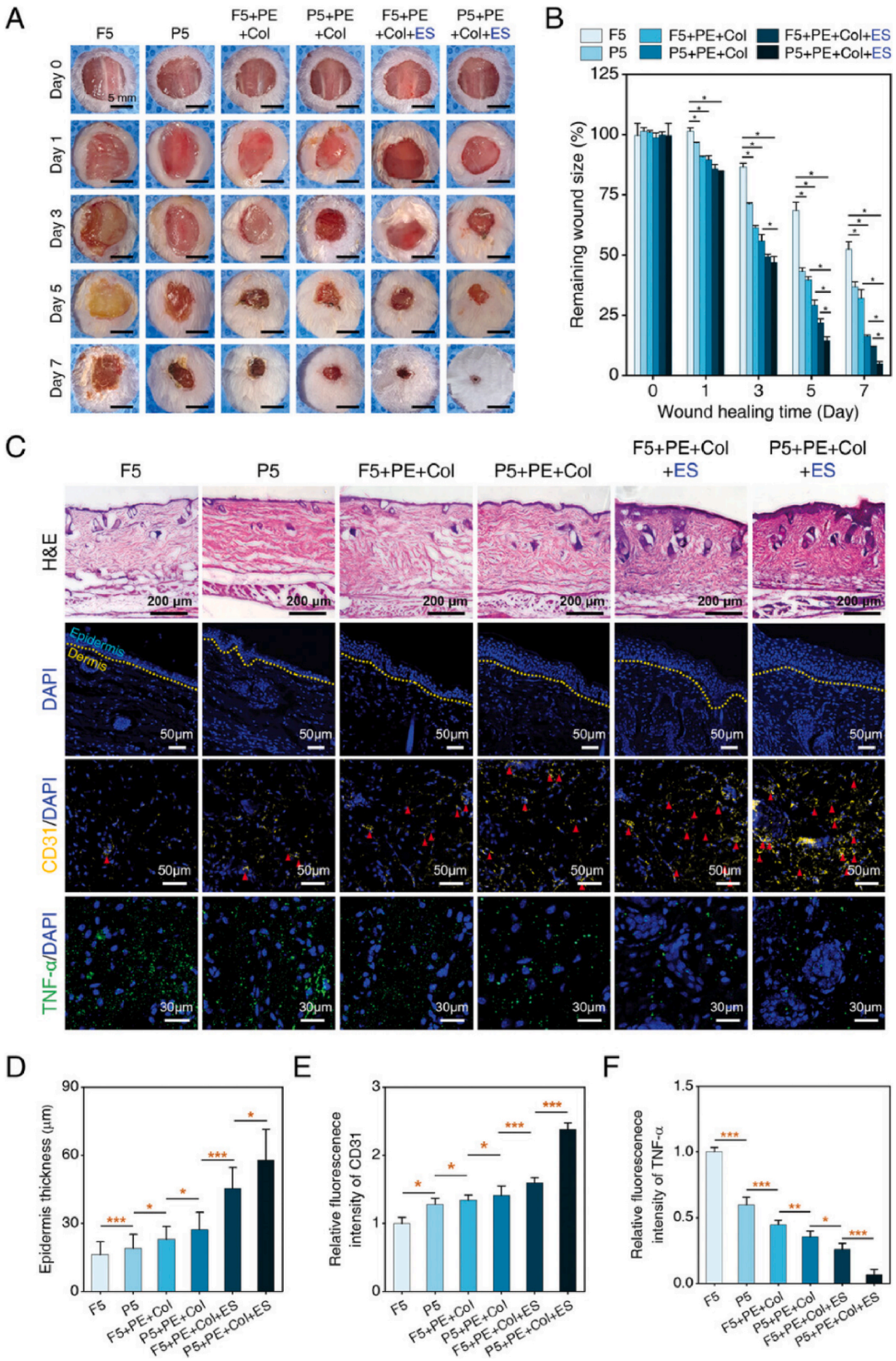

Fig. 4. In vivo studies on healing wounds. A) Pictures of injured tissues and B) proportions of wound healing among various groups at 0, 1, 3, 5, and 7 days. Photos of H&E, CD31, and TNF-α staining in the sections with DAPI under different conditions on day 7. All images are enlarged at 200 μm for H&E, 50 μm for CD31, and 30 μm for TNF-α. Arrows indicate newly formed blood vessels. D) Quantitative statistical evaluation of epidermal thickness, E) fluorescence level of CD31, and F) TNF-α, indicated by a red arrow, at 7 days after surgery. Reprinted with permission from Ref [47]. (For interpretation of the references to color in this figure legend, the reader is referred to the Web version of this article.)

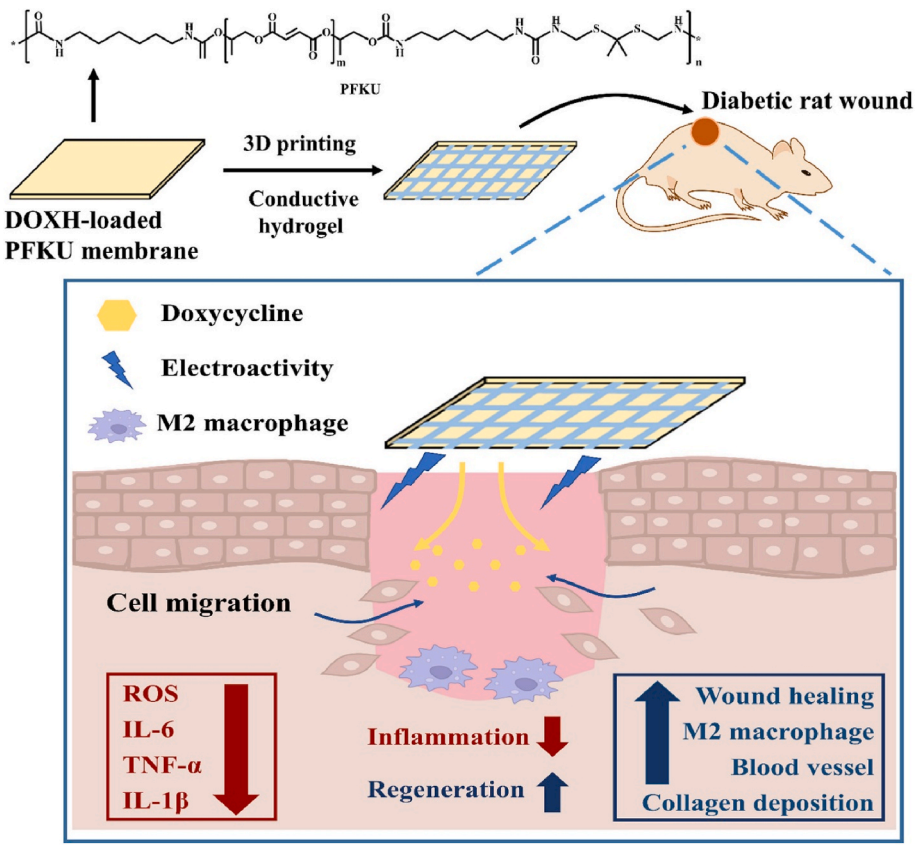

Fig. 5. The treatment of diabetic wounds with a composite dressing composed of conductive hydrogel strips and DOXH-loaded PFKU fiber membrane improves wound healing by facilitating collagen accumulation and the formation of new blood vessels. The composite wound dressing modulates the inflammatory environment by encouraging M2 polarization of macrophages and reducing the levels of reactive oxygen species and inflammatory indicators. Published again with consent from Elsevier [48].

or iodine, which are associated with delayed healing and other side effects. 3ABAPANI-PLA nanofibers are positioned as a potential, biocompatible option for improved wound care applications [49]. While 3ABAPANI-PLA nanofibrous scaffolds exhibit enhanced conductivity, mechanical properties, biocompatibility, and antibacterial activity, several limitations warrant further exploration. The long-term stability and degradation behavior of the conductive polymer under physiological conditions remain unclear, potentially impacting safety and performance in chronic wound environments. Additionally, in vivo studies are needed to confirm the scaffold's efficacy and biocompatibility beyond in vitro observations. Future research should focus on optimizing the balance between conductivity and biodegradability, assessing performance in relevant animal models, and exploring integration with bioactive agents or smart drug delivery systems to further enhance wound healing and tissue regeneration capabilities.

Electrospun silk fibroin (SF) meshes, covered with PPy, were created and assessed for their electrochemical, structural, mechanical, and biological characteristics to determine their appropriateness for tissue engineering applications. PPy coating did not substantially modify the average transverse fiber size (≈2300–2630 nm) or diminish the mesh porosity, hence maintaining the design conducive to cell adhesion. The homogenous PPy coating, obtained via in situ polymerization, constituted around 52 % by mass and exhibited electrical activity, as confirmed by cyclic voltammetry, demonstrating sustained redox behavior and the ability to facilitate ionic exchange without degradation under physiological settings. FTIR demonstrated effective coating and minor alterations in the silk's molecular structure, implying interactions between PPy and the silk backbone through hydrogen bonding or electrostatic interactions. Mechanical tests revealed improved tensile strength and elasticity in the coated meshes, with Young's modulus rising from 266.7 ± 17.3 MPa (SF) to 310.5 ± 37.6 MPa (PPy-SF). Cell culture experiments utilizing human fibroblasts (hFb) and adipose-derived human mesenchymal stem cells (ahMSCs) demonstrated that both cell types adhered and proliferated effectively on the meshes, with hFb displaying markedly superior proliferation on PPy-SF at 1 and 21 days, although no differences were noted at intermediate time points. In contrast, ahMSCs exhibited superior proliferation on uncoated SF over time, indicating that although the PPy coating improves electroactivity and mechanical qualities, it may somewhat diminish the bioactivity of silk for certain cell types, possibly due to polymer impurities. Nonetheless, PPy-SF composites maintained adequate biocompatibility and electrochemical responsiveness, rendering them appropriate for subsequent investigations into electrically-stimulated cell proliferation and differentiation, thereby positioning them as viable materials for bioelectronic interfaces in regenerative medicine [50].

Electrical fields naturally exist in biological systems and are crucial in controlling numerous physiological processes. External ES has been employed to modify cellular function and expedite the wound healing process. Scaffolds made from silk fibroin micro- and nanofibers were produced using electrospinning and then coated with PPy by means of chemical polymerization. This procedure, validated through SEM and IR spectroscopy, improved the scaffolds' mechanical strength and electroactivity, facilitating anion storage in redox reactions. Both coated and uncoated scaffolds facilitated the adhesion and proliferation of adult human mesenchymal stem cells and human fibroblasts, with uncoated meshes exhibiting greater bioactivity [51].

Microfibrous scaffolds of poly(L-lactic acid) (PLLA) covered with PEDOT were created and thoroughly described to assess their electrical, structural, thermal, mechanical, and biological characteristics for prospective biomedical applications. Surface resistivity had a strong

dependence on EDOT concentration, decreasing dramatically from 49.4 KΩ/sq to 0.4 KΩ/sq as the concentration rose to 0.25 mol/L, after which no notable enhancement was detected. Morphological examination demonstrated that the PEDOT coating maintained the original fibrous structure of PLLA, exhibiting only a little decrease in fiber diameter. XPS validated the effective deposition of PEDOT, indicating alterations in carbon-oxygen bonding and surface composition; however, sulfur, anticipated in PEDOT was not seen in the final composite, maybe due to surface constraints. The hydrophilicity of the fibers improved with PEDOT coating, reducing the water contact angle from 125.3° (PLLA) to 93°, signifying higher wettability. The PEDOT coating markedly boosted tensile strength and stiffness while reducing elongation, indicating increased rigidity. Differential scanning calorimetry (DSC) and thermogravimetric analysis (TGA) indicated that the thermal breakdown characteristics of the composite were akin to those of pure PLLA, although the glass transition temperature decreased markedly, implying a disturbance in the polymer's amorphous phase. Electrical stability assessments indicated that PEDOT-coated scaffolds preserved electrical conductivity in humid and culture environments, but conductivity progressively diminished over time. Cytocompatibility assessments utilizing human dermal fibroblasts revealed favorable cell adhesion, proliferation, and scaffold infiltration, with no harmful effects detected. ES administered to the conductive PLLA/PEDOT scaffold moderately improved cellular activity, suggesting the potential of these scaffolds as bioelectrically active platforms for tissue regeneration [52].

Bacterial infections and inflammation impede wound healing; however, adding electrically conductive nanoparticles to dressings can boost cell proliferation via natural electrical signals. A multifunctional hydrogel comprising CS, gelatin (Gel), β-cyclodextrin (β-CD), and dopamine–polypyrrole (DA-PPy) conductive nanofibers was formulated, characterized, and evaluated for wound healing applications, exhibiting improved adhesive, antimicrobial, photothermal, and immunomodulatory properties. FTIR and NMR measurements validated the effective grafting of β-CD onto gelatin and hydroxycinnamic acid (HCA) onto chitosan, therefore enhancing the hydrogel's structural integrity and catechol-rich chemistry, which improved Fe^{3+}-mediated crosslinking, rheological stability, and tissue adhesion. SEM and TEM images demonstrated a uniform distribution of DA-PPy nanofibers inside the hydrogel matrix, markedly enhancing its electrical conductivity and facilitating photothermal response under NIR light. The hydrogel exhibited remarkable water stability, robust tissue adhesion (sustained under flowing water), and modifiable swelling characteristics. Photothermal investigation demonstrated that the addition of DA-PPy facilitated a rapid temperature increase to about 60 °C under 808 nm NIR irradiation, enough for photothermal treatment. Antibacterial experiments exhibited significant suppression of *E. coli* and *S. aureus*, particularly under NIR stimulation, attributable to the synergistic effects of chitosan and the thermal influence of DA-PPy. Cytocompatibility assays with L929 fibroblasts demonstrated over 90 % vitality in all formulations, exhibiting no toxicity and improved cytoskeletal growth and intercellular connection over time. The addition of ES and DA-PPy significantly improved cell migration and diminished ROS, indicating the antioxidative potential of the hydrogel. Flow cytometry verified that the hydrogel facilitated the polarization of macrophages from the pro-inflammatory M1 phenotype to the anti-inflammatory M2 phenotype, signifying advantageous immunomodulation. In a rat model of infected full-thickness skin wounds, CG/DA-PPy hydrogel mixed with NIR irradiation expedited wound healing, augmented granulation tissue development, elevated collagen deposition, facilitated capillary growth, and reinstated skin appendages, including hair follicles. Immunofluorescence confirmed the hydrogel's function in inhibiting inflammatory cytokines (IFN-γ, IL-6, TNF-α) while enhancing IL-10 and CD206, facilitating a shift from inflammation to regeneration (Fig. 6) [53].

Despite the excellent electrochemical properties, mechanical

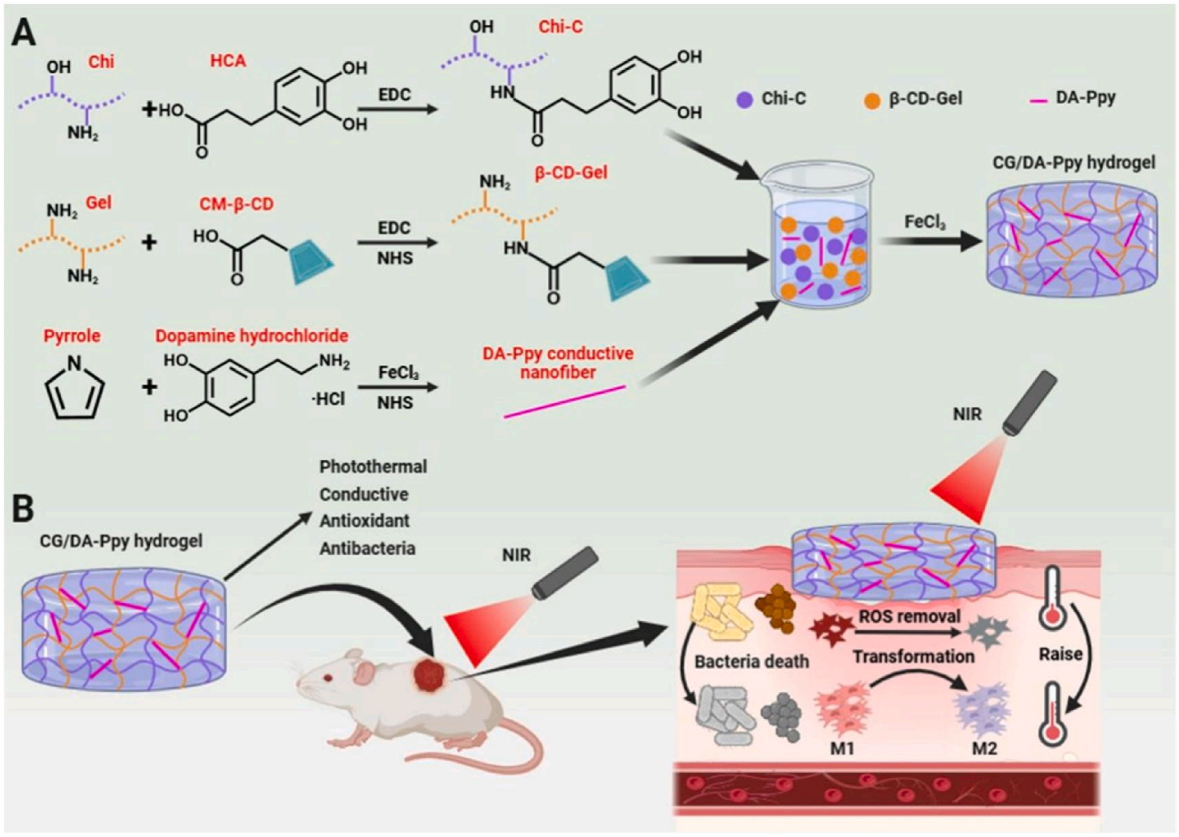

Fig. 6. (A) Diagram illustrating the synthesis of CG/DA-Ppy hydrogel. Application of CG/DA-Ppy hydrogel in the treatment of infected wounds. Reprinted with permission from Elsevier [53].

reinforcement, and notable biological functions such as improved cell adhesion, proliferation, antibacterial efficacy, and immunomodulation of the conductive biomaterials discussed, including PPy-coated silk fibroin (SF), PEDOT-coated poly(L-lactic acid) (PLLA), and DA-PPy-enhanced hydrogels, several significant limitations persist. Certain coatings, such as PPy, may diminish the inherent bioactivity of base materials for particular cell types, shown by the decreased proliferation of ahMSC on PPy-SF meshes, maybe attributable to changes in surface chemistry or residual polymer contaminants. Likewise, whereas PEDOT-coated scaffolds exhibit robust initial conductivity, their electrical efficacy deteriorates over time in humid or cultural environments, prompting questions over long-term dependability. The integration of multifunctional components and external stimuli, such as NIR light or electrical fields, while effective in improving regenerative results, complicates fabrication and application, potentially obstructing clinical scalability and cost-efficiency. Future views must concentrate on optimizing material synthesis to maintain or augment cellular compatibility, enhancing the longevity of conductive characteristics in physiological settings, and streamlining fabrication methods to facilitate scale manufacturing. Furthermore, extensive in vivo investigations across diverse wound models, encompassing infected and chronic wounds, are crucial to substantiate therapeutic efficacy and safety, facilitating the advancement of intelligent, patient-specific wound care systems that incorporate real-time monitoring, targeted drug delivery, and regulated bio ES.

Electrospun membranes made of PLA and poly(3-hydroxybutyrate-co-3-hydroxyvalerate) (PHBV) were created and refined for shape, surface characteristics, conductivity, and cellular interactions, especially following the application of the conductive polymer PEDOT:PSS. The fiber shape was significantly affected by polymer concentration, solvent, and mix ratios. Pure PHBV exhibited difficulty in complete dissolution in chloroform, leading to the formation of particles instead of fibers, but a 50:50 PLA/PHBV mix at 20 % (w/v) produced homogeneous, bead-free fibers appropriate for biomedical applications. SEM demonstrated consistent morphology with PEDOT:PSS coatings up to 30 % (v/v), which did not obstruct membrane pores. EDX analysis verified the successful surface deposition of PEDOT:PSS by detecting sulfur content, which rose with coating concentration. Contact angle measurements indicated enhanced wettability, decreasing from 133° (PLA) to 83° with a 30 % PEDOT:PSS coating. Concurrently, AFM and porosity analyses revealed increased surface roughness and minor reductions in porosity, both advantageous for cellular adhesion. FTIR validated the chemical composition of the mixtures and coatings. The PEDOT:PSS coating imparted conductivity to the otherwise non-conductive membranes, with a 30 % concentration producing roughly 1.45 μS/m, nearly sevenfold the conductivity of the 10 % coating. Biologically, PEDOT:PSS markedly improved human skin fibroblast (HSF) vitality (~97 %), adhesion, and proliferation over time, as validated by MTT, live/dead tests, and SEM imaging. Coated membranes enhanced cellular spreading and decreased the number of dead cells. The hydrophilicity and conductivity of the PEDOT:PSS surface promote cell-material interactions, promoting better adhesion, accelerated proliferation, and increased biointegration potential [54].

There is a significant demand for the development of multifunctional nanofibrous wound dressings that combine adequate mechanical strength, electroactivity, antioxidant properties, and natural antibacterial functions to meet the growing clinical needs for improved wound management. A collection of electroactive, antibacterial, and antioxidant nanofibrous membranes (NFMs) made from polycaprolactone (PCL) and quaternized chitosan–polyaniline (QCSP) was effectively produced for enhanced wound healing applications. SEM investigation revealed smooth, randomly oriented fibers with diameters that increased in proportion to QCSP concentration, while FTIR validated the integration of QCSP into the PCL matrix. The mechanical parameters of the NFMs, such as tensile strength and Young's modulus, fell within the optimal range for skin tissue, and their swelling behavior exhibited adequate fluid absorption capacities, which are crucial for managing wound exudate. Electrochemical analysis demonstrated that NFMs containing QCSP had considerable electroactivity, facilitating electrical signaling that promotes cell proliferation, particularly in fibroblasts. Furthermore, these NFMs exhibited significant antioxidant activity by neutralizing DPPH free radicals and shown strong antibacterial efficacy against *E. coli* and *S. aureus*, particularly at elevated QCSP concentrations. PCL/QCSP15 was shown to be the ideal formulation, achieving a balance between antibacterial effectiveness and superior cytocompatibility, facilitating L929 fibroblast growth while preventing the cytotoxicity noted at elevated QCSP concentrations. In vivo wound healing studies in a murine model further validated the enhanced efficacy of PCL/QCSP15 relative to commercial Tegaderm™ film and pure PCL (PCL/QCSP0) membranes. PCL/QCSP15 markedly expedited wound healing, augmented granulation tissue thickness, raised collagen deposition (as shown by elevated hydroxyproline levels), and facilitated the creation of hair follicles and blood vessels. Histological examination revealed decreased inflammation, enhanced epithelial regeneration organization, and elevated fibroblast activity in the PCL/QCSP15 group. Immunofluorescence labeling demonstrated reduced TNF-α expression and elevated VEGF levels, validating successful inflammation reduction and enhanced angiogenesis [55].

Recent advancements in tissue engineering have focused on developing multifunctional, smart, and responsive scaffolds that mimic the dynamic physiological conditions to enhance wound healing and tissue regeneration. Many sophisticated nanofibrous scaffolds incorporating CPs and nanomaterials have shown promising results. Similarly, highly conductive coatings of PPy and PANI were successfully applied to Antheraea mylitta silk fibroin fibers without affecting their β-sheet structure, resulting in thermally stable, conductive scaffolds that enhanced keratinocyte adhesion and survival. Moreover, the electrospun polyvinyl alcohol/graphene oxide (PVA/GO) nanofibrous scaffolds exhibited improved mechanical strength, hydrophilicity, protein adsorption, and cellular compatibility, with the scaffold containing 0.25 % GO achieving over 90 % wound closure in 9 days in animal models. An essential approach involved the development of aligned chitin/polyaniline (Chi/PANI) nanofiber scaffolds, which significantly enhanced electrical conductivity and promoted guided growth and faster proliferation of human dermal fibroblasts compared to random fiber arrangements. Together, these studies highlight the growing potential of CP-based scaffolds especially those that combine electroactivity, biocompatibility, antioxidant, and antibacterial features in revolutionizing wound dressings and regenerative medicine by boosting cell proliferation, guiding tissue development, and promoting swift healing responses in both healthy and diseased conditions [56–58].

Electrospun scaffolds made from biopolymers and CPs hold great potential in skin tissue engineering and wound healing by promoting cell growth, adhesion, and regeneration. Scaffolds made from PVP and coated with PPy/iodine showed improved survival and adhesion of HaCaT, while FE-SEM and FTIR confirmed the successful incorporation of the conductive coating and beneficial surface morphology. Electrospun nanofibers composed of chitosan, collagen, and polyethylene oxide, which included varying concentrations of polypyrrole, showed enhanced electrical conductivity and biocompatibility. Significantly, 10 % polypyrrole offered the best balance between cell growth and scaffold properties, making them suitable for electrically responsive tissues like nerves and heart muscle. Additionally, CPSA doped PANI was blended with poly(L-lactide-co-ε-caprolactone) (PLCL) to create uniform nanofibers demonstrating improved conductivity and strong cell adhesion, especially for fibroblasts and myoblasts. The CPSA-PANI/PLCL nanofibers promoted cell growth when exposed to ES, indicating their possible use as bioactive platforms in regenerative medicine to guide cell behavior via electrical signals [59–61].

Despite the promising advancements in electroactive and multifunctional nanofibrous scaffolds for wound healing and tissue regeneration, several limitations persist that require further exploration. First,

Table 2
The key performance and features of (nano)fibers for wound healing acceleration.

Feature Category	Key Attributes	Examples/Details	Refs for further information about such platforms for wound healing
Electrical Conductivity	Ranges from μS/cm to mS/cm; stable or time-dependent degradation	3ABAPANI-PLA: 8.1 mS/cm; PEDOT: 0.4 KΩ/sq; PEDOT:PSS: 1.45 μS/m	[49–55]
Cellular Response	Enhanced adhesion, proliferation, and migration (especially fibroblasts); phenotype modulation	COS-1, hFb, HSF, L929 showed increased growth; PES induced α-SMA expression and regenerative phenotype	
Antibacterial Activity	High antibacterial effect against *S. aureus*, *E. coli*; enhanced by ES or NIR stimulation	3ABAPANI-PLA: reduced *S. aureus* viability to 31 %	
Immunomodulation	Reduced pro-inflammatory cytokines; increased anti-inflammatory markers and M2 polarization	IL-6, TNF-α ↓; IL-10, CD206 ↑	
Mechanical Properties	Increased tensile strength and stiffness; reduced elongation in some systems	pPy-SF: Young's modulus ↑ to 310.5 MPa; 3ABAPANI-PLA: tensile strength ↑ to 30 MPa; PEDOT increased rigidity	
Surface Wettability	Ranges from hydrophobic to hydrophilic depending on coating	3ABAPANI-PLA: 72.8° → 93.5° (↑ hydrophobic); PEDOT:PSS: 133° → 83° (↑ hydrophilic)	
Porosity & Morphology	Retained porous, nanofibrous structure; bead-free, roughened surfaces promote cell infiltration	Honeycomb (3ABAPANI-PLA); random/smooth fibers (PCL/QCSP, PLA/PHBV)	
Thermal Stability	Generally preserved; some decrease in Tg or amorphous structure alteration	PEDOT-coated PLLA: decreased Tg; DSC/TGA showed comparable decomposition behavior to base polymers	
Chemical Composition	Successful polymer integration and surface chemistry modifications	Verified by FTIR, XPS, EDX, Raman; sulfur, β-CD, or DA-Ppy confirmed by characteristic peaks or elemental mapping	
In Vivo Performance	Enhanced wound closure, angiogenesis, collagen deposition, and immune regulation	DA-Ppy hydrogel, PCL/QCSP15	
Stimuli-Responsiveness	Responsive to electrical fields, temperature, pH, or NIR light	PANI–MWCNT/PNIPAm: thermoresponsive; PES: dose-dependent cell activation	

while many materials including conductive polymers like polypyrrole, polyaniline, and PEDOT:PSS demonstrate enhanced cellular adhesion, proliferation, and differentiation, the long-term stability and biocompatibility of these materials under physiological conditions remain uncertain, particularly in chronic or infected wounds. Degradation byproducts, potential polymer impurities, and variability in electrical conductivity over time may limit clinical translation. Furthermore, advanced composite scaffolds often require external stimuli such as NIR irradiation or electrical fields, which, although effective, introduce logistical and technological challenges for bedside or outpatient clinical use. Future research should prioritize the development of simplified, smart, and self-regulating scaffolds capable of responding to endogenous wound cues (pH, ROS levels, enzymatic activity) without reliance on complex equipment or continuous external stimulation. Biodegradable, electrically conductive polymers with tunable degradation profiles and minimal cytotoxicity should be further refined to ensure both functionality and safety. Long-term in vivo studies in relevant models, especially diabetic or immunocompromised conditions, are essential to validate therapeutic efficacy, tissue integration, and immune compatibility. Moreover, multifunctional scaffolds that integrate bio ES with on-demand, targeted drug delivery (via photothermal triggers like rGO) offer promising avenues for dual-action therapies against infection and inflammation. Ultimately, future perspectives should focus on translating these advanced materials into scalable, cost-effective, and clinically accessible solutions that combine real-time responsiveness with robust healing capacity for both acute and chronic wounds.

5.2.2.2. Critical analysis of (nano)fibers. Conductive nanofibrous scaffolds designed for wound healing exhibit multifunctional performance by integrating enhanced electrical conductivity, biocompatibility, mechanical reinforcement, and bioactivity. Materials such as 3ABAPANI-PLA, polypyrrole (pPy)-coated silk fibroin, PEDOT-coated PLLA, and dopamine–polypyrrole (DA-Ppy) hydrogels significantly improve cell proliferation, adhesion, and migration, especially under ES. These scaffolds also demonstrate potent antibacterial effects against *S. aureus* and *E. coli*, with some systems (DA-Ppy and rGO-infused hydrogels) utilizing photothermal effects to enhance antimicrobial efficacy without cytotoxic additives. In vivo studies confirm accelerated wound closure, granulation tissue formation, collagen deposition, and angiogenesis, with immunomodulatory effects that shift macrophages toward pro-regenerative M2 phenotypes. Physicochemically, these materials exhibit tunable conductivity (from μS/cm to mS/cm), high porosity, and nanoscale fibrous morphology that supports cell infiltration. Surface wettability can be modulated by polymer type or coating, with contact angles ranging from hydrophilic (~83°) to hydrophobic (~133°). Mechanical properties are generally improved upon conductive polymer incorporation, with increased tensile strength and stiffness while maintaining flexibility. Chemical and structural characterization confirms successful integration of conductive elements (via FTIR, XPS, Raman), and thermal analyses indicate preserved or slightly altered stability. Overall, these nanofibrous platforms are promising for next-generation wound dressings that combine bioelectrical responsiveness, antibacterial action, and tissue-regenerative potential. Table 2 surther summarizes the key features and performance of these structures.

5.2.3. Conductive 3D scaffolds

The growing occurrence of chronic wound infections caused by antibiotic-resistant bacteria is a significant issue in healthcare. These infections are often worsened by biofilm formation, as bacterial groups create a protective environment that reduces the effectiveness of antibiotic treatments. MRSA is a commonly encountered bacterium associated with considerable morbidity in the management of clinical wounds. There is an immediate need for alternative therapies that do not involve antibiotics. H_2O_2 is recognized for its antibacterial and antibiofilm properties; however, its continuous application presents a technological hurdle. A conductive e-scaffold made of carbon fabric has been developed to produce H_2O_2 through the electrochemical reduction of dissolved oxygen when subjected to a polarization of $-0.6\ V_{Ag/AgCl}$. This e-scaffold functions as a novel antibiofilm covering for managing wounds. The in vitro evaluation showed that the e-scaffold effectively eliminates MRSA biofilms, confirmed through bacterial quantification and ATP assays. Additionally, imaging research suggests that the disruption of bacterial cell membranes could contribute to its mechanism of action [63].

A study illustrates that a polarized carbon-based conductive e-scaffold successfully eradicates Acinetobacter baumannii biofilms both in vitro and on infected pig explants, principally via the electrochemical production of hydrogen peroxide (H_2O_2). The e-scaffold, selected for its biocompatibility and conductivity, was tuned to generate maximal H_2O_2 concentrations when polarized at $-600\ mV_{Ag/AgCl}$. Microelectrode experiments indicated that H_2O_2 is produced at quantities (~25 μM) enough to eliminate biofilms while preserving adjacent tissue, with the concentration rapidly decreasing beyond 300 μm from the scaffold

surface. In vitro investigations demonstrated a significant drop in biofilm surface coverage (from 25.0 % to 7.0 %) and viable bacterial cells (about a 4-log reduction in CFU/cm^2), whereas control samples with non-polarized scaffolds exhibited biofilm proliferation. Upon the addition of catalase, an enzyme that decomposes H_2O_2 to mitigate its oxidative effects, a mere ~1-log decrease was noted, therefore affirming H_2O_2 as the principal biocidal agent. Furthermore, trials including the external administration of H_2O_2, using both bolus and continuous low-dose methods, replicated certain effects of the scaffold, indicating a more effective localized dispersion of H_2O_2 via the e-scaffold, maybe facilitated by electrokinetic forces. In swine explants, the e-scaffold attained approximately a 3-log CFU decrease while maintaining tissue viability, as shown by viability staining and histological examination. These findings confirm the e-scaffold as a viable, tissue-compatible approach for biofilm control via continuous, localized H_2O_2 production. The research indicates that performance may be improved by oxygen enrichment or electrolyte replenishment to facilitate sustained operation in clinical environments [64].

Managing chronic skin ulcers caused by diabetes is difficult. The transplantation of mesenchymal stem cells (MSCs) presents a possible remedy, yet it is challenging to stabilize and deliver MSCs in wounds with high proteolytic activity. To tackle this issue, a study details the creation and assessment of a conductive, multifunctional bio-nanocomposite scaffold, DAT-pMXene@bFGF, aimed at enhancing diabetic wound healing through synergistic enhancement of electrical conductivity, neuro-immune regulation, antioxidant protection, and growth factor delivery. The scaffold was constructed by incorporating polydopamine-modified MXene (pMXene) infused with basic fibroblast growth factor (bFGF) into a decellularized adipose tissue (DAT) matrix. In vitro studies exhibited superior biocompatibility, cell adhesion, proliferation, angiogenesis, and robust ROS scavenging capacity, successfully safeguarding HUVECs and NIH-3T3 cells from oxidative stress. The scaffold boosted neuronal cell activity, increased Schwann cell marker expression, and promoted M2 macrophage polarization through neuro-immune communication, principally by modulating the NF-κB pathway. In vivo investigations using a streptozotocin-induced diabetic rat model demonstrated that DAT-pMXene@bFGF markedly expedited wound closure, re-epithelialization, neovascularization (CD31, α-SMA), and collagen deposition, while concurrently diminishing pro-inflammatory cytokines (TNF-α, IL-6) and in vivo ROS. Furthermore, it increased the production of calcitonin gene-related peptide, therefore associating nerve regeneration with immunological regulation. Limitations encompass the utilization of H_2O_2 instead of hyperglycemic circumstances to replicate oxidative stress in vitro, as well as the necessity for more mechanistic investigations regarding electric field-mediated healing. The findings underscore the therapeutic potential of this bioelectrically active, immuno-modulatory scaffold for chronic diabetic wound treatment, while recognizing that scaling production, ensuring clinical-grade consistency, and elucidating EF-related mechanisms are significant challenges for clinical translation [65]. Current challenges in chronic wound management include the persistent threat of antibiotic-resistant infections, particularly those complicated by biofilm formation from pathogens like MRSA and Acinetobacter baumannii, which significantly impair the efficacy of conventional antibiotic treatments. Although electrochemically active scaffolds generating H_2O_2 have emerged as promising alternatives by disrupting biofilms and preserving tissue viability, limitations persist in sustaining localized H_2O_2 production, managing oxygen availability, and ensuring biocompatibility over prolonged periods. Additionally, in diabetic wound care, difficulties in delivering and stabilizing MSCs within protease-rich wound environments hinder regenerative outcomes, despite the promise shown by multifunctional bio-nanocomposites such as DAT-pMXene@bFGF, which offer synergistic benefits through conductivity, immunomodulation, and growth factor release. However, future advancements are anticipated in enhancing electrochemical scaffold efficiency through oxygen-enrichment strategies, improving electrolyte replenishment for prolonged activity, and fine-tuning bioelectric cues to further regulate immune and neural pathways. Moreover, scalable fabrication of clinically consistent, bioactive scaffolds, along with deeper mechanistic insight into electric field-mediated healing, particularly under true hyperglycemic and inflammatory conditions, remains a critical focus to bridge the gap from experimental validation to widespread clinical application.

5.2.4. Hydrogels

5.2.4.1. Development and application. Burn injuries have emerged as a significant public health concern globally. It is essential to investigate novel techniques to mitigate thermal damage and enhance healing efficacy in the treatment of burn injuries. A new thermoresponsive hydrogel (PMO-CNT) was created by integrating hydroxyl-functionalized carbon nanotubes (CNT-OH) into a copolymer matrix of OEGMA and MEO2MA using in situ free radical polymerization. The incorporation of CNT-OH, evenly distributed using SDS and ultrasonic treatment, established a conductive network that markedly improved the hydrogel's thermal conductivity, mechanical strength, and swelling capacity. Cryo-SEM demonstrated a well-defined, porous morphology, with CNT-OH uniformly dispersed in the gel, enhancing the hydrogel's thermal conductivity and mechanical performance under stress. In comparison to P and PMO hydrogels, the PMO-CNT hydrogel exhibited enhanced compressive strength (reaching 581.9 kPa), significant stretchability (with an elongation at break of almost 300 %), and remarkable fatigue resistance. Thermal evaluations indicated an elevated heating and cooling rate, enhanced thermal conductivity (0.73 W/m·K), and an augmented heat storage capacity (ΔHm ~601.8 J/g), ascribed to the thermoresponsive polymer matrix and the carbon nanotube network. Swelling tests demonstrated notable temperature-responsive characteristics, essential for regulating wound wetness and facilitating heat dissipation. The PMO-CNT hydrogel demonstrated robust adhesion characteristics and excellent cytocompatibility, enhancing cell survival to over 80 %. In vivo investigations utilizing a rat scald model revealed that PMO-CNT significantly lowered wound surface temperature without inducing hypothermia, in contrast to ice therapy, and expedited wound healing by promoting granulation tissue development, re-epithelialization, and diminishing inflammation. Histological study verified enhanced tissue regeneration and decreased heat injury [66].

Burn injuries frequently result in considerable dermal damage, aggravated by bacterial infections and severe inflammation. Conductive hydrogels employed as electroactive wound dressings have significant potential in facilitating burn wound healing; yet, they encounter obstacles in achieving a balance between high electrical conductivity and mechanical strength, limiting dehydration, and enhancing transparency. A new conductive eutectogel (HPDChCl-1.0 gel) was synthesized utilizing a polymeric deep eutectic solvent (PDES) including acrylamide (AM), glycerol (Gly), and choline chloride (ChCl), in conjunction with thiolated hyaluronic acid (HA-SH). Among the formulations examined, PDESChCl exhibited less hydrogen bonding compared to its betaine-based equivalent (PDESBet), leading to a more relaxed network structure characterized by enhanced conductivity, reduced viscosity, and advantageous electrostatic interactions. The incorporation of these features into the HPDChCl-1.0 gel conferred exceptional mechanical flexibility, electrical conductivity (up to 0.25 S m^{-1}), self-healing capability, and skin-like ductility to the gel. The gel's architecture, distinguished by substantial holes and significant swelling capacity, proved ideal for nutrition transfer in burn wounds, while its adhesive strength (50 ± 2 kPa) facilitated robust yet removable adhesion to diverse biological and synthetic substrates. The gel demonstrated 90 % antibacterial efficacy against *E. coli* and *S. aureus*, attributed to the antimicrobial properties of ChCl. The gel, when used with exogenous ES (3 V, 1 Hz, 1 h/day), facilitated in vitro fibroblast proliferation and

migration, expedited wound closure, increased collagen deposition (71.47 %), and promoted vascular regeneration by enhancing VEGF production. Immunofluorescence demonstrated a transition in the wound microenvironment characterized by reduced inflammation (low TNF-α) and an enhanced anti-inflammatory response (high IL-10). In vivo experiments on a deep second-degree burn model shown that the HPDChCl-1.0 gel with ES achieved 98 % wound healing after 14 days, surpassing independent therapies (Fig. 7) [67].

The conventional hydrogel dressings promote wound healing by maintaining moisture and preventing infection; however, they do not actively influence cellular activity. This constraint is alleviated by using ES, known for its ability to affect skin cell function and speed up healing. A study introduces the design and multifunctional application of an innovative conductive hydrogel, DES-SH/PDA/TTO/PNE, which integrates a deep eutectic solvent (DES, composed of glucose and choline chloride) with thiolated polymers (SH), PDA, tea tree oil (TTO), and Panax notoginseng extract (PNE). The hydrogel was synthesized using hydrogen bonding and electrostatic interactions, resulting in a resilient 3D porous architecture with viscoelastic and self-healing properties. Characterization using SEM, XPS, FT-IR, and rheological study validated its structural integrity, modest swelling ratio (102 %), elevated conductivity attributed to DES, and mechanical robustness under strain with rapid recovery. TTO and PNE markedly improved the hydrogel's antioxidant properties (as shown by DPPH and ABTS tests) and antibacterial efficacy against *E. coli* and *S. aureus*, whilst PDA facilitated robust tissue adhesion across diverse substrates. The hydrogel exhibited flexibility and adhesiveness throughout an extensive temperature range (−20–40 °C), rendering it suitable for clinical applications. Biocompatibility experiments demonstrated hemolysis rates under 5 % and cell survival above 85 %, while scratch testing validated its capacity to enhance endothelial cell migration. In a full-thickness wound mouse model, the hydrogel, particularly when utilized with ES, markedly expedited wound healing (99.7 % closure in 12 days), augmented vascularization and hair follicle regeneration, and improved collagen deposition (up to 58.2 %). The hydrogel exhibited real-time reactivity to joint movement and vocalization, operating successfully as a flexible bioelectronic sensor. This dual-functional material facilitates fast wound healing via antibacterial, antioxidant, and pro-angiogenic activities under ES, while also demonstrating significant potential in wearable health monitoring systems [68]. Current challenges in the treatment of burn injuries using hydrogel-based materials revolve around the difficulty of simultaneously optimizing multiple critical parameters such as mechanical strength, electrical conductivity, thermal regulation, biocompatibility, and multifunctionality. Although hydrogels like PMO-CNT, HPDChCl-1.0, and DES-SH/PDA/TTO/PNE have demonstrated promising results by integrating conductive nanomaterials, eutectic solvents, and bioactive compounds to promote wound healing, each formulation still encounters trade-offs. For instance, enhancing electrical conductivity often compromises flexibility or swelling capacity, and achieving stable adhesion without compromising removability remains difficult. Moreover, while certain hydrogels show excellent thermal management or antibacterial activity, few can provide long-term performance stability under physiological conditions or adapt dynamically to wound environments. A further concern is achieving precise control over ES parameters to prevent tissue damage while maximizing healing efficacy. Future perspectives should focus on developing smart, adaptive hydrogel systems that can dynamically modulate their properties (conductivity, adhesiveness, drug release) in response to real-time wound signals such as temperature, pH, or inflammation markers. Incorporating advanced nanomaterials with programmable responsiveness, multi-layered or gradient structures to localize functionalities, and biodegradable, self-deactivating ES circuits can overcome current limitations. Additionally, integrating biosensing capabilities with wireless feedback systems can elevate these hydrogels from passive dressings to active therapeutic platforms. Improvements in design should prioritize synergistic combinations of bioactive molecules, advanced manufacturing methods (4D printing), and sustainable biomaterial sources to create personalized, scalable, and multifunctional

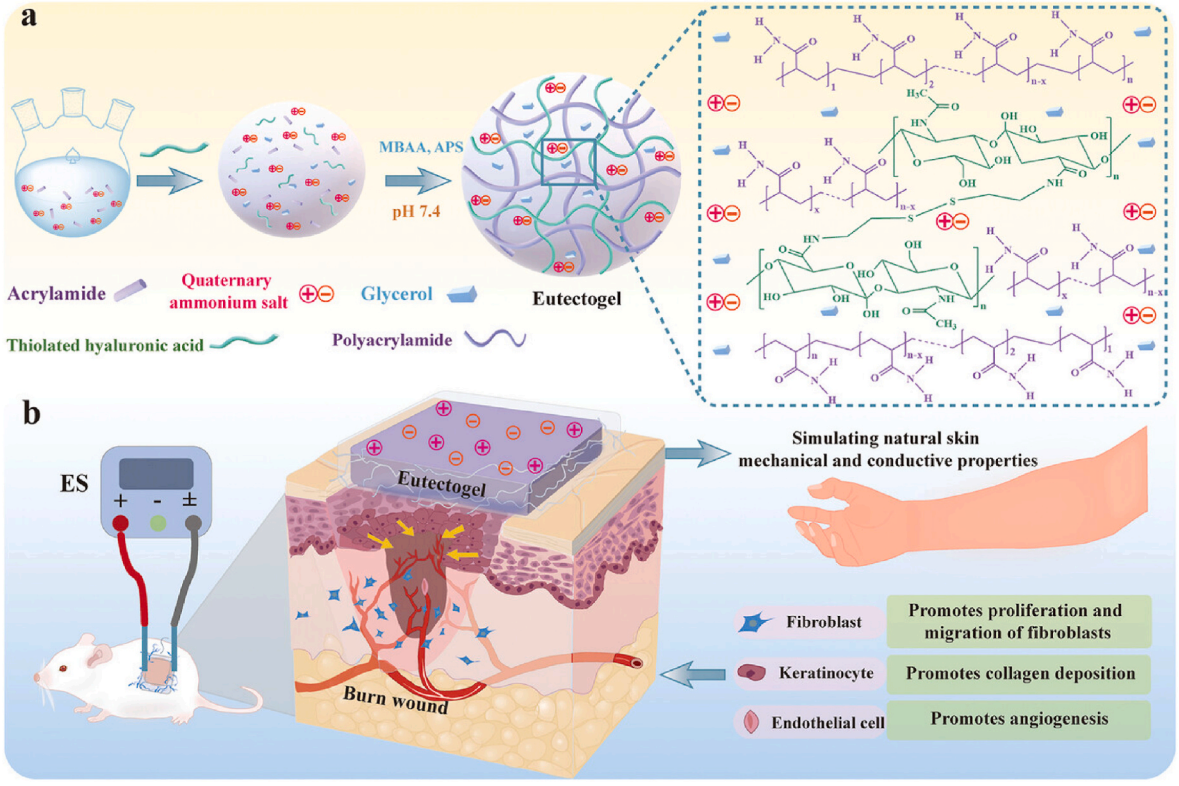

Fig. 7. Schematic illustration of the design approach and application of conductive DN eutectogel. a) Method for preparing eutectogel. b) Eutectogel displaying dermal properties, in combination with ES, improves the healing process of burn injuries. Reproduced with approval from Wiley [67].

burn treatment solutions that support not only wound closure but also functional tissue regeneration and systemic integration with wearable health-monitoring systems.

Oral mucosal diseases present treatment difficulties because of their common prevalence and the complexities involved in managing symptoms. A study introduces the creation and assessment of a new bioelectric hydrogel, PAA-SA@rGO, intended for the expedited healing of oral mucosal lesions under difficult, damp conditions. The hydrogel, synthesized through free radical polymerization of poly(acrylic acid) (PAA) and sodium alginate (SA) augmented with reduced graphene oxide (rGO), establishes a "completed circuit" that restores the impaired bioelectric field at the wound site, converting the disrupted "short circuit" into a favorable healing microenvironment. rGO markedly improves the hydrogel's mechanical strength, electrical conductivity, antioxidant capacity, and antibacterial characteristics, essential for preserving integrity in dynamic oral environments. The hydrogel exhibits remarkable flexibility (threefold stretchability), robust wet adhesion, little swelling, and biocompatibility, displaying negligible cytotoxicity, low hemolysis rates (<5 %), and safe in vivo disintegration. In vitro, it efficiently scavenges ROS, safeguards fibroblasts from oxidative injury, diminishes inflammatory responses (TNF-α, IL-6), and enhances angiogenesis (CD31) and collagen production (Col-1). Antibacterial experiments demonstrated its substantial activity against *S. aureus*, *E. coli*, and *S. mutans*, exhibiting much bigger inhibition zones compared to controls. In infected rat buccal models, PAA-SA@rGO enhanced wound closure to 92.21 % by day 7, surpassing both commercial bFGF gel and PAA-SA alone, and attaining total mucosal regeneration by day 10. Histological examination validated decreased inflammation and improved tissue remodeling. Molecular docking and qRT-PCR demonstrated significant interactions and upregulation of sex-determining region Y-box 2 (SOX2), paired-like homeodomain 1 (PITX1) and paired-like homeodomain 2 (PITX2), transcription factors linked to wound healing. PAA-SA@rGO triggered the Nrf2/HO-1 antioxidant pathways and reinstated electrical conductivity at the wound site, emulating the voltages and resistances of normal tissue (Fig. 8) [69].

Recent advancements in electroactive hydrogels demonstrate potential for improving wound healing, especially for challenging cases such as diabetic wounds and joint injuries. Conventional hydrogels encounter issues from toxic conductive additives and inadequate dispersibility, emphasizing the necessity for biocompatible substitutes. Novel formulations, including a hydrogel composed of oxidized sodium alginate, carboxymethyl chitosan, and silver nanoparticles, demonstrate remarkable self-healing and antibacterial capabilities. Moreover, multifunctional hydrogels that integrate polysaccharides with other substances provide quick healing and bacterial detection, whereas gelatin (Geln)/CS-based ones enhance angiogenesis and alleviate inflammation in diabetic wounds [70–72]. Injectable hydrogels capable of creating a hypoxic microenvironment hold significant potential for enhancing innovative therapeutics in tissue regeneration. Nonetheless, investigations in this domain predominantly remain theoretical and are still in the nascent phases of advancement. A research illustrates the enhanced efficacy of an innovative sequentially interpenetrating polymer network (IPN) hydrogel, formulated from PBAE-TA/HA-SH and Geln-Van/Lac, for wound healing, especially in diabetes mice. The hydrogel has robust rheological characteristics, improved electrical conductivity, and a rapid gelation rate, facilitating superior mechanical stability in dynamic tissues. Vanillin is conjugated to Geln to enhance biocompatibility and induce hypoxia through a Lac-mediated enzymatic reaction, which efficiently reduces oxygen levels and replicates a hypoxic wound microenvironment within 60–90 s, 20–30 times more rapidly than conventional systems and sustains it for over 13 h. Mathematical modeling demonstrated that oxygen consumption adheres to Michaelis–Menten kinetics, enabling the programmability of hypoxic duration by the modulation of Lac concentration. In vitro, adipose-derived stem cells (ADSCs) encased in the hydrogel exhibited over 85 % vitality and a significant increase in the expression of genes linked to angiogenesis (HIF-1α, VEGF, ANG-1) and anti-inflammatory responses (TGF-β1/3). Subcutaneous injections in rats exhibited the hydrogel's biocompatibility, showing minimal inflammation and signs of angiogenesis by day two. In a humanized diabetic rat skin wound model, the hydrogel, particularly when paired with ADSCs, achieved over 95 % wound healing within 21 days, enhanced collagen remodeling, and the regeneration of blood vessels and hair follicles. RT-PCR and immunofluorescence validated a marked upregulation of gene expression and protein levels of angiogenic and ECM markers, indicating that conductivity-enhanced cell–cell interactions and hypoxia-induced signaling effectively facilitate vascular regeneration, anti-inflammatory responses, and scar-free wound healing [73].

ES is regarded as a potential method for the treatment of chronic wounds utilizing conductive dressings. A significant difficulty exists due to the absence of conductive dressings that are therapeutically appropriate for clinical use. This paper offers a thorough assessment of an innovative conductive MT-MAA hydrogel, created by integrating microtubules (MTs) into a methacrylic acid (MAA)-based hydrogel, to improve wound healing. Structural characterisation using TEM and SEM validated the tubular shape of MTs and the porous, nanofibrous architecture of the MT-MAA hydrogel. Fluorescence microscopy confirmed the effective labeling of microtubules, which maintained steady conductivity (~0.14 S/m) for 14 days in vitro. The conductivity of the hydrogel augmented with elevated MT concentrations (0.5–2 wt%) and aligned with human skin values at 1 % MT. Nonetheless, its conductivity diminished under acidic and divalent cation conditions, which are characteristic of wound sites. Mechanical investigation indicated enhanced Young's and compressive moduli with elevated MAA content, identifying 2 % MAA as ideal. The MT-MAA hydrogel shown little cytotoxicity, facilitated NIH3T3 cell adhesion and proliferation, and showed biodegradability after 10 days in vivo. The hydrogel, when used in conjunction with ES, markedly improved NIH3T3 cell migration, proliferation, alignment, and paracrine signaling, resulting in elevated production of growth factors (VEGF, TGF-β, EGF) and facilitating endothelial tube construction. In diabetic full-thickness wound models, the MT-MAA hydrogel under ES expedited wound closure, re-epithelialization, and angiogenesis by enhancing microvessel density and epidermal tongue length, while simultaneously diminishing T/B cell infiltration and promoting M2 macrophage polarization. RT-PCR and western blot analyses indicated increased expression of growth factor genes and proteins. Significantly, ES with MT-MAA hydrogel enhanced nerve regeneration and shown antibacterial effectiveness against *E. coli* and *S. aureus* in both in vitro and in vivo settings. The hydrogel further facilitated MSC function, hence enhancing tissue regeneration [74]. Hydrogel patches, modeled after biological systems, are designed with features including temperature-sensitive adhesion, regulated drug release, antibacterial traits, and physiological tracking, employing materials such as gelatin with tannin grafting, Ag-tannin nanoparticles, and PNIPAm. Conductive hydrogels like SFMA@IL have been created for spinal cord repair, promoting neuroelectric signal conduction and reducing inflammation. In the care of diabetic wounds, hydrogels such as PPCA, which incorporate Ag-coated polypyrrole nanotubes and Co^{2+} ions, offer skin-like conductivity, strong tissue adhesion, and antibacterial features. Furthermore, self-healing hydrogels that can be injected and are made of QCSP and PEGS-FA demonstrate electroactivity, antioxidant features, and enhanced healing by influencing gene expression [75–78].

Conventional approaches to managing diabetic wounds primarily emphasize reducing inflammation or enhancing angiogenesis, while less focus is placed on adjusting the neuro-immune microenvironment. A multifunctional, injectable, self-healing, and conductive hydrogel, PQCD-A@Cur was created, integrating AMNP@Cur nanoparticles to enhance wound healing and nerve regeneration, specifically for diabetic wounds and peripheral nerve injuries. The AMNP@Cur nanoparticles were produced using oxidative polymerization and successfully loaded

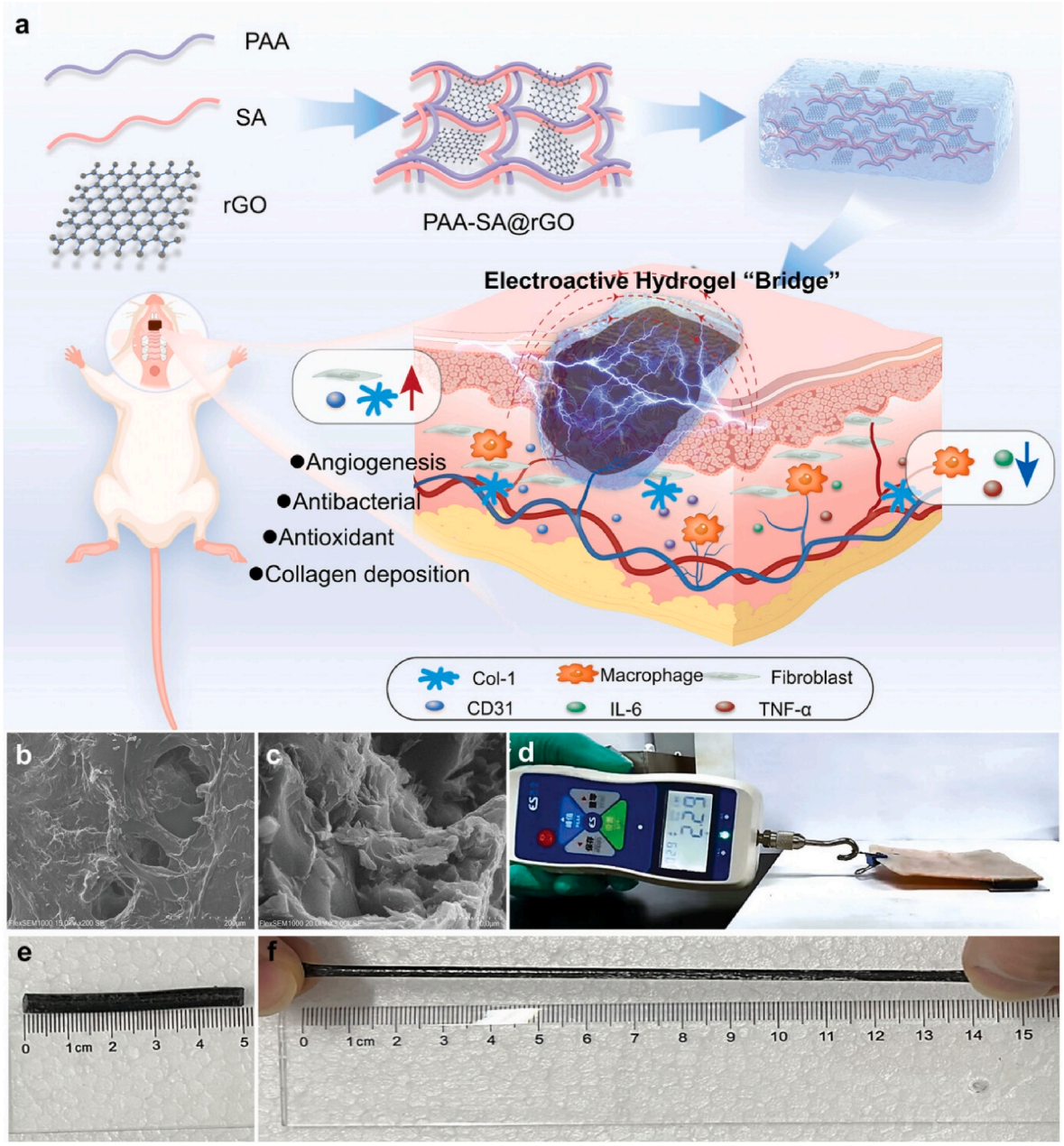

Fig. 8. Approach for reconstructing the electric field and properties of the PAA-SA@rGO hydrogel. The PAA-SA@rGO hydrogel bridge creates a bioelectric "closed circuit" therapy for oral wounds, addressing the "short circuit" issue at the injury location. This revival of the electric field microenvironment accelerates the recovery of oral mucosal wounds. SEM image of PAA-SA and PAA-SA@rGO c) Hydrogel. d) Adhesion of the PAA-SA@rGO hydrogel in dry conditions. Evaluation of the flexibility of the PAA-SA@rGO hydrogel. Reproduced with authorization from Wiley [69].

with curcumin via π-π stacking, demonstrating robust antioxidant, photothermal (PTT), and NIR-triggered drug release properties. The composite exhibited improved mechanical strength, rheological stability, conductivity, injectability, and superior biocompatibility when included into polyaniline-grafted quaternized chitosan (PQCS)/oxidized dextran (OD) hydrogel. Upon NIR irradiation, the hydrogel exhibited enhanced photothermal efficiency (~26.2 %), facilitated the regulated release of curcumin, and demonstrated significant antibacterial action through the synergistic effects of quaternary ammonium groups and moderate photothermal therapy. In vitro experiments demonstrated significant ROS scavenging, enhancement of fibroblast migration, angiogenesis, and M2 macrophage polarization. The hydrogel enhanced recovery in a rat peripheral nerve crush model by facilitating axonal regeneration, remyelination, reducing inflammation, and reinstating muscle innervation and sensory function. Moreover, in a diabetic wound model with infection, the hydrogel markedly accelerated wound healing, improved blood perfusion and collagen deposition, and promoted cutaneous nerve regeneration. Transcriptomic study demonstrated the elevation of myelination-related genes (SOX10, MBP, MPZ, PLP1) and the downregulation of inflammatory genes (IL12B, CXCL17), therefore affirming a neuro-immune modulation mechanism (Fig. 9) [79].

Despite rapid progress in hydrogel engineering for complex wound environments such as oral mucosal injuries, diabetic ulcers, and nerve-damaged tissues, several material-specific challenges persist. A major hurdle is achieving stable electrical conductivity in hostile physiological environments, such as the fluctuating pH and enzyme-rich settings of chronic wounds or the constantly wet, mechanically stressed oral cavity. Materials like rGO or microtubule composites show initial conductivity

but degrade under acidic conditions or lose uniform dispersion over time, compromising bioelectric modulation. Additionally, while multifunctional hydrogels such as PQCD-A@Cur exhibit remarkable neuroregenerative and antibacterial properties, controlled release triggered by external stimuli (NIR or temperature) still faces challenges in terms of spatial precision and scalability in deep tissue applications. Swelling control is another bottleneck many hydrogels exhibit uncontrolled expansion in wet conditions, which can hinder adhesion and drug diffusion, particularly in the oral or mucosal environment. Moreover, synchronizing angiogenesis, anti-inflammatory responses, and nerve regeneration within one system is rare, and balancing these biological signals remains difficult. Future improvements should focus on hierarchically structured hydrogels with spatially programmed domains, for instance, a layered hydrogel with an inner conductive core, a drug-loaded responsive shell, and an outer adhesive interface, each optimized for specific functions like mechanical support, controlled delivery, and biointegration. Introducing enzyme-inert conductive polymers or self-assembling nanofillers that maintain long-term conductivity in biofluids can help overcome current degradability issues. Also, integrating real-time sensing capabilities directly into the hydrogel network (ROS- or pH-responsive colorimetric signals) could enable dynamic, on-demand therapeutic adjustments. Injectable systems should be enhanced with programmable gelation kinetics, allowing in situ conformation to irregular wound shapes while retaining electrical and mechanical integrity. Finally, advanced biofabrication techniques like 4D printing or microfluidic-assisted patterning can be used to spatially pattern biological cues, enabling synchronized vascular, neural, and epithelial regeneration tailored to wound-specific healing phases.

Clinical settings presently do not have effective wound dressings that integrate robust resistance to drug-resistant bacteria with dependable self-healing properties. To tackle this issue, a variety of multifunctional self-healing antibacterial conductive hydrogel dressings (OSD/CMC/Fe/PA) were developed and assessed for the treatment of MRSA-infected full-thickness skin wounds. The hydrogels were synthesized via a combination of dynamic Schiff base and coordination bonds utilizing dopamine-grafted oxidized sodium alginate (OSD), carboxymethyl chitosan (CMC), Fe^{3+} ions, and polydopamine-coated poly(thiophene-3-acetic acid) (PA), which imparted the hydrogels with advantageous mechanical properties, conductivity, antioxidant activity, photothermal responsiveness, adhesion, biocompatibility, and self-healing capabilities. Rheological investigation demonstrated an elevated storage modulus with increasing PA concentration, signifying improved network crosslinking, while SEM pictures indicated a decrease in pore size with higher PA content. Tests on swelling and degradation indicated that elevated concentrations of Fe^{3+} and PA improved hydrogel stability. The hydrogels demonstrated enhanced conductivity with the inclusion of PA, emulating the electrical conductivity of native skin to facilitate wound healing. The OSD/CMC/Fe/PA3 hydrogel exhibited remarkable self-healing capabilities, restoring itself upon mechanical damage. Antioxidant tests (DPPH and NBT) validated robust free radical scavenging attributed to dopamine and PA. Lap shear tests and in vivo liver hemorrhage models demonstrated robust adhesion and enhanced hemostatic characteristics, exceeding those of commercial gelatin sponges. Hemolysis and cytocompatibility assays validated biocompatibility, demonstrating cell viability over 80 %. The hydrogels had remarkable photothermal effects under NIR light, particularly OSD/CMC/Fe/PA3, which consistently elevated in temperature by more than 23 °C and exhibited significant photothermal antibacterial efficiency, eliminating over 99 % of MRSA and *E. coli* within minutes. In vivo investigations utilizing MRSA-infected murine wound models demonstrated that OSD/CMC/Fe/PA3 hydrogels, especially under NIR irradiation, markedly expedited wound healing, improved granulation tissue development, facilitated re-epithelialization, and stimulated angiogenesis and hair follicle regeneration. Histological and

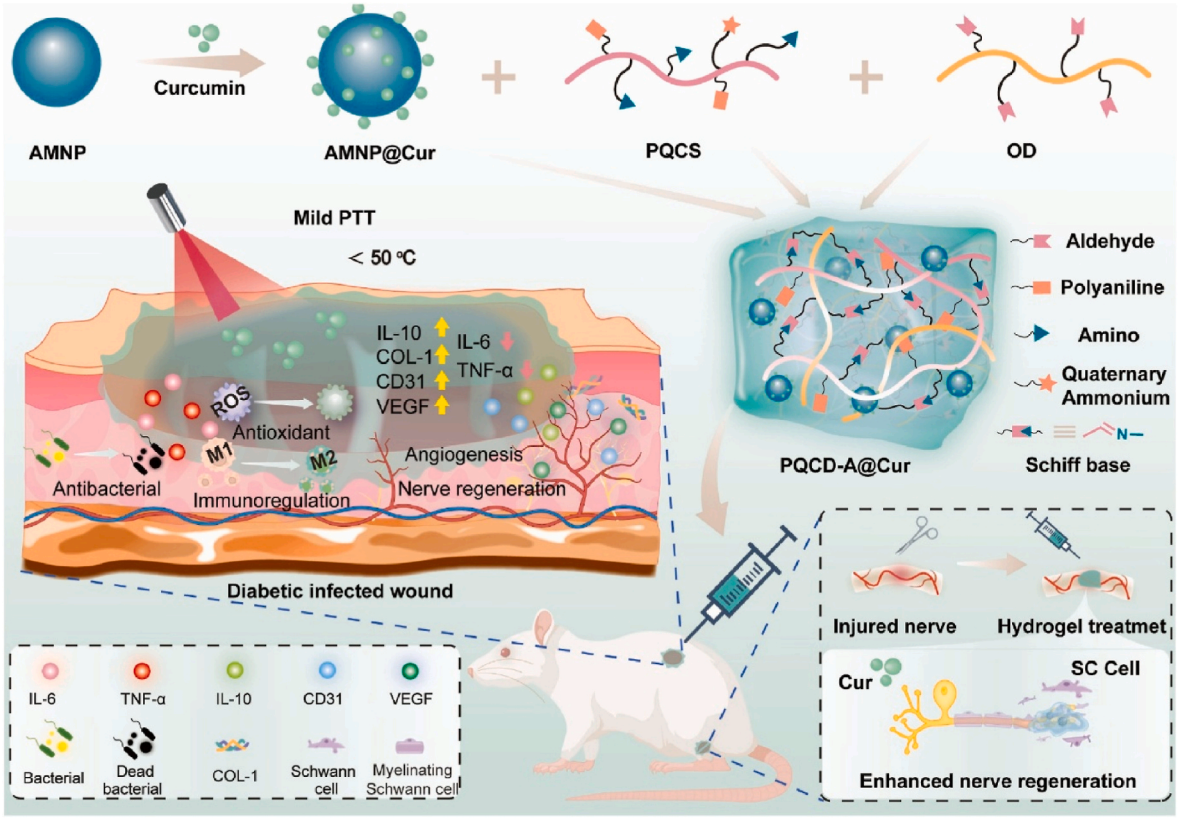

Fig. 9. Schematic illustration of hydrogel production and its effectiveness in treating peripheral nerve damage and promoting healing of diabetic wounds. Reproduced with authorization from Elsevier [79].

immunofluorescence investigations corroborated less inflammation (lower TNF-α) and increased VEGF expression, signifying improved tissue regeneration and neovascularization [80].

A series of multifunctional adhesion-enhanced self-healing hydrogels (PC hydrogels) were engineered for the management of athletic diabetic foot wounds by integrating dual dynamic bonds (Schiff base and phenylboronate ester) between CS-DA-LAG (catechol- and arginine-modified chitosan) and polyethylene glycol-*co*-poly(glycerol sebacic acid) (PEGS-PBA-BA), yielding hydrogels with superior mechanical strength, antioxidant and antibacterial properties, conductivity, pH/glucose-responsive drug release, tissue adhesion, and biocompatibility. Rheological and compression assessments revealed that augmenting the concentration of CS-DA-LAG and including rGO@PDA markedly improved the hydrogel's strength and elasticity, whilst swelling and degradation analyses indicated advantageous water absorption and degradation rates. PC hydrogels demonstrated strong self-healing properties and distinctive removability in acidic or high-glucose environments due to bond dissociation, facilitating safe removal of wound dressings. The hydrogels demonstrated a regulated release of metformin under acidic or hyperglycemic conditions, corresponding with the inflammatory milieu of diabetic wounds. Moreover, the hydrogels exhibited significant conductivity in both dry and wet conditions, facilitating electrical signal transfer to enhance healing, while the cationic properties of L-arginine imparted strong antibacterial efficacy against both *E. coli* and MRSA. Lap-shear tests demonstrated superior wet tissue adherence compared to commercial dressings, whereas PC2 hydrogel exhibited remarkable hemostatic efficacy in both in vitro and in vivo liver hemorrhage models in diabetic rats, thereby minimizing blood loss and lowering clotting duration. The DPPH and ROS tests validated the robust antioxidant properties of the catechol-modified hydrogels, which exhibited little hemolysis and enhanced HUVEC cell proliferation and angiogenesis, attributed to the synergistic effects of L-arginine and rGO@PDA. In vivo, PC hydrogels, particularly those co-loaded with rGO@PDA and metformin (PC2/GO2/Met), markedly expedited wound closure in diabetic foot models, diminished inflammation (as evidenced by reduced IL-6 expression), augmented collagen deposition, facilitated epidermal regeneration, enhanced granulation tissue formation, and stimulated vigorous angiogenesis and hair follicle regeneration. Immunofluorescence examination corroborated that the dual-loading of rGO@PDA and metformin synergistically enhanced vascular regeneration, evidenced by increased expression of CD31 and α-SMA, indicating a proliferation of nascent and mature blood vessels [81].

Despite promising performance, current hydrogel dressings such as OSD/CMC/Fe/PA and PC hydrogels face several critical challenges, including limited long-term mechanical stability in dynamic wound environments, suboptimal integration of drug release kinetics with fluctuating wound conditions, and difficulty maintaining consistent conductivity and bioactivity under chronic inflammation or infection. Additionally, while photothermal and glucose-responsive features are promising, they require precise tuning to avoid tissue overheating or premature drug depletion. Future research should focus on incorporating multi-scale reinforcement strategies, such as dual-network architectures or nanofiber reinforcement, to improve mechanical resilience and fatigue resistance. Enhancing spatiotemporal control over drug release can be achieved by embedding multi-compartmental drug carriers (core-shell nanoparticles or vesicles) that release payloads in response to specific biomarkers (IL-6 or ROS levels). To improve conductivity and cellular signaling, hybrid nanomaterials like MXenes or Au@PDA nanocomposites can be introduced in place of or alongside rGO, ensuring stable electrical performance even in wet, inflamed tissue. The design of adhesion mechanisms should also evolve, potentially by mimicking mussel-inspired adhesion combined with enzyme-triggered debonding, for strong yet removable dressings. Lastly, integrating microelectronic biosensors into the hydrogel matrix could enable real-time monitoring of pH, glucose, temperature, or bacterial load, facilitating personalized, closed-loop wound management strategies.

5.2.4.2. Critical analysis of hydrogels. Based on the discussions of previous section, it can be concluded that hydrogels are promising for wound healing acceleration. Therefore, this section is based on previous discussions and provide a critical analysis of their performance. Recent advancements in conductive hydrogels have yielded impressive performance benchmarks, including electrical conductivity values ranging from 0.14 to 0.73 S/m, aligning with physiological requirements for skin or nerve tissue. Mechanically, these hydrogels offer high compressive strength (up to 581.9 kPa), excellent stretchability (up to 300 %), and fast self-healing capabilities. Swelling properties are carefully tuned for specific wound environments, while biocompatibility is consistently high, with >80–90 % cell survival and minimal hemolysis. Antibacterial effectiveness, reaching up to 99 % against pathogens like *E. coli* and *S. aureus*, complements their wound healing performance, which typically achieves over 90 % closure within 10–21 days. Some systems also deliver thermal regulation, antioxidant activity, and controlled drug release in response to environmental stimuli. The hydrogels are constructed from a diverse array of functional materials to meet mechanical, electrical, and biological demands. Base polymers such as poly(acrylic acid), sodium alginate, PEG, and methacrylic acid provide structure and biocompatibility. Conductive fillers like hydroxyl-functionalized carbon nanotubes (CNT-OH), rGO, polythiophene derivatives, microtubules, and silver nanoparticles enable electrical conductivity and mechanical reinforcement. Crosslinkers including dopamine, thiolated HA, and catechol groups enhance self-healing and adhesion. Bioactive compounds like tea tree oil, curcumin, metformin, and L-arginine deliver antibacterial, antioxidant, or anti-inflammatory effects, while deep eutectic solvents and enzymes (lactate oxidase) introduce stimuli-responsive behaviors such as hypoxia induction or thermal responsiveness. Conductive hydrogels are being customized for various wound types, including burns, oral mucosal injuries, diabetic foot ulcers, and peripheral nerve injuries. Each hydrogel is engineered with specific functionalities tailored to its target environment: for example, PMO-CNT and HPDChCl-1.0 emphasize thermoregulation and electroactive healing in burn wounds, while rGO-enhanced formulations like PAA-SA@rGO address wet adhesion and inflammation in oral lesions. Diabetic and nerve-related wounds benefit from multifunctional systems such as PQCD-A@Cur or MT-MAA, which deliver nerve regeneration, angiogenesis, and immune modulation. Across all applications, features like antibacterial action, ES response, and controlled drug release significantly accelerate healing and support complex tissue remodeling.

Despite promising results, conductive hydrogels face key limitations related to stability, responsiveness, and multifunctional integration. Maintaining consistent conductivity in hostile environments such as acidic, enzyme-rich wounds or constantly moist oral tissues is difficult, as fillers like rGO or MTs tend to degrade or disperse unevenly over time. Over-swelling in high-moisture areas can impair adhesion and drug diffusion, while synchronizing biological processes like angiogenesis, neurogenesis, and anti-inflammatory responses in a single platform remains complex. Additionally, external stimuli-triggered release (NIR or pH) often lacks spatial control, especially in deep wounds. These trade-offs highlight the need for next-generation hydrogels featuring smart hierarchical architectures, enzyme-inert conductive polymers, dynamic biosensing, and programmable gelation tailored to wound-specific conditions.

5.2.5. Carbon nanomaterials

5.2.5.1. Development of platforms. Wounds in diabetics pose a significant healthcare issue because of their slow healing and increased risk of infection. This study details the creation and assessment of multifunctional CNT-reinforced BSA-cellulose composite hydrogels as sophisticated wound dressings, exhibiting remarkable conductivity, mechanical

strength, photothermal responsiveness, antibacterial and antioxidant properties, biocompatibility, and real-time imaging capabilities. CNTs were analyzed using TEM and DLS, demonstrating nanoscale tubular structure and enhanced hydrodynamic size resulting from aggregation in aqueous conditions. The hydrogels, created by heat-induced gelation of BSA and cross-linked with cellulose and CNTs, demonstrated both chemical (C-O-C bonds in cellulose) and physical (hydrogen bonding, π–π stacking) interactions. SEM demonstrated a concentration-dependent reduction in pore size of CNTs, enhancing the structural compactness and swelling capacity of the hydrogel. The incorporation of CNT markedly improved hydrogel conductivity (reaching 8.77 S/m) and mechanical characteristics, including as compressive modulus and tissue adhesion, rendering them appropriate for dynamic wound conditions. Rheological study validated robust elastic properties and structural stability at diverse stresses and frequencies. Photothermal tests demonstrated that CNT hydrogels produced temperatures of up to 43 °C under NIR irradiation, allowing efficient photothermal bacterial elimination (up to 81 % inhibition) and a significant enhancement in antioxidant activity (up to 89 % DPPH scavenging). In vitro assays demonstrated superior cytocompatibility, hemocompatibility, and cell survival, with CNTs and NIR-treated groups enhancing fibroblast proliferation. In vivo diabetic rat wound models treated with CNT-based hydrogels, namely the B + C + CNT1+NIR group, exhibited expedited wound closure (96 % by day 14), augmented collagen deposition, enhanced tissue architecture, and increased vascularization. Photoacoustic imaging and Doppler scans demonstrated significant improvements in oxygen saturation (up to 66 %) and vascularity (up to 74 %), validating the hydrogel's dual therapeutic and diagnostic applications. Immunohistochemistry corroborated these results, demonstrating decreased inflammation (CD68), enhanced wound contraction (α-SMA), and significant angiogenesis (CD31) in the B + C + CNT1+NIR group, surpassing other groups [82].

The creation of stable, multifunctional silver-based materials for wound dressings remains a significant challenge. The Ag-pDA/bacterial cellulose (BC) (rGO) composite film was meticulously studied to assess its structure, functioning, and potential as an antibacterial wound dressing. FT-IR and Raman investigations validated the efficient incorporation of graphene oxide and silver nanoparticles into the bacterial cellulose matrix, with changes in hydroxyl and carbon-oxygen peaks signifying interactions between Ag and BC components. XRD examination demonstrated the retention of crystalline structures in BC, with modest peaks indicative of decreased graphene oxide and Ag nanoparticles, implying good integration without substantial GO aggregation. SEM and AFM imaging demonstrated that dopamine coating enhanced the distribution of silver nanoparticles and minimized agglomeration, while also filled spaces in the BC matrix to increase compactness; the silver nanoparticles maintained a uniform dispersion with diameters below 50 nm. Thermal study (TG-DSC/DTA) revealed that the composite exhibited thermal stability below 100 °C, with identifiable degradation phases associated with BC, DA, and rGO. Freeze-drying and nanoparticle incorporation enhanced tensile strength while diminishing swelling capacity, indicating structural densification and decreased water permeability. Conductivity assessments indicated diminished electrical performance relative to rGO-only composites; nonetheless, the current generation (average resistance: 0.5062 Ω; current: 2.388×10^{-5} A) was adequate to facilitate modest Joule heating, resulting in heat production of 7 J after 6 h, which may enhance wound healing. The composite exhibited significant antibacterial activity, with inhibition zones reaching 7.8 mm attributed to silver ion release (≤0.005 mg/L), and maintained 84 % antibacterial efficacy after 72 h, demonstrating its endurance. Biocompatibility tests with NIH3T3 fibroblasts demonstrated elevated cell viability (>90 %) and no cytotoxicity, confirming its appropriateness for biological applications. A proposed mechanism demonstrates that AgNPs function as antibacterial agents, while the conductive, thermally active film structure facilitates cell migration and regulates wound temperature under ES, rendering Ag-pDA/BC (rGO) a multifunctional material with significant potential for advanced wound care [83].

Flexible hydrogel sensors have advantageous mechanical qualities and biocompatibility; nevertheless, typical rGO has limits in reduction degree and dispersion, which impede the development of high-sensitivity sensors. Developing conductive hydrogels that exhibit high sensitivity, antibacterial properties, and antioxidative functions continues to pose significant challenges. A two-step process was established to manufacture Hep-PDA-rGO nanosheets, which were integrated into PAM hydrogels to provide multifunctional, electroconductive, and biocompatible materials suitable for wearable sensors and wound healing applications. The reduction and functionalization of GO with heparin and PDA improved dispersion, thermal stability, and surface charge, while simultaneously attaining a significant level of reduction, as verified by UV–vis, Raman, FTIR, TGA, and AFM analyses. Incorporating heparin (Hep)-PDA-rGO into PAM hydrogels markedly enhanced mechanical strength, electrical conductivity (3.63 S/m at only 1 wt% loading), and cycle endurance, facilitating excellent sensitivity and repeatability under compressive and tensile strain, with strain detection reaching 350 %. The hydrogels operated efficiently as epidermal sensors, identifying human movements such as finger flexion, ambulation, and deglutition. Biocompatibility studies demonstrated little hemolysis (<5 %) and elevated 3T3 cell viability (>90 %), with the Hep-PDA combination alleviating GO-induced cytotoxicity by improving water stability and diminishing membrane rupture. Moreover, Hep-PDA-rGO hydrogels had significant antioxidant activity by effectively scavenging DPPH and hydroxyl radicals (>80 % efficiency) and displayed potent antibacterial capabilities against *S. aureus* and *P. aeruginosa* (>99 % kill rate), attributable to the synergistic antimicrobial actions of PDA, heparin, and rGO. In vivo investigations in diabetic rats shown that the Hep20-PDA0.8-rGO-PAM hydrogel, especially when paired with ES, markedly expedited the healing of infected wounds, attaining virtually complete closure (99.7 %) after 14 days. Histological and immunohistochemical evaluations validated improved tissue regeneration, diminished inflammation, increased collagen deposition, neoangiogenesis, and heightened expression of angiogenic factors (VEGF, PDGF, VEGFR2) in the rGO + ES group, illustrating the hydrogel's effectiveness as both a biosensor and therapeutic dressing for chronic wounds (Fig. 10) [84].

A research created a GO-infused poly (lactic-co-glycolic acid) (PLGA) composite (PLGA/GO) and assessed its physicochemical characteristics, biocompatibility, and wound-healing effectiveness, both independently and in conjunction with ES. SEM examination indicated that GO augmented surface roughness, while contact-angle measurements demonstrated increased hydrophilicity in proportion to GO concentration, both of which facilitated cell adhesion and proliferation. Mechanical testing revealed that a modest quantity of graphene oxide (specifically at 2 %) markedly improved tensile strength, but excessive graphene oxide resulted in agglomeration and a little reduction in performance. The PLGA/GO composites had significant antibacterial efficacy against *E. coli* and *S. aureus*, which intensified with higher GO concentrations. In vitro cell viability studies with fibroblasts demonstrated enhanced proliferation, particularly at 2 % GO, although elevated doses exhibited harmful effects. Moreover, the application of ES (optimal at 500 Hz) synergistically promoted fibroblast proliferation, adhesion, and increased the production of VEGF and COL-1, which are essential for angiogenesis and tissue remodeling. Immunofluorescence and qRT-PCR corroborated these results, revealing that the PLGA/GO + ES group had the greatest levels of gene and protein expression. In vivo investigations utilizing a full-thickness skin-defect rat model revealed that PLGA/GO + ES expedited wound healing, enhanced epithelium thinning and granulation tissue development, facilitated collagen deposition, and markedly augmented neovascularization relative to other groups. Histological investigations and CD31 staining demonstrated superior epidermal remodeling and capillary development in the PLGA/GO + ES group [85].

Antibacterial hydrogel wound dressings have attracted interest for

improving wound healing, but the risk of bacterial infection persists. The advancement and multifunctional capabilities of a unique indocyanine green (ICG)-PDA-mediated graphene oxide (PGO)-amorphous calcium phosphate (CaP)-incorporated poly(vinyl alcohol) (PVA) hydrogel, which integrates photothermal, photodynamic, electroactive, and self-healing qualities to improve wound healing. Characterization validated the effective alteration of GO with PDA to produce PGO, whereas amorphous CaP was generated in situ inside the PVA matrix. The addition of CaP and PGO markedly enhanced the mechanical characteristics of the hydrogel, demonstrated by increased tensile strength, compressibility, and elasticity. The hydrogel demonstrated remarkable photothermal effects under NIR light, with PGO and ICG collaboratively increasing temperatures and facilitating reversible gel–sol transitions that enhance self-healing and calcium ion release. The ICG-PGO-CaP-PVA hydrogel exhibited significant photothermal and photodynamic antibacterial efficacy against S. epidermidis and *E. coli*, with reactive oxygen species production resulting in substantial decreases in bacterial viability. In vivo research utilizing rat models validated its enhanced anti-inflammatory and antibacterial properties, diminishing infection and expediting tissue regeneration. The hydrogel's conductivity, enhanced by PGO and CaP, facilitated bioelectric signal transmission and device integration, while fostering myoblast adhesion, elongation, and initial myotube creation under ES. In full-thickness wound models, the ICG-PGO-CaP-PVA hydrogel markedly expedited wound closure and improved collagen deposition, vascularization, and hair follicle regeneration. The results were ascribed to PDA-enhanced cellular affinity and immunomodulation, ICG-mediated photodynamic activation of repair mechanisms, and synergistic photothermal effects that induced gel liquefaction and promoted Ca^{2+} release, thereby amalgamating various biological signals to enhance effective tissue repair (Fig. 11) [86].

5.2.5.2. Critical analysis. The integration of carbon nanomaterials into wound-healing platforms has led to the creation of multifunctional dressings that significantly outperform conventional materials by synergistically combining electrical conductivity, mechanical robustness, biocompatibility, antibacterial activity, and bioresponsiveness. The use of CNTs, rGO, and their functionalized derivatives enables the design of wound dressings that are not only structurally resilient but also

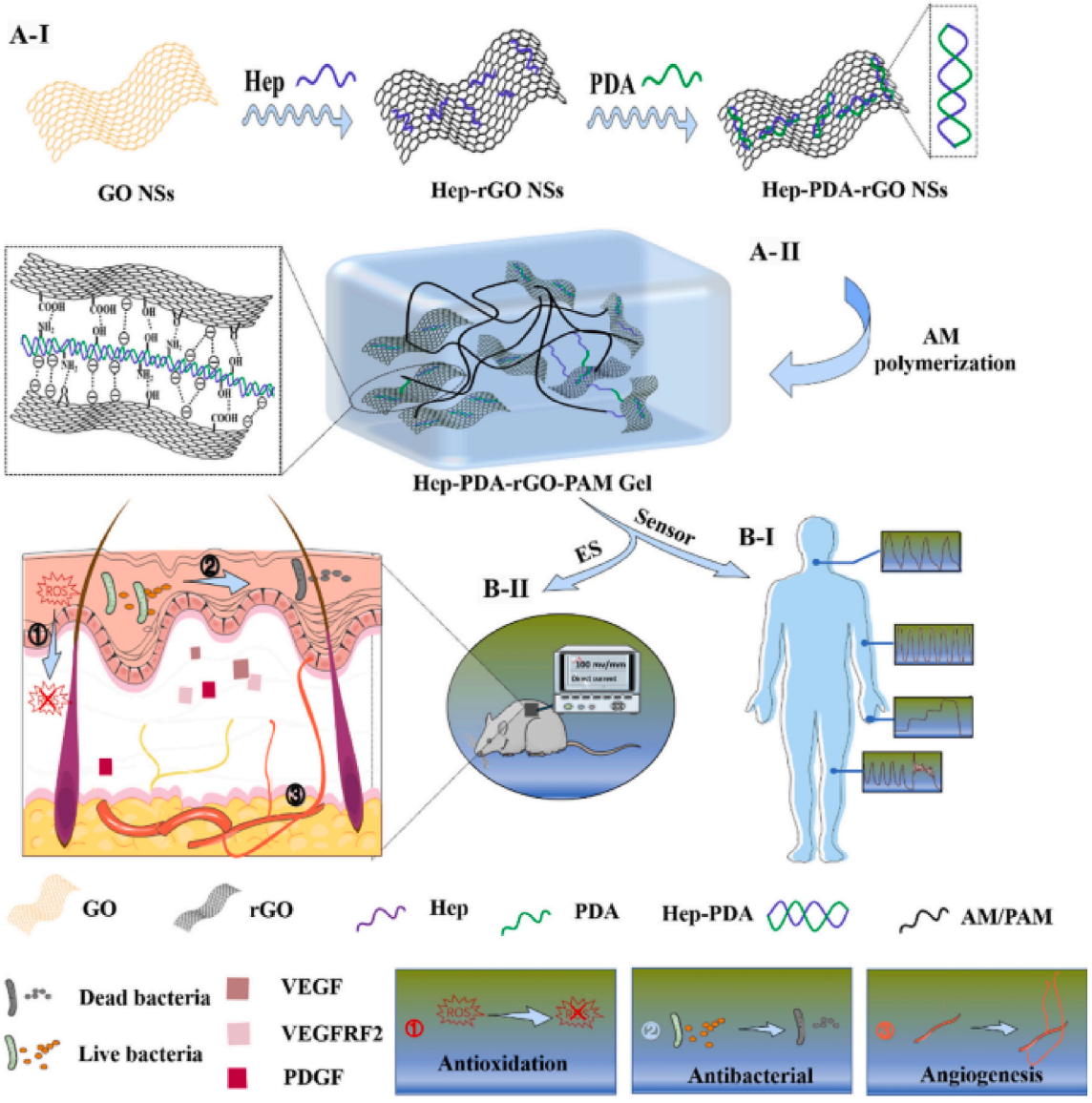

Fig. 10. Schematic illustration of the creation and application of multifunctional hydrogels. Hep-PDA-rGO nanosheets were created in two phases, showing improved stability owing to strong negative repulsion (A–I), and later incorporated into a hydrogel matrix to create a conductive Hep-PDA-rGO-PAM gel (A-II). The gel was utilized in two roles: as an epidermal sensor (B–I) and as a diabetic wound dressing integrated with ES, due to its multifunctional characteristics (B-II). Reproduced with consent from BMC Springer Nature [84].

therapeutically and diagnostically potent. CNT-reinforced BSA-cellulose hydrogels, for instance, demonstrated exceptional performance in diabetic wound models, exhibiting high electrical conductivity (up to 8.77 S/m), superior compressive strength, and tissue adhesiveness, essential for dynamic wound environments. These materials leveraged photothermal conversion under NIR light to eradicate bacteria and improve antioxidant activity, with real-time imaging capabilities such as photoacoustic and Doppler scans confirming enhanced vascularization and oxygenation. Similarly, the Hep-PDA-rGO-PAM hydrogel sensor platforms showcased the dual functionality of biosensing and therapeutic delivery, where rGO functionalized with heparin and polydopamine achieved enhanced dispersion, thermal stability, and cytocompatibility. These hydrogels efficiently supported fibroblast proliferation, diminished inflammation, and promoted angiogenesis, particularly when combined with ES leading to near-complete wound closure and improved tissue remodeling in diabetic rat models.

Furthermore, hybrid systems integrating metal ions and carbon nanostructures have broadened the scope of advanced wound care. For example, silver-incorporated BC-rGO composites utilized dopamine-mediated coating techniques to uniformly disperse nanoparticles, enhancing antibacterial efficacy and structural compactness while maintaining biocompatibility. These dressings demonstrated stable antibacterial performance (up to 84 % inhibition after 72 h) and supported fibroblast viability, positioning them as promising long-term wound dressings. Similarly, ICG-PGO-CaP-PVA hydrogels combined photothermal and photodynamic properties with electroactivity and self-healing capabilities. These multifunctional gels, formed through freeze-thaw cycling and incorporating amorphous calcium phosphate and ICG-functionalized PGO, demonstrated substantial antibacterial and regenerative outcomes. They facilitated cell adhesion, modulated immune responses, and promoted tissue regeneration under NIR stimulation by integrating Ca^{2+} release and ROS production into the healing process. The collective findings underscore the vital role of multifunctional carbon-based materials in addressing complex wound healing challenges, particularly in chronic and infected wounds, by offering an integrated approach that encompasses antimicrobial defense, tissue regeneration, real-time monitoring, and enhanced bioelectrical communication.

5.2.6. *Metals and metal oxides*

The treatment of skin wounds remains a significant healthcare concern. Although electric stimulation is known to effectively enhance wound healing, its application in clinical settings has been hindered by bulky and inconvenient electrical devices. The self-activated electrotherapy bandage device consists of a biomechanical energy conversion unit (NG) and dressing electrodes, employing a multilayer Cu/PTFE-Cu on PET configuration that facilitates flexibility and safe skin application, as verified by MTT tests indicating little cytotoxicity. The NG transforms mechanical motion from respiration into distinct electrical pulses that promote wound healing, with voltage amplitude according to rat breathing rates. Preliminary experiments on rats with linear incisional wounds demonstrated markedly accelerated healing with NG stimulation relative to controls, ascribed to the enhancement of the endogenous electric field (TEP disruption) facilitating epithelial migration. Finite element study indicated that the produced electric field (~10 V/cm) was concentrated and intense at the electrode teeth, exerting no influence

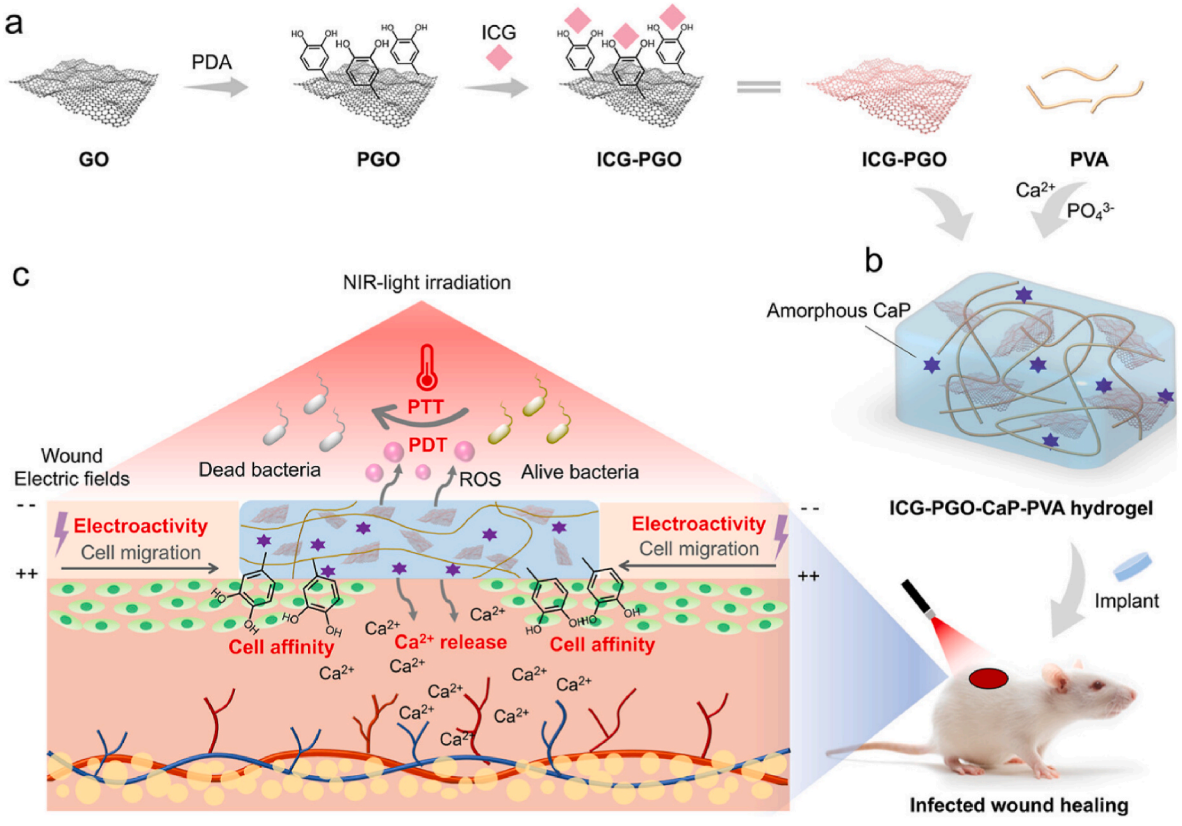

Fig. 11. Schematic illustration of the creation of the ICG-PGO-CaP-PVA hydrogel demonstrating multifunctional properties for managing infected wounds. (a) PGO was produced by reducing GO with PDA, subsequently loading ICG onto the PGO surface via the catechol groups present in PDA. ICG-PGO, Ca(OH)2, and H3PO4 were incorporated into the PVA matrix to form the ICG-PGO-CaP-PVA hydrogel through freeze-thaw cycling. Amorphous calcium phosphate was generated in place within the PVA hydrogel throughout this process. The ICG-PGO-CaP-PVA hydrogel has multiple functions. The photothermal effect generated heat energy to eliminate germs while promoting Ca2+ release. The photodynamic effect generated reactive oxygen species to eliminate the pathogens. Electroactivity impacted cellular activity. Cell affinity improved cell adhesion. The ICG-PGO-CaP-PVA hydrogel was employed for the treatment of infected wounds with near-infrared light exposure. Published again with authorization from ACS [86].

beyond that region. Wounds subjected to perpendicular electric fields healed much more rapidly than those exposed to parallel fields or lacking stimulation. In a more measurable assessment, full-thickness rectangular wounds were subjected to treatment with parallel electrodes generating an approximate 250 V/m electric field, resulting in virtually complete healing after 72 h under NG stimulation, compared to around 10–12 days for the control group. H&E staining verified a more thorough epithelialization in the treated wounds. In vitro experiments demonstrated higher fibroblast vitality (up to 127 %) and directed migration and differentiation in response to NG electric fields, accompanied by increased production of growth factors (TGF-β, EGF, VEGF), notably EGF ($P = 0.0085$). Moreover, the formation of reactive oxygen species (ROS) was markedly reduced in NG-driven stimulation relative to normal AC pulses, suggesting a decreased potential for cytotoxicity. The results underscore the NG device's effectiveness in facilitating rapid and safe wound healing by using naturally occurring, low-intensity electric fields to augment cellular activity and tissue regeneration [87].

Conventional wound healing treatments primarily support passive recovery and typically do not possess the ability to actively influence skin cell functions. EFs, generated by variations in electric potential, have been shown to influence numerous functions of skin cells. A study details the creation, characterization, and therapeutic assessment of a piezoelectric patch (PZP) consisting of bilaterally domain-grown (BDG) ZnO nanorods (NRs) embedded in a polydimethylsiloxane (PDMS) matrix, intended to produce endogenous electric fields (EFs) to promote wound healing. BDG ZnO nanorods were manufactured using hydrothermal techniques and aligned using unidirectional rubbing to enhance piezoelectric response, as validated by SEM imaging and finite element modeling, which exhibited symmetrical charge polarization during bending. Multilayered PZPs (up to nine layers) demonstrated exceptional flexibility, stretchability, and consistent piezoelectric outputs ($\sim$1.8 V and 85 nA cm^{-2}) when aligned NRs were subjected to bending, markedly surpassing randomly aligned variants. The piezoelectric output enhanced with NR alignment, layer count, and filling density, reaching a maximum at 95.2 % NR density. In vitro studies revealed that PZPs with aligned NRs exhibited no cytotoxicity and facilitated dermal fibroblast proliferation, myofibroblastic differentiation, migration, and the expression of regenerative markers (FGF-2, TGFβR, COL III), while also augmenting calcium signaling and COL IV expression in keratinocytes. The administration of PZPs to murine skin wounds in vivo markedly expedited wound closure, re-epithelialization, and tissue remodeling, accompanied by elevated expression of angiogenic (VEGF, CD31), inflammatory (CD68), and matrix remodeling proteins (MMP2, COL I/III/IV, fibronectin). Augmented microvessel and arteriole development was noted, ascribed to continuous piezoelectric stimulation. PZP therapy mechanistically elevated essential intracellular signaling molecules linked to electrotaxis and cell proliferation, such as phosphorylated Akt, phosphoinositide 3-kinase (PI3K), ERK1/2, and Rho-GTPase. The PZPs preserved their structural integrity and piezoelectric functionality for 15 days without nanorod degradation or leaching, confirming their long-term biocompatibility and effectiveness [88].

Externally applied electric fields can efficiently direct cell movement and improve wound healing; however, their practical use is constrained by device accessibility and insufficient knowledge of associated molecular pathways. This work delineates and assesses an innovative silver/zinc bioelectric dressing (Ag/Zn BED) intended to expedite wound healing via endogenous electric field production and redox-mediated molecular signaling. The dressing, consisting of alternating microreservoirs of high-purity silver and zinc particles printed on a polyester substrate, creates redox couples spaced 1 mm apart, producing localized electric fields of up to 13.5 V/cm and potentials reaching 1 V when hydrated. SEM and EDS verified the existence of elemental silver and zinc, as well as their oxides. Numerical modeling demonstrated that electric fields decrease at sub-millimeter distances from the BED surface, affecting adjacent cells without external power. The BED markedly enhanced keratinocyte migration in scratch experiments, a mechanism associated with the production of endogenous hydrogen peroxide (H_2O_2) and mitochondrial activation. Keratinocytes exposed to the BED exhibited elevated mitochondrial membrane potential, enhanced glucose absorption, and increased intracellular H_2O_2 levels. Inhibiting H_2O_2 signaling or neutralizing ROS with catalase or NAC eliminated this migratory impact. Mechanistically, the BED prompted activation of the IGF1 receptor, diminished cellular protein thiols without altering glutathione levels, and increased integrinαv expression near wound margins, suggesting involvement in redox-regulated signaling pathways. These integrated electrical and biochemical signals replicate the physiological "injury potential" and promote re-epithelialization. The structured electric field produced by the Ag/Zn BED offers a power-free, biocompatible method to influence cellular function, with potential benefits for enhanced wound care, especially in chronic or non-healing wounds [89].

Future developments in bioelectric wound healing are poised to revolutionize regenerative medicine by combining advanced materials science, bioengineering, and cellular biology to produce more intelligent, adaptable, and clinically viable therapeutic platforms. A key direction involves the integration of wireless, self-powered systems with multifunctional capabilities such as real-time monitoring, targeted drug delivery, and adaptive ES within flexible, skin-conforming dressings. Innovations in nanomaterials like 2D piezoelectric layers, conductive hydrogels, and biocompatible polymers could yield highly sensitive, stretchable devices that not only harvest biomechanical energy more efficiently but also tailor electric field parameters dynamically in response to healing progress or tissue feedback. Machine learning and biosensing technologies may soon be incorporated to analyze wound biomarkers and optimize stimulation protocols in a closed-loop system, ensuring patient-specific treatment with minimal clinical oversight. Moreover, combining electric field therapy with emerging fields such as gene editing, immunomodulation, and stem cell delivery could open novel pathways to synergistically activate cellular regeneration and angiogenesis while suppressing chronic inflammation or fibrosis. Research is also expected to expand beyond acute injuries to tackle complex cases such as diabetic ulcers, burn wounds, and post-surgical complications, with a focus on regulatory approval and manufacturability for large-scale deployment. Additionally, the elucidation of electrotaxis-related molecular pathways including redox signaling, ion channel dynamics, and intracellular transport will be critical for refining stimulation strategies and minimizing off-target effects. Ultimately, the convergence of bioelectronic design with precision medicine promises to create a new generation of "smart" wound care systems that are not only curative but also preventative, capable of diagnosing, treating, and reporting in a seamless, patient-friendly manner.

6. Conductive polymers in infected and diabetic wound healing

6.1. Infected wounds

Contemporary viewpoints underscore that dependence on a singular therapeutic approach is inadequate for attaining effective wound healing. Wound dressings have to be engineered for the prolonged release of therapeutic medicines, including epidermal growth factors, to facilitate skin regeneration. Moreover, sophisticated combination treatments using photothermal, acoustic, electrical, and other physical modalities have been devised to enhance skin healing and more effectively battle infections. A multifunctional PPy@PDA/PANI hydrogel sensor, combined with a PANI/PVDF substrate, was created for real-time detection of ammonia gas and accurate drug administration, especially in wound healing applications. The hydrogel, composed of polypyrrole-polydopamine nanowires (PPy@PDA) and PANI, demonstrated a highly porous architecture with evenly dispersed nanoparticles, offering a substantial specific surface area ($\sim$64 μm pore size) and multiple active sites favorable for effective gas sensing. The best configuration, PPy@PDA/PANI(3/6), exhibited superior gas-sensing capability,

characterized by a rapid reaction time of 23.2 s, a swift recovery time of 42.9 s, and a sensitivity of 23.5 % at 1 ppm NH_3, with a theoretical detection limit of 49 ppt. The increased sensing was ascribed to the creation of p–p heterojunctions between PPy@PDA and PANI, which enabled enhanced charge carrier modulation, while the 3D porous PVDF layer promoted expedited gas transport. Remarkable selectivity against other gases, reliable performance under diverse humidity and pH conditions, and a steady charge-transfer-based sensing mechanism were noted. A wireless app-controlled system was constructed, enabling real-time monitoring of ammonia concentration and precise regulation of electrically triggered medication release, therefore establishing a closed-loop feedback system to assure appropriate dose. The hydrogel system exhibited superior ionic and electronic conductivity, exceptional mechanical stability, demonstrated biocompatibility and antibacterial properties, responsiveness to humidity fluctuations, and adaptability to various pH levels, rendering it highly appropriate for wearable biomedical sensing and advanced wound management [90].

TENGs have significant potential as autonomous devices for administering therapeutic ES to facilitate various phases of wound healing. However, a substantial constraint exists in the challenge of attaining total (100 %) contact in conventional TENG designs, which considerably impedes their capacity to generate greater current outputs, an crucial element for improving the efficacy of wound healing. A thorough assessment was performed on a multifunctional wound healing system utilizing aqueous-aqueous triboelectric nanogenerators (A-A TENGs), which demonstrated a marked improvement in wound repair due to increased current output. Biocompatible dextran (DEX) and PEG solutions were employed due to their low viscosity, steady interfacial tension, and cytocompatibility, facilitating stable contact-separation cycles and effective charge transfer absent in traditional liquid or solid TENGs. Sixteen DEX-PEG droplet pairs were serially coupled, yielding an output of roughly 790 nA and 5.4 V, while exhibiting robust performance across varying humidity and temperature conditions, and sustaining over 4000 operating cycles. In comparison to solid-solid (S-S) TENGs, liquid-liquid (A-A) TENGs demonstrated a current density over 500 times greater, attributable to enhanced charge transfer at liquid-liquid interfaces, as corroborated by experimental data and COMSOL finite element simulations. The electrical output was conveyed through a conductive K_2CO_3/PAA/$CaCl_2$ hydrogel, facilitating uniform ES over wound areas devoid of electrodes. Augmented antimicrobial efficacy was noted, especially against *S. aureus*, due to heightened membrane disruption and enhanced minocycline absorption, as validated by SEM imaging and SYTO 9/PI staining. Cell viability and scratch studies demonstrated that fibroblast proliferation and migration were markedly enhanced under electric stimulation from A-A TENGs in comparison to S-S TENGs, presumably owing to more robust divided-voltage fields. In vivo, expedited wound closure was attained in S. aureus-infected rat models administered M-H-A-A TENGs, with full healing noted by day 10. Histological investigations demonstrated increased granulation tissue development, diminished inflammation characterized by lowered TNF-α and IL-6 levels, augmented collagen deposition, and elevated angiogenesis as shown by VEGF and CD31 expression (Fig. 12) [91].

Infection constitutes a substantial impediment to efficient wound healing. To enhance the recovery of infected wounds, there is a significant demand for dressings that exhibit antibacterial qualities and multifunctional attributes that facilitate the healing process. A multifunctional hydrogel system, GT-DA/CS/CNT, was created by combining gelatin-grafted-dopamine (GT-DA), CS, and polydopamine-coated carbon nanotubes (CNT-PDA) to facilitate the healing of infected skin wounds through structural support, bioactivity, and conductive properties. Gelatin offered biocompatibility and extracellular matrix mimicking, whereas dopamine imparted sticky and antioxidative characteristics through EDC/NHS coupling. CS was included to improve mechanical stability and degradation resistance, with 5 wt% determined as best for preserving hydrogel integrity. CNTs covered with PDA enhanced dispersion, bioactivity, and decreased cytotoxicity, resulting in crosslinked hydrogels by H_2O_2/HRP-catalyzed oxidative coupling. The resultant hydrogels exhibited fast gelation, water absorption depending on swelling, and adjustable breakdown rates contingent upon CNT-PDA concentration. Elevated CNT-PDA levels improved pore density, mechanical strength, and conductivity, with GT-DA/CS/CNT4 attaining the maximum modulus and conductivity (7.2×10^{-2} S/m). Hydrogels exhibited robust tissue adhesion, efficient form restitution post-compression, and considerable hemostatic efficacy, markedly reducing hepatic hemorrhage in vivo. The antioxidant activity was validated using DPPH scavenging, achieving practically total radical neutralization at a concentration of 5 mg/mL hydrogel. Antibiotic loading (doxycycline) facilitated prolonged drug release controlled by Fickian diffusion, preserving antibacterial efficacy for a duration of up to 9 days. Furthermore, CNTs imparted robust photothermal characteristics to the hydrogel under NIR irradiation, facilitating efficient in vitro and in vivo elimination of *S. aureus* and *E. coli*. Biocompatibility was confirmed through L929 fibroblast viability and minimal hemolysis rates (<4 %), while in vivo investigations utilizing an infected full-thickness mouse skin model exhibited enhanced wound closure, granulation tissue thickness, and collagen deposition in the GT-DA/CS/CNT2 and GT-DA/CS/CNT2/Doxy hydrogel groups relative to a Tegaderm™ control. Histological examination demonstrated decreased inflammation, improved epidermal regeneration, neovascularization, and increased hair follicle density in CNT- and antibiotic-embedded hydrogels. Immunofluorescence validated reduced TGF-β expression and elevated CD31 levels, indicating successful inflammation regulation and angiogenesis [92].

Wound infections pose major health risks, and recent studies suggest that conductive composite materials could enhance the effectiveness of ES and promote cell migration, thus accelerating the healing process. A multifunctional conductive hydrogel (CPH) incorporating AgNPs was synthesized utilizing a PVA matrix augmented with gelatin and PANI, presenting potential applications in infected wound healing due to its enhanced mechanical strength, conductivity, antibacterial properties, and biocompatibility. The mechanical properties of the hydrogel were adjusted by altering the PVA concentration (2.5–12.5 wt%), with increased PVA content resulting in better tensile strength, elongation, and storage modulus, signifying greater stiffness and endurance. Nonetheless, 5 wt% PVA was determined to be ideal for attaining a compromise between mechanical strength and moldability. Conductivity was augmented by the incorporation of CNT-PDA and aniline (AN), resulting in hydrogels exhibiting an increase in conductivity from 0.032 to 0.069 S/cm with the rising volume of AN. The gelatin content was tuned to 1.5 wt% to preserve porosity and provide enough Ag NP loading and sustained release. SEM scans validated a porous architecture conducive to fluid absorption and medication administration. The hydrogel exhibited significant water absorption (up to 180 %) and extended swelling, facilitating effective exudate control. Swelling experiments indicated that the Ag NPs may be progressively released, sustaining localized antibacterial effectiveness. Antibacterial assays against *E. coli* and *S. aureus* demonstrated significant inhibitory zones correlated with Ag NP concentration, and optical density (OD) assessments over 48 h validated dose-dependent bacterial suppression. XPS and FTIR analysis confirmed the effective incorporation of Ag NPs and PANI inside the hydrogel. Cytotoxicity evaluations on HaCat, LO2, and 293T cells demonstrated no toxicity, even at elevated Ag NP concentrations, with modest evidence of increased cell proliferation at lower levels. In vivo wound healing experiments involving mice with S. aureus-infected wounds revealed enhanced healing in the Ag NPs/CPH group relative to the CPH and control groups, as indicated by accelerated wound closure, low adhesion during dressing changes, decreased inflammation, and significant tissue regeneration. Histological investigation corroborated these findings, revealing a reduced presence of inflammatory cells, enhanced neovascularization (as shown by CD31 staining), and elevated collagen deposition in wounds treated with Ag NPs/CPH [93].

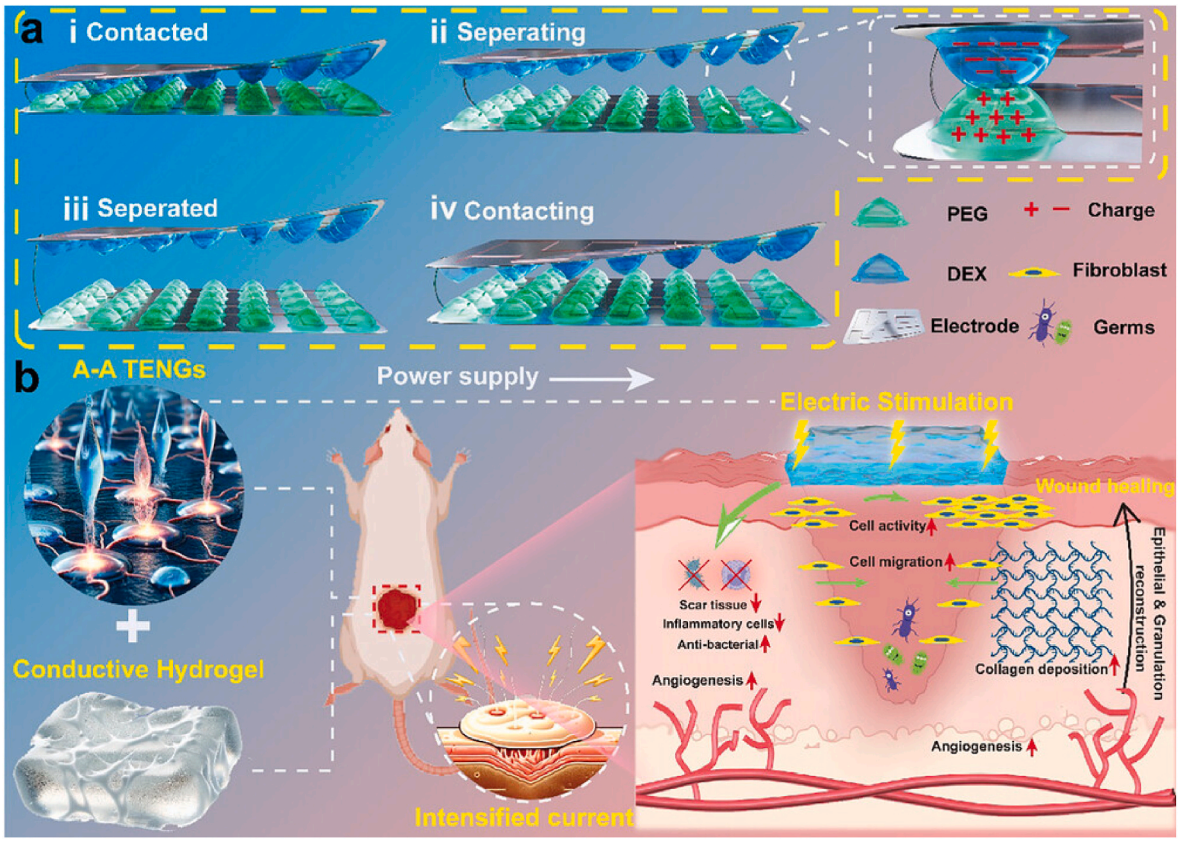

Fig. 12. Schematic representation of the suggested A-A TENGs-powered multifunctional wound healing system aimed at accelerating wound recovery. a) Functional principles of ATPS-based A-A TENGs. b) The improved current promoted the wound healing process through our engineered M-H-A-A TENGs. Reproduced with authorization from Wiley [91].

The treatment and management of infected skin wounds remain considerable therapeutic challenges. The PDES electroactive eutectogel, developed via a one-pot synthesis utilizing quaternized chitosan (QCS), acrylic acid (AAc), acrylamide (AAm), 2-acrylamido-2-methyl-1-propanesulfonic acid (AMPS), and additional monomers, has proven to be a multifunctional material adept at tackling various issues in tissue engineering, particularly in wound healing, biosensing, and infection management. This hydrogel system combines the mechanical strength of polymeric networks with the adjustable ionic characteristics of deep eutectic solvents (DESs), yielding a material that exhibits rapid gelation (<20 s), exceptional swelling capacity (up to 1100 %), significant mechanical strength, and outstanding fatigue resistance over 9000 compression cycles. Its elevated porosity and adjustable microstructure facilitate cellular penetration and nutrient exchange while markedly improving water absorption and tissue compatibility. The eutectogel exhibits exceptional universal adhesion (up to 75 kPa on pig skin), far exceeding that of traditional fibrin glue, attributed to substantial hydrogen bonding interactions. It exhibits remarkable conductivity (>1 S/m) and a significant ionic piezoelectric effect, allowing it to serve as a sensitive biosensor for detecting physical inputs such as joint movement, voice, and handwriting, with elevated signal-to-noise ratios. The antibacterial efficiency is notable, achieving approximately 100 % suppression of *E. coli* and *S. aureus*, due to the zwitterionic and amphiphilic characteristics of the hydrogel matrix. In vitro biocompatibility studies demonstrate its low cytotoxicity, superior support for fibroblast motility, robust resistance to protein adsorption, and little hemolysis (<5 %). In a liver hemorrhage model, the PAAAQ hydrogel exhibited rapid hemostatic effects, drastically decreasing blood loss and clotting time due to its positive surface charge that enhances platelet aggregation. In vivo, in a rat model of acute wound infection, the hydrogel expedited healing, diminished inflammation (through a transition from M1 to M2 macrophages), improved vascularization (indicated by elevated α-SMA and vWF levels), and facilitated structured collagen deposition, particularly type III collagen over type I, implying reduced scarring. Subsequent immunofluorescence examination demonstrated less oxidative stress (DHE staining) and increased cellular proliferation (Ki-67 staining) in hydrogel-treated tissues [94].

Chronic wounds infected with antibiotic-resistant bacteria, such as MRSA, are difficult to manage because there are few approaches that effectively tackle both the infection and the healing process without the use of antibiotics. The HPEM scaffolds, created by a dynamic Schiff-base reaction involving oxidized hyaluronic acid (HCHO), poly(glycerol-ethylenimine) (PGE), and MXene@PDA, provide a multifunctional, conductive, and biocompatible hydrogel system specifically intended for infected wound healing. Their structural integrity and network creation were validated using NMR, FTIR, SEM, and TEM investigations, demonstrating a porous architecture and the effective incorporation of MXene@PDA nanosheets, which markedly improved mechanical strength, thermal stability, and electrical conductivity (2.89 S/m). Rheological evaluations demonstrated exceptional shear-thinning properties, a remarkable self-healing capability (G' recovery rate of 99.1 %), and robust tissue adhesion attributed to dynamic bonding and mussel-inspired PDA chemistry. In antibacterial research, HPEM scaffolds shown significant suppression of *E. coli*, *S. aureus*, and particularly MRSA, surpassing conventional medicines such as ampicillin. Bacterial membrane rupture was mechanistically validated by zeta potential lowering, protein leakage tests, SEM, and TEM imaging, which combined demonstrated significant cytoplasmic leakage and cell wall destruction. The hemostatic assessment utilizing a murine liver hemorrhage model demonstrated that HPEM drastically decreased blood loss and abbreviated bleeding duration, highlighting its fast coagulation capability. Cytotoxicity assays on L929, HUVEC, and NIH-3T3 cells

demonstrated substantial biocompatibility, characterized by little LDH release and the absence of severe histopathological damage in primary organs. Cell proliferation studies further evidenced HPEM's capacity to augment cellular growth over a five-day period, ascribed to its conductivity-enhanced electrical signaling. Gene expression analyses indicated that HPEM markedly elevated α-actin, COL III, and VEGF, which are essential regulators of fibroblast function, collagen production, and angiogenesis. In vivo, utilizing an MRSA-infected full-thickness wound model, HPEM expedited wound closure (96.31 % by day 14), diminished bacterial load, and alleviated inflammation by downregulating IL-6 and decreasing macrophage and neutrophil infiltration. Histological investigations demonstrated increased granulation tissue development, denser collagen deposition, and angiogenesis, accompanied with pronounced expression of Ki67, α-SMA, and CD31, signifying proliferative and vascular responses [95].

Bioelectroactive materials has the capacity to augment cell proliferation and tissue regeneration, while concurrently reducing infection-related problems, hence facilitating scar-free wound healing. The QCS/OD/SDI/PANI/PS/Plasma (QOSP) hydrogel is a sophisticated multifunctional dressing designed to meet the intricate requirements of burn wound healing, especially in contaminated environments. The hydrogel is synthesized via a Schiff base reaction between quaternized chitosan (QCS) and OD, subsequently crosslinked with sulfadiazine (SDI). It incorporates conductive polyaniline (PANI) nanowires and polystyrene (PS) to improve electrical conductivity, mechanical stability, and antibacterial properties. An essential advancement in the QOSP hydrogel is its high-voltage plasma charge injection, which enables the creation of a homogeneous conductive network and markedly enhances charge retention, surface potential, and dielectric breakdown strength. This electroactive matrix facilitates prolonged charge storage and emulates the natural electric fields of skin, allowing for uninterrupted bioelectric stimulation without external power sources crucial for enhancing fibroblast proliferation, tissue regeneration, and epithelialization. Morphological and structural investigations using SEM, TEM, XRD, FTIR, and XPS validated the development of a porous, crystalline, and chemically altered network exhibiting enhanced hydrophilicity and polarity as a result of surface oxidation and molecular realignment. Rheological, thermal, and dielectric analyses demonstrated enhanced elasticity, thermal stability, and electrochemical performance, especially in QOSP-5, the optimized variation. The hydrogel demonstrated superior cytocompatibility, little hemolysis, and significant antibacterial efficacy against *Staphylococcus aureus* and *Pseudomonas aeruginosa*, with SDI release enhanced in acidic environments characteristic of infected wounds. In a mouse model of second-degree burn wounds infected with mixed bacterial strains, QOSP-5 markedly surpassed uncharged and non-conductive variations, expediting wound healing, diminishing infection, and lowering scarring. Histological and proteomic evaluations revealed increased granulation tissue thickness, collagen organization resembling normal skin, and reduced markers of fibrosis (TGF-β, α-SMA) and inflammation (iNOS), alongside a transition from Th2-dominated immune responses to a Th1 bias an effect essential for curtailing excessive fibrotic deposition. Label-free proteomics and pathway studies indicated a downregulation of inflammatory, coagulation, and necroptotic pathways, and decreased activity in proteasome and autophagy-related proteins, signaling a regulated immunological system conducive to recovery (Fig. 13) [96].

Wound infections present a growing therapeutic challenge because of persistent inflammation and the rise of drug-resistant bacteria. A set of self-repairing, conductive hydrogels, named COGFe, was created using CMC, oxidized sodium alginate (OSA), polymerized gallic acid (pGA), and Fe^{3+} ions. These hydrogels feature a dynamic dual network created by Schiff base bonds and catechol-Fe^{3+} coordination, which grants them exceptional toughness, conductivity, self-healing abilities, and strong adhesion, allowing for effective adaptation to the changing conditions of skin wounds. Along with mechanical flexibility, the hydrogels provide UV shielding and efficiently remove ROS, thereby decreasing oxidative stress at the injury location. Under NIR light, the hydrogels exhibited notable photothermal antibacterial effectiveness, achieving a 95 % rate of bacterial death in 5 min by disrupting bacterial membranes through localized thermal effects. The inherent antibacterial qualities of gallic acid successfully reduced accidental heat damage to nearby healthy tissue. The COGFe hydrogels promoted fibroblast growth and movement, demonstrated outstanding biocompatibility, and assisted in effective hemostasis. In a rat model of a full-thickness infected wound, treatment with the COGFe5 hydrogel along with NIR irradiation significantly enhanced bacterial clearance, promoted macrophage polarization from the pro-inflammatory M1 to the reparative M2 phenotype, and accelerated wound healing. This was shown by increased levels of the collagen-associated factor TGF-β and the angiogenesis indicator CD31, indicating improved tissue regeneration and immune regulation [97].

The extensive application of antibiotics has resulted in the emergence of drug-resistant bacteria, making wound treatment more complex. To tackle this, the H-NPs-12 hydrogel is a multifunctional, bioactive wound dressing designed to enhance healing, especially in MRSA-infected wounds, via a dynamic integration of structural, biochemical, and immunomodulatory approaches. This hydrogel, created by grafting 4-carboxyphenylboronic acid onto hydroxypropyl cellulose (HPC) and integrating silver-lignin nanoparticles (Ag-Lignin NPs), establishes a durable, injectable, self-healing, and conductive matrix crosslinked by dynamic borate ester linkages and hydrogen bonding. Structural investigation validated the effective production and incorporation of Ag-Lignin nanoparticles (~31–78 nm), which imparted a homogeneous porous shape, improved mechanical strength, and increased conductivity (up to 0.85 mS/cm) to the hydrogel. The conductivity, akin to that of biological tissues, allowed the hydrogel to facilitate bioelectrical signal transmission, while rheological assessments revealed shear-thinning properties, frequency-dependent viscoelasticity, and significant resilience to mechanical deformation, signifying exceptional self-healing and adaptability. Moreover, the hydrogel demonstrated minimal swelling ratios, extended in vivo stability (8–13 days), and robust adherence to moist and active biological tissues, such as skin and organs, preserving integrity even after stretching or washing, with adhesive strengths reaching 9.18 kPa. Biological experiments demonstrated significant antioxidant activity (exceeding 92 % DPPH scavenging), hemostatic effectiveness in a rat liver hemorrhage model (blood loss decreased to around 332 mg), and total antibacterial efficacy (100 % eradication) against *E. coli*, *S. aureus*, *C. albicans*, and MRSA. The hydrogel exhibited non-cytotoxicity (viability >90 %) and shown minimal histological damage in key organs, confirming superior biocompatibility. In vivo, H-NPs-12 hydrogel-treated MRSA-infected wounds exhibited markedly expedited closure, full healing by day 15, decreased inflammatory infiltration, and improved epithelialization, relative to commercial dressings and controls. Histologically, there was an increased collagen deposition (26.4 % by day 15), enhanced neovascularization (shown by heightened CD31 expression), and a rise in M2 macrophage polarization (high CD206/CD68 ratio), signifying a pro-regenerative immunological milieu (Fig. 14) [98].

6.2. Diabetic wounds

Chronic diabetic wounds show impaired angiogenesis and a heightened risk of bacterial infections because of the hyperglycemic environment, greatly hindering the healing process. The QP-P-D hydrogel is a multifunctional, injectable, conductive, and self-healing wound dressing developed via the chemical modification of CS, which was initially QCS to improve antibacterial properties and subsequently grafted with PANI to provide conductivity. The hydrogel, crosslinked by Schiff base interactions between the amine groups of QCS/PANI and the aldehyde groups of 4-arm PEG-CHO, exhibited significant porosity (~200 μm), remarkable swelling capacity (>2000 %), and pH-responsive drug

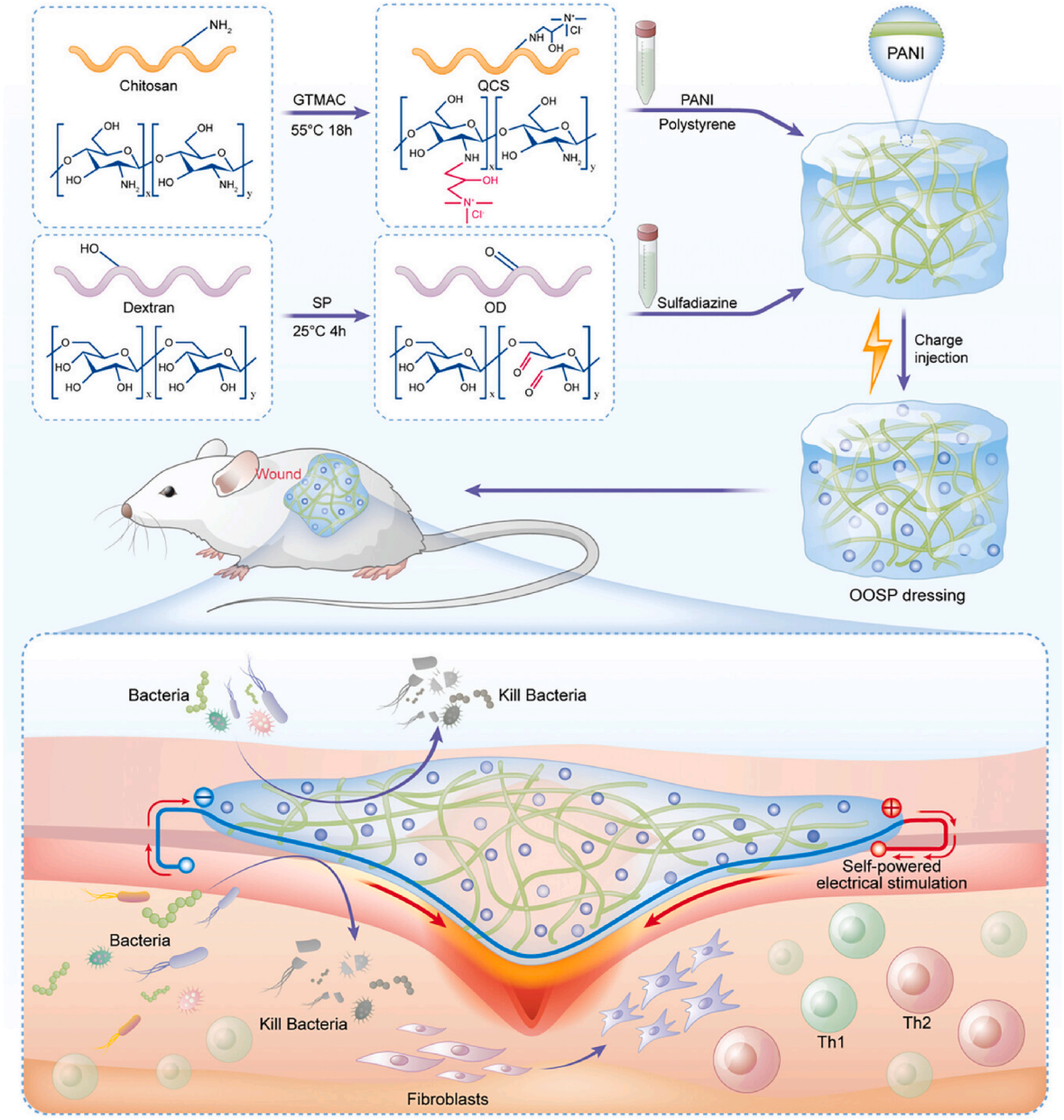

Fig. 13. The creation of QOSP hydrogel entails preparing QCS and OD, then merging PS and polyaniline nanowires (PANI), and finally adding charge to the QOSP hydrogel to develop a unique self-powered hydrogel dressing, which is then applied to the skin wounds of bacterially infected second-degree burn mice for the purpose of providing ES. QOSP hydrogel promotes wound healing without scars mainly by producing bioelectricity, ensuring cleanliness, and modulating the immune response to avoid excessive fibrosis. Reproduced with authorization from Wiley [96].

release. Structural characterisation using FTIR and NMR validated effective alteration, whilst UV–Vis and rheological tests demonstrated improved conductivity and mechanical tunability attributed to PANI. The hydrogel demonstrated smooth extrusion via thin needles (as small as 26G) and autonomously repaired upon mechanical rupture, so demonstrating its excellent injectability and self-healing properties essential for addressing irregular wounds. Mechanical tests indicated an enhanced compressive modulus with PANI, while the addition of deferoxamine (DFO), a medicinal drug that facilitates angiogenesis, resulted in a marginal decrease in stiffness. The hydrogel's conductivity (about 0.1–0.26 mS/cm) emulated that of human skin, facilitating its application in ES-based treatments. DFO was released in a regulated, pH-sensitive manner (74 % at pH 5.6), suitable for chronic wounds with acidic microenvironments, facilitating fibroblast migration, diminishing inflammation, and inducing VEGF and HIF-1α production to enhance vascularization. Antibacterial experiments exhibited around 90 % lethality against *S. aureus*, principally due to the quaternary ammonium groups of QCS and the interaction of PANI with lipoteichoic acid. Biocompatibility was outstanding, characterized by reduced hemolysis (<1 %), increased fibroblast proliferation, and FDA-stained morphology indicative of robust cell development. In vitro scratch studies demonstrated over 95 % fibroblast migration in QP-P-D groups, signifying a fast wound closure capability. Moreover, in HUVEC experiments, DFO markedly enhanced proliferation and migration, elevated angiogenic markers (VEGF and HIF-1α), and decreased cell death. The combination with ES enhanced cell viability through synergistic stimulation of the PI3K/Akt pathway. In vivo, utilizing a diabetic rat model, QP-P-D + ES therapy achieved near-complete wound healing by day 14, exceeding all other groups, alongside substantial epidermal regeneration and dense collagen deposition. Immunohistochemical staining demonstrated

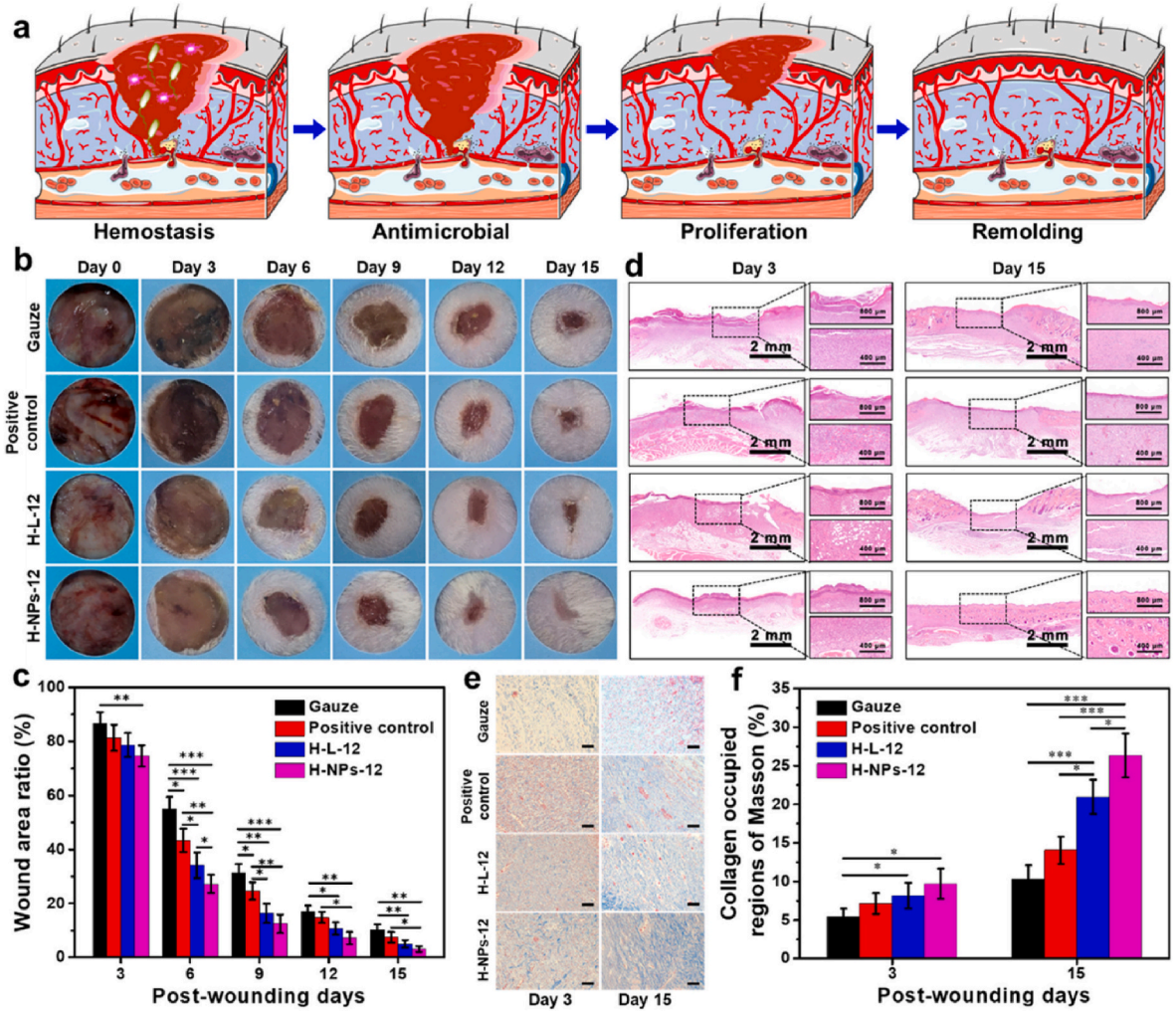

Fig. 14. Diagrams illustrating wound healing using hydrogel therapy. Visual depictions of the injuries managed with gauze, Tegaderm Film (positive control), H-L-12, and H-NPs-12. The diameter of the circle is 1.5 cm. The ratio of the wound area after treatment with gauze, Tegaderm Film, H-L-12, and H-NPs-12 at different time intervals. H&E-stained sections of skin tissue from the gauze, Tegaderm Film, H-L-12, and H-NPs-12 groups on days 3 and 15. Representative images of Masson staining on wound tissue (Scale bar: 30 μm). Examination of the collagen occupancy ratio in the newly formed tissue using Masson's trichrome staining. Reproduced with authorization from ACS [98].

significantly enhanced neovascularization (by CD31) and reduced inflammation (via $CD68^{+}$ cell infiltration) in the QP-P-D + ES group, corroborating the hydrogel's dual function in infection management and tissue regeneration [99].

Dissolving microneedles (DMNs) present a hopeful method for painless drug administration and biosensing; however, attaining multifunctionality with eco-friendly recyclability through photo-curable additive manufacturing is difficult. A DMN system has been created through the strategic design of photoprintable deep eutectic solvent (PDES)-based eutectogels to tackle the issues of diabetic wound healing and transdermal medication administration. The dissolving needle component was fabricated using an innovative ternary PDES comprising choline chloride (ChCl), itaconic acid (IA), and N-vinylpyrrolidone (NVP), referred to as CIN-PDES. This mixture provided a harmonious blend of mechanical durability and rapid breakdown, essential for skin insertion and effective drug release. NVP provided mechanical strength, IA promoted dissolution, and hydrogen bonding within the PDES network accelerated polymerization kinetics, as shown by FTIR, GPC, and heat studies. The CIN eutectogels exhibited remarkable solubility for hydrophobic drugs, up to 15,880-fold for curcumin and 8883-fold for insulin, demonstrating substantial drug-loading capacity attributed to interactions such as hydrogen bonding and ion-dipole forces. A glucose-responsive CHPG eutectogel was developed for the adhesive backing layer by integrating HEMA, glucose, and AAPBA to facilitate adhesion and responsive release, with TA included for antibacterial properties. This backing layer demonstrated exceptional mechanical tunability, adhesion to various substrates (up to 48.12 kPa on porcine skin), thermal stability (Tg = −31.5 °C), and prolonged integrity at sub-zero temperatures. The materials were produced via high-resolution DLP 3D printing, resulting in customized needle geometries and consistent nanoparticle dispersion attributed to PDES viscosity. The CHPG eutectogel backing layer facilitated recyclable 3D printing by dissolving in ethanol, resulting in about 90 % recovery of mechanical qualities. Mechanical tests and finite element analysis demonstrated that DMNs with square bases and a 4:1 aspect ratio provided the best penetration force (0.54 N) and fracture strength (0.95 N). Upon application, more than 80 % of the DMNs disintegrated within 10 min, facilitating rapid and thorough medication administration with minimum dermal injury. In vitro studies demonstrated superior biocompatibility (hemolysis <5 %, >90 % cell viability), facilitation of cell migration (up to 93.67 % scratch closure with curcumin), and significant antibacterial efficacy (>95 % eradication of *S. aureus* and *E. coli*). Glucose- and pH-responsive insulin-loaded nanoparticles (CMCS-PBA-based) demonstrated adjustable insulin release patterns, discharging over 91 % of insulin at 20 mM glucose and up to 32.64 % at pH 8.5, suitable for diabetic wound conditions. In diabetic rat models, the DMNs facilitated regulated, sustained

insulin release, maintaining stable glycemic control without inducing hypoglycemia in healthy subjects. Research on wound healing indicated expedited closure (up to 68.08 % by day 10), augmented collagen deposition, heightened neovascularization (elevated CD31 expression), and diminished inflammation (lower IL-6 levels) [100].

Hydrogels hold significant promise for addressing DFUs, yet their efficacy can be diminished due to adverse immune reactions and difficult wound environments, including elevated ROS and low oxygen availability. A multifunctional nanozyme-decorated hydrogel, MnCoO@PDA/CPH, was developed to tackle the complex problems of diabetic wound healing, especially in environments characterized by oxidative stress and hypoxia. The hydrogel was manufactured by a sequential procedure that included the production of $Mn_3[Co(CN)_6]_2$-based metal-organic frameworks, surface coating with mesoporous silica, calcination to produce MnCoO nanoparticles, and further PDA modification to improve stability and biocompatibility. The hydrogel matrix was synthesized by integrating MnCoO@PDA nanozymes with PVA, HA, aniline (AN), and 3-aminophenylboronic acid (ABA), then undergoing in situ polymerization and crystallization-induced cross-linking to provide a porous, elastic, and conductive hydrogel. The dynamic boronate bonds and hydrogen bonding enhanced its mechanical strength, self-healing capabilities, and superior rheological performance. Characterization demonstrated elevated conductivity (sufficient to illuminate an LED), consistent electrochemical impedance, and adjustable mechanical strength comparable to biological tissue. The inserted MnCoO@PDA nanozymes effectively replicated catalase function by degrading excess H_2O_2 into oxygen, thus mitigating oxidative stress and tissue hypoxia, exhibiting kinetic behavior akin to natural enzymes and maintaining catalytic stability. In vitro investigations including keratinocytes, fibroblasts, and endothelial cells under simulated diabetic foot ulcer (DFU) conditions validated the hydrogel's capacity to diminish intracellular ROS, increase oxygen levels, and markedly improve cell survival, proliferation, and migration. The hydrogel had significant anti-inflammatory properties, shown by reduced production of NO, TNF-α, and IL-1β in macrophages, combined with elevated levels of IL-10 and TGF-β, and facilitated a phenotypic transition of macrophages from M1 to M2 in both in vitro and in vivo settings. In a streptozotocin-induced diabetic rat model, the 2-CPH-NPs hydrogel expedited wound closure, markedly enhanced epithelial regeneration, diminished inflammation, increased collagen I and III deposition, and promoted neovascularization, as evidenced by elevated CD163+, integrin α3+, α-SMA+, and VEGF/PDGF expression levels. Immunostaining demonstrated reduced HIF-1α and ROS levels in treated wounds, confirming alleviation of hypoxia and oxidative injury (Fig. 15) [101].

6.3. Comparative analysis of conductive polymers in the infected and diabetic wound healing

CPs have emerged as versatile platforms for addressing complex wound environments, especially those complicated by infections or diabetes. In the case of infected wounds, the focus lies primarily on antimicrobial efficacy, bio ES, and responsive drug delivery. Several multifunctional hydrogels and nanogenerator-based systems such as PPY@PDA/PANI, CPH-AgNPs, HPEM, and PDES-based eutectogels demonstrate robust antibacterial performance (up to 100 % bacterial inhibition, including MRSA), mechanical resilience, and high conductivity (up to 2.89 S/m). These materials often utilize dynamic chemical bonding (Schiff-base reactions, catechol-Fe^{3+} coordination) for self-healing and adhesion. Technologies like A-A TENGs and QOSP hydrogels further integrate ES via triboelectricity or internal charge storage, promoting enhanced fibroblast migration and inflammation control. Advanced systems even allow real-time sensing of wound biochemistry (ammonia detection), enabling precise, app-controlled drug release. Most infected-wound-targeting systems also prioritize rapid hemostasis, photothermal antibacterial action, and immune modulation (macrophage M1-to-M2 switching), leading to complete healing in preclinical models within 10–15 days. In contrast, diabetic wound healing demands added functionality, as the hyperglycemic microenvironment impairs angiogenesis, oxygenation, and immune responses. Conductive hydrogels such as QP-P-D and MnCoO@PDA/CPH have been tailored to overcome oxidative stress and hypoxia through integration of nanozymes (MnCoO) and angiogenesis-enhancing drugs like DFO. These systems often feature pH- or glucose-responsive mechanisms for controlled drug release, targeting the acidic and fluctuating diabetic wound milieu. ES plays a pivotal role, enhancing angiogenesis via pathways such as PI3K/Akt and promoting neovascularization through upregulated CD31 and VEGF expression. Advanced delivery modalities such as photoprintable DMNs using eutectogels allow for customized, minimally invasive administration of insulin or curcumin, with rapid needle dissolution and high drug-loading efficiency. These diabetic-focused materials display remarkable porosity (up to 200 μm), swelling (≥2000 %), and conductivity (~0.26 mS/cm), supporting cellular proliferation even under stress. Healing times in diabetic rat models are slightly longer than for infected wounds (~14 days to near-complete closure), likely due to systemic metabolic impairment, but the outcomes show reduced scarring and restored tissue function. Overall, while both systems share core attributes biocompatibility, conductivity, antibacterial efficacy, and controlled drug release they differ in strategic emphasis. Infected wound systems focus more on broad-spectrum antimicrobial activity, mechanical robustness, and sensing or photothermal destruction of pathogens. Diabetic wound platforms prioritize angiogenesis, ROS regulation, and metabolic responsiveness, often requiring more sophisticated signal-responsive drug delivery and enzyme-mimicking functionalities. Yet, in both cases, the use of CPs like polyaniline, polypyrrole, and their composites proves central in achieving electroactive, smart wound care that adapts to complex healing environments. Table 3 further provides a comparative table of the studies based on previous discussions.

7. Wound monitoring

Flexible biosensors made from conductive hydrogels possess great promise for health tracking and interactions between humans and machines. Nonetheless, developing robust and stable hydrogels continues to be a challenge. A new conductive nanocomposite hydrogel has been developed via one-pot radical polymerization of 3-acrylamidophenylboronic acid (APBA) and acrylamide (AM), integrating CNTs with LAPONITE® XLG nanosheets. The hydrogel exhibits outstanding mechanical characteristics as a result of non-covalent interactions such as B–N coordination and hydrogen bonding, presenting a tensile strength of 252–323 kPa, fracture strain of 880 %–1200 %, and Young's modulus of 48–50 kPa. It offers a significant gauge factor (reaching 9.43) and extensive detection ranges, allowing for accurate motion sensing [102]. Efficient wound care remains a clinical obstacle due to the complex healing process and the need for continual monitoring. A hydrogel dressing with multifunctional capabilities has been developed, incorporating conductivity, temperature sensitivity, antimicrobial features, and biocompatibility. The hydrogel, made of polyacrylic acid (PAA)--grafted poly(N-isopropylacrylamide) (PNIPAM), vinyl-based polyacrylamide (PAM) and silver nanowires (AgNWs), features a conformal, temperature-responsive matrix, enhanced mechanical strength from semi-interpenetrating polymer networks, and a three-dimensional conductive framework with antibacterial and sensing capabilities. The gadget, featuring a Bluetooth module, permits wireless, instant tracking of wound temperature, facilitating prompt detection of infections. This innovative technique shows considerable potential for advanced wound care and diagnostic applications [103].

Serious skin cuts require extended healing times, during which outside elements can cause pain, re-injury, and fluid leakage, thus increasing the risk of complications. Traditional dressings do not provide timely feedback, making immediate wound monitoring essential.

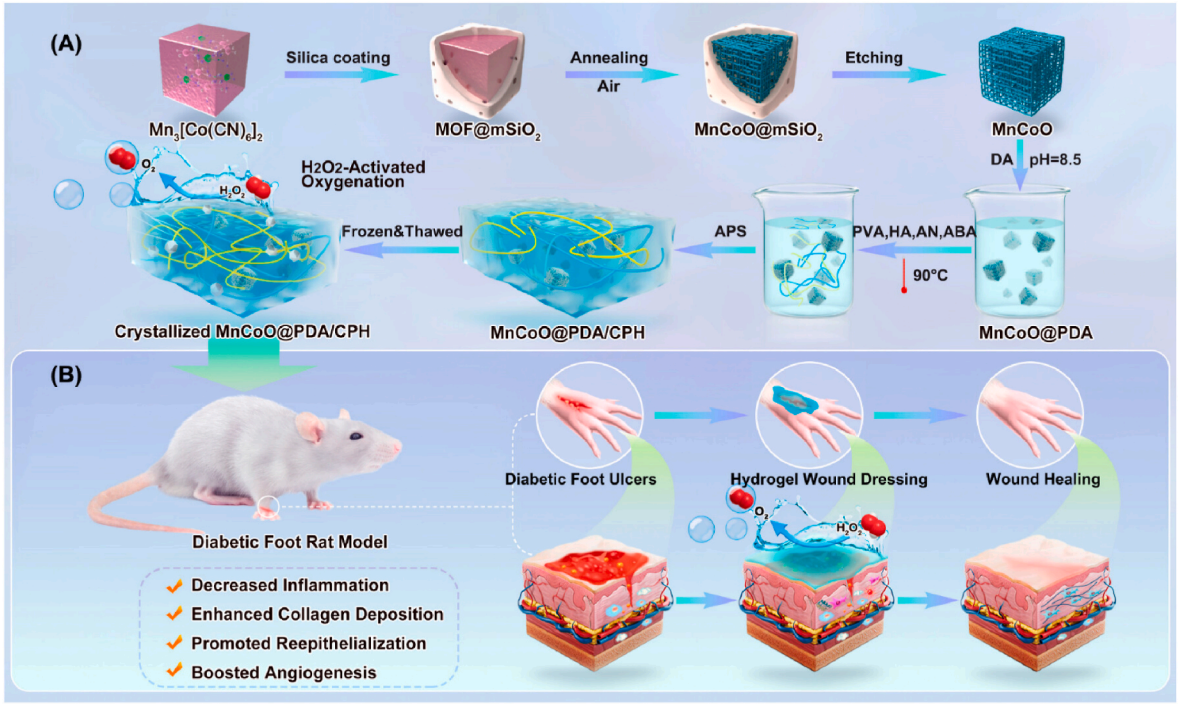

Fig. 15. Illustration showing the manufacturing process and later utilization of the hydrogel. A chart depicting the manufacturing methods of MnCoO@PDA/CPH hydrogels. (B) Diagram showing MnCoO@PDA/CPH hydrogels with H2O2-triggered oxygenation properties to improve healing of diabetic wounds. Reproduced with authorization from ACS [101].

The research details the creation, characterisation, and use of an innovative CNTs/graphene/GelMA mat produced using electrospinning and UV-crosslinking of GelMA, subsequently incorporating CNTs and graphene in situ, with chitosan employed for adhesive integration. Electrical resistance studies indicated that 0.04 g of CNTs gave excellent conductivity (110 Ω/sq) without aggregation. Structural and compositional investigations by FTIR and Raman spectroscopy validated robust hydrogen bonding, van der Waals interactions, and π-π stacking among GelMA, graphene, and CNTs. Rheological assessments revealed enhanced mechanical capabilities and solid-like characteristics, with the CNTs/graphene/GelMA matrix exhibiting a superior storage modulus compared to both GelMA and graphene/GelMA matrices. The findings of breathability, porosity, swelling/deswelling ratios, and water vapor transmission rate demonstrated that the incorporation of CNTs optimized gas permeability and moisture regulation, which are critical for wound healing. SEM pictures demonstrated that CNTs augmented surface roughness and porosity, boosted conductivity, and functioned as connectors between graphene sheets. The mat demonstrated excellent structural integrity under mechanical stress and regained its original shape post-deformation. Biocompatibility experiments demonstrated exceptional cytocompatibility and facilitated cell growth and attachment. Mechanical studies indicated that the CNTs/graphene/GelMA mat had superior tensile strength and Young's modulus compared to GelMA alone, while preserving flexibility and demonstrating little hysteresis under cyclic loading. The mat operated efficiently as a strain sensor, demonstrating a linear and reproducible $\Delta R/R_0$ response over strain levels (0–85 %) and frequencies (0.125–1 Hz), exhibiting remarkable endurance over 700 cycles. It functioned as a moisture sensor, accurately detecting artificial interstitial fluid (AIF) with great sensitivity, while exhibiting no influence from ambient humidity or temperature fluctuations (35–42 °C). Demonstration trials with a balloon model and a rat wound model exhibited real-time, wireless monitoring of strain and moisture through a mobile device, with dependable signal output. Histological study (H&E staining) in rats demonstrated accelerated wound healing and reduced inflammation in mat-treated groups relative to controls, with the CNTs/graphene/GelMA mat exhibiting performance comparable to GelMA alone, hence confirming its biocompatibility and therapeutic safety [104].

Skin-electronic interfaces hold considerable promise for diagnostics, treatment, health monitoring, and wearable technology; however, they face challenges like poor adhesion in wet or dynamic environments, leading to reduced signal precision. This paper details the creation, characterisation, and deployment of a multifunctional PAMS composite hydrogel, designed for sophisticated biomedical applications like wound healing, physiological monitoring, and skin-electronics interfaces. The researchers developed PAMS hydrogels by integrating MXene nanosheets and SDS into a PA hydrogel matrix, resulting in improved conductivity, mechanical characteristics, and micro-nanostructures favorable for adhesion. Chitosan-based priming solutions, sensitive to pH and ultrasonic (US), created a topologically entangled third network with hydrogel-tissue hybrids, facilitating reversible and improved adhesion by US cavitation and hydrogen bonding. The optimization of digital light-processing (DLP) 3D printing enabled the accurate production of octopus-inspired adhesive patterns, with performance adjusted by altering sucker diameter and spacing. Finite element models and experimental measurements validated maximum adhesion at ideal suction chamber dimensions under defined preload and ultrasound conditions. The PAMS hydrogels exhibited remarkable electromechanical sensitivity, characterized by elevated gauge factors and consistent strain response throughout an extensive deformation range, including sub-zero temperatures. Their photothermal and thermally responsive characteristics, stemming from the semiconducting capabilities of MXene, enabled real-time observation of strain and temperature variations, rendering them suitable for dynamic anatomical areas like joints. Biocompatibility was validated using cell viability studies with Saos-2 cells, demonstrating over 90 % survival, while antibacterial evaluations against *E. coli* and *S. aureus* revealed over 99 % inhibition attributable to the synergistic effects of MXene-induced membrane rupture and SDS's biofilm interference. In vivo frostbite wound models in rats shown markedly enhanced healing using hydrogel patches, particularly when

Table 3
A comparative analysis of using conductive platforms in infected and diabetic wound healing.

Feature	Infected wounds	Diabetic wounds	Further information can be found in these studies abound diabetic and infected wound healing
Primary Challenges	Bacterial infection, inflammation, biofilm formation	Impaired angiogenesis, oxidative stress, delayed healing due to hyperglycemia	[90–101]
Conductive Materials Used	Polyaniline (PANI), polypyrrole (PPY), CNT-PDA, AgNPs, MXene@PDA, QCS, eutectogels	QCS-PANI, MnCoO@PDA nanozymes, PDES-based eutectogels, DFO, CMCS-PBA	
Key Functionalities	Antibacterial, photothermal therapy, ES, real-time sensing, drug release	Angiogenesis promotion, ROS scavenging, pH/glucose-responsive drug release, oxygen generation	
Drug Delivery Mechanisms	Electrically-triggered, photothermal, prolonged Fickian diffusion	Responsive to pH/glucose, injectable hydrogels, dissolving microneedles	
Bacteria Targeted	*S. aureus*, *E. coli*, MRSA, C. albicans	*S. aureus*, *E. coli*, occasionally MRSA	
Electrical Conductivity	Up to 2.89 S/m	0.1–0.26 mS/cm	
Self-Healing and Adhesion	Strong, via dynamic covalent bonds and mussel-inspired adhesion	Present, often via borate ester bonds and hydrogen bonding	
Biocompatibility	High: minimal cytotoxicity and hemolysis, promotes fibroblast growth	High: supports cell proliferation under stress, low ROS, low inflammatory cytokines	
Mechanical Strength	High modulus, shear-thinning, suitable for dressing replacement	Tunable for injectable and 3D-printed formats	
Stimulation Source	Triboelectric (A-A TENGs), app-triggered, internal bioelectricity	Exogenous ES or internal, via plasma charging or nanozymatic effects	
Healing Time in Animal Models	10–15 days (infected full-thickness wounds, MRSA models)	~14 days (diabetic rat models, DFUs)	
Angiogenesis Support	Moderate to high (via VEGF, CD31, α-SMA)	High (VEGF, HIF-1α, CD31, TGF-β, improved oxygenation)	
Advanced Features	Ammonia gas sensing, app-controlled release, NIR photothermal therapy	Nanozyme-based oxygenation, 3D-printed microneedles, glucose-responsive insulin delivery	
Scarring and Fibrosis Control	Reduced fibrosis, some systems (QOSP) downregulate TGF-β and α-SMA	Significant reduction, especially in systems that regulate immune polarization and collagen architecture	
Overall Focus	Infection control, electrotherapy, smart monitoring	Regeneration, metabolic regulation, oxidative stress mitigation	

paired with ultrasound therapy, resulting in decreased wound size, re-epithelialization, hair follicle regeneration, and superior histology results without detectable toxicity [105].

Despite remarkable progress in the development of flexible, conductive hydrogels for biomedical and health-monitoring applications, significant challenges remain in enhancing their mechanical robustness, long-term stability, biocompatibility, and multi-functionality, particularly in dynamic or moist biological environments. Current research emphasizes addressing these hurdles through advanced material integration, such as combining conductive nanomaterials (CNTs, graphene, MXene) with smart polymers and nanosheets (LAPONITE®, CS, SDS), which provide improved mechanical strength, elasticity, and electrical performance via non-covalent interactions like hydrogen bonding, B–N coordination, and π-π stacking. Yet, the pursuit of hydrogels with enhanced adhesion, environmental tolerance (sub-zero operation), and tissue-integration remains complex, especially for applications requiring real-time, wireless feedback in wound care or motion sensing. Future innovations will likely focus on developing hydrogels with programmable, responsive properties such as those that alter conductivity, adhesion, or drug release in response to temperature, pH, or ultrasound stimulation, while leveraging technologies like DLP 3D printing and bioinspired microstructuring to customize device performance and interface precision. Moreover, integrating multifunctionality (antimicrobial, strain sensing, moisture detection) into a single hydrogel platform without compromising biocompatibility or mechanical integrity is critical. As such, the convergence of materials science, electronics, and tissue engineering is expected to yield next-generation skin-electronic interfaces and wound dressings that offer precise diagnostics, accelerated healing, and robust, personalized monitoring across varied physiological and environmental conditions.

The PAMS hydrogel patch demonstrates strong potential for real-time wound monitoring, particularly through its strain- and temperature-sensitive properties, which are critical for managing complex wound environments. Its integration of MXene nanosheets endows the hydrogel with high conductivity and photothermal responsiveness, enabling the detection of subtle physiological changes. When applied to joints or other dynamic areas, the patch effectively tracks mechanical strain during movement, offering insights into wound mobility and healing progress. Furthermore, the hydrogel's negative temperature coefficient allows for accurate temperature sensing in the wound area, which is essential for identifying inflammation, infection, or changes in blood flow. Infrared-induced heating tests revealed that the patch responds rapidly and uniformly to temperature changes, with resistance decreasing as temperature rises, indicating high thermal sensitivity. This ability to monitor both strain and temperature in a continuous and noninvasive manner positions the PAMS hydrogel as a valuable tool for assessing wound healing status, particularly in conditions prone to complications such as frostbite or infection.

8. The overall trend in conductive polymers for wound healing

The previous discussions highlighted the importance of using CPs for the process of wound healing. In order to facilitate in understanding the landscape of the field, we have summarized most of the studies in Table 4. Since Table 4 provides a good summary and main results of the studies, we further analyzed the composition of these platforms, other features including biological functions and the cell lines as well as animal models utilized in the studies. Describing and analysing these studies can further summarize the key progresses and trends in the field and provide better understanding of what is the current status (analysis was solely performed based on Table 4).

8.1. Conductive polymer/platform, material form and composition components: a critical analysis

The diverse conductive platforms used in wound healing can be broadly categorized by their material form, with notable prevalence of hydrogels, electrospun fibrous membranes, and coated/printed composites. Among these, hydrogels dominate due to their tunable

viscoelasticity, injectability, water content, and tissue-like softness, making them ideal for conforming to irregular wound geometries and providing a moist healing environment. Electrospun membranes are frequently used owing to their high surface area, nanofibrous architecture mimicking the ECM, and their ability to be loaded with drugs, conductive fillers, or antibacterial agents. Additionally, coated woven fabrics and composite films though less represented are gaining traction for their mechanical robustness and flexibility, suitable for wearable or reusable systems. A clear trend is the combination of synthetic and natural polymers, often merged with conductive polymers or nanofillers to create multifunctional platforms that support not just passive wound coverage but also active therapeutic roles such as ES, drug delivery, or ROS scavenging. Over time, these forms are converging into smart wound dressings, integrating multiple properties like self-healing, conductivity, and biocompatibility, thereby moving beyond simple scaffolding to bio-interactive and bioresponsive platforms.

A critical examination of the CPs across the dataset reveals a strategic selection based on desired bioelectronic functionality, processability, and biocompatibility. PPy and PANI are the most commonly utilized, primarily because of their ease of synthesis, cost-effectiveness, and moderate biocompatibility; however, they are non-biodegradable and require careful modification or blending with biopolymers to avoid long-term toxicity. PEDOT:PSS stands out for its superior electrical conductivity and long-term stability, making it a favored choice for coatings in systems intended for extended bioelectronic interface, such as those employing ES. In contrast, carbon-based alternatives like MXenes, rGO, and CNTs offer exceptionally high conductivity and mechanical strength, but raise toxicity and environmental persistence concerns, particularly if not adequately functionalized. As the field advances, the choice of conductive polymer is becoming more nuanced, driven by a need to balance biofunctionality (cell signaling, wound pH response), ES capabilities, and in vivo safety. The inclusion of dopants, nanoparticles (Ag, Fe^{3+}), and functional side chains (catechol, quaternary amines) is indicative of a shift from simple conductive scaffolds to multifunctional, responsive bioelectronic materials.

The design of composite conductive platforms in wound healing is increasingly focused on modular, synergistic systems that combine the strengths of multiple materials to enhance both functionality and biocompatibility. A recurring strategy is the incorporation of natural polymers such as gelatin, chitosan, silk fibroin, and collagen, which not only offer intrinsic bioactivity (promoting cell adhesion, providing antibacterial effects, or ROS scavenging) but also help mitigate the cytotoxic effects of synthetic conductive polymers such as PANI and PPY. These base polymers are frequently functionalized or crosslinked with agents like Fe^{3+}, catechol groups, or β-cyclodextrin to enable self-healing, adhesive, or injectable properties. Simultaneously, inorganic nanoparticles such as silver (AgNPs), ZnO, or calcium phosphates are integrated for antimicrobial or osteogenic enhancements, particularly for infected or deep wounds. There is also a notable emergence of stimuli-responsive composites that release drugs or change behavior in response to ROS, pH, temperature, or mechanical stress (DOXH-loaded PFKU, PQCD-A@Cur). This layered design philosophy reflects a shift toward bioelectronic therapeutics, where a single wound dressing can simultaneously monitor, stimulate, protect, and regenerate tissue underscoring the importance of interdisciplinary material engineering in the next generation of wound care platforms.

To advance the efficacy and clinical potential of conductive wound healing platforms, next-generation design strategies should focus on biointegration, responsive functionality, and regenerative microenvironment control. One novel approach is the incorporation of multimodal, spatiotemporally controllable drug delivery systems into the conductive scaffold. While some current systems offer ROS-responsive or pH-sensitive release (PFKU/DOXH membranes), these could be further refined by integrating layer-by-layer nanostructures, microcapsules, or 3D-printed reservoirs that allow for sequential or on-demand release of bioactive agents, such as anti-inflammatories, growth factors, or even exosomes. Coupling this with electroactive control mechanisms, for instance, using mild ES to trigger release from electro-responsive carriers would make wound therapy highly customizable. Additionally, improving cell-instructive conductivity could be achieved by using gradient conductivity designs, where conductivity increases toward the wound core to promote directed cell migration and tissue regeneration. Incorporating anisotropic architectures (aligned nanofibers or micropatterned hydrogels) can also enhance electro-guided cellular behavior, especially for re-epithelialization and angiogenesis. These architectural and release features should be tightly integrated with real-time biosensing elements (for pH, glucose, lactate, or cytokines) that can inform both therapy and clinical decision-making. On the material composition front, innovations should aim at balancing biofunctionality with electrical performance while ensuring biosafety and degradability. Conductive polymers like PPY, PANI, and PEDOT:PSS, while effective, can be structurally brittle and biologically inert, so functionalization with short peptides (RGD), anti-inflammatory moieties (curcumin, flavonoids), or extracellular vesicle-binding ligands could add bioactivity to their surface chemistry. Additionally, novel bioconductive hybrids could be developed by blending enzymatically degradable polymers (gelatin methacrylate, HA-SH) with biominerals or plant-based antioxidants to address chronic inflammation and oxidative stress, two major barriers to healing in diabetic or infected wounds. Emerging materials like 2D nanomaterials (black phosphorus, boron nitride nanosheets) or MXene variants with surface-modified functional groups hold promise for delivering controllable degradation rates and ultra-high conductivity while maintaining biocompatibility. Another exciting avenue is the development of biodegradable ionic liquids and conductive zwitterionic polymers that mimic native ion transport mechanisms of the skin, thereby restoring electrophysiological homeostasis during healing. Ultimately, these material systems should be designed for scalable, one-pot synthesis, with minimal cytotoxicity and efficient integration into wearable, stretchable, and breathable constructs, pushing the boundaries from passive scaffolds toward fully interactive, therapeutic bioelectronics for wound care. Fig. 16 further demonstrates these discussions.

8.2. Fabrication methods

Many of the listed fabrication methods such as in situ chemical polymerization, multiple functionalization steps, or sequential layer assembly offer precise control over composition, architecture, and biofunctionality, but often at the cost of scalability and reproducibility. For instance, soft-template synthesis of AgPPy nanotubes, ultrasonic self-assembly of Me-PANI NPs, or Schiff-base/IPN hydrogels enable intricate structures and responsive behavior but would face significant challenges during mass production, sterile packaging, and batch-to-batch consistency. In contrast, methods like electrospinning and UV-crosslinkable hydrogels are more aligned with industry standards, providing better throughput, structural uniformity, and design tunability. The use of spin-coating, 3D printing, and freeze–thaw cycles also indicates a shift toward fabrication techniques compatible with wearable and patch-like wound dressings, but they must be further simplified or automated for clinical translation. A key strength seen across the fabrication methods is the integration of multiple functionalities during synthesis. Many systems simultaneously incorporate conductive agents (PPy, PANI, rGO) and bioactive elements (AgNPs, VEGF, curcumin) through co-polymerization, nanoparticle templating, or sequential crosslinking strategies. For instance, Fe^{3+}-mediated crosslinking not only supports hydrogel formation but also offers ionic conductivity and wound responsiveness, while Schiff-base bonding facilitates injectability, self-healing, and pH-sensitivity. Moreover, the use of dynamic covalent chemistry (imine, borate ester, catechol-metal interactions) enables adaptability, on-tissue adhesion, and responsiveness to biochemical cues, which is critical for chronic wound environments. These advanced chemistries, however, require tight control over

Table 4
The application of conductive platforms in wound healing acceleration.

Conductive Polymer/platform	Material Form	Composite Components	Fabrication Method	Key Functional Properties	Biological Effects	In Vivo/In Vitro Model	Healing Outcome/ Performance	Refs
Polypyrrole (PPY)/TENG Patch	Electrospun membrane	PPY, PCL, PLGA	Electrospinning + Chemical Vapor Deposition	High conductivity, breathability, flexibility, wettability, mechanical strength, self-powered electrical output	Antibacterial (*E. coli* & *S. aureus*), enhanced fibroblast proliferation, migration, adhesion; reduced inflammation	In vitro (NIH-3T3 cells, bacterial cultures); In vivo (infected diabetic rat model)	Faster wound closure, better collagen deposition and organization, reduced inflammation (IL-6), increased angiogenesis (CD31, VEGF), enhanced ECM formation (TGF-β), complete epithelialization	[37]
PDA@AgNPs-PPyGel-Fe	Hydrogel	Polydopamine-coated Ag nanoparticles (PDA@AgNPs), PPy, gelatin, Fe^{3+}	In situ chemical reduction, Fe^{3+}-mediated crosslinking to form hydrogel	Porous, flexible, high swelling ratio, high water content (~85 %), conductivity (24–36 mS/cm), compressive strength (up to 55 kPa), self-healing (30 min at 37 °C), antioxidant (DPH/ABTS scavenging), rheological stability	Antibacterial (*S. aureus*, *E. coli*), antioxidant activity, hemostasis, non-hemolytic, supports L929 fibroblast viability (>80 %), promotes coagulation (low BCI)	In vitro: L929 cells, *E. coli*, *S. aureus*, blood compatibility tests	Strong antibacterial activity (>90 % kill), excellent cytocompatibility, non-hemolytic, rapid self-healing (30 min), high antioxidant efficiency (100 %), potential for wound exudate absorption and infection control	[40]
PPy-BiOCl intercalated nanosheets	Nanosheets (2D intercalated)	Polypyrrole (PPy), Bismuth Oxychloride (BiOCl)	Solvothermal synthesis of BiOCl + in situ ultrasonic polymerization of PPy (space-confined intercalation approach)	NIR photoresponsiveness, high photothermal conversion (~50 °C in 10 min), strong NIR absorption, enhanced ROS generation (PDT), improved photocarrier separation, atomic-level intercalation, good dispersion, excellent photothermal and photodynamic stability, biocompatibility, hemocompatibility, low PL emission, conductivity through π–π* transitions, crystalline stability, amorphous PPy intercalation in BiOCl layers	Excellent antibacterial effect under NIR light (99.2 % against *E. coli* and *S. aureus*), stable across 3 cycles, low cytotoxicity (BMSC viability >98 %), low hemolysis (<1 %), reduced inflammation, increased ROS production, destruction of bacterial membranes, enhanced collagen deposition	In vitro: *E. coli*, *S. aureus*, BMSC cells; In vivo: full-thickness infected wound mouse model	>91 % wound area closure at 14 days; significant reduction in pus/inflammation; enhanced collagen deposition; re-epithelialization; antibacterial rate >91.9 % in vivo; rapid local temperature rise (30 °C–50 °C); no organ toxicity in major organs; shows synergistic PDT/PTT healing effects and high biocompatibility for wound infection treatment	[42]
PANI (polyaniline)	Hydrogel (PSP hydrogel)	PAM (polyacrylamide), SHA (sulfonated hyaluronic acid), PANI	In situ polymerization of aniline in pre-formed PAM matrix	High conductivity (~1.05–1.20 mS/cm), mechanical strength, swelling capacity (SR ~1373 %), dynamic mechanical stability	Cytocompatibility with L929 fibroblasts, antibacterial activity (especially against Gram-positive bacteria)	In vitro: Biofilm assays, bacterial viability; In vivo: Infected chronic wound model in mice	Enhanced wound closure rate, epithelial thickness, collagen deposition, granulation tissue maturation, and angiogenesis ($CD31^+$)	[44]

(*continued on next page*)

Table 4 (*continued*)

Conductive Polymer/platform	Material Form	Composite Components	Fabrication Method	Key Functional Properties	Biological Effects	In Vivo/In Vitro Model	Healing Outcome/ Performance	Refs
PANI (polyaniline), MXene ($Ti_3C_2T_x$)	Hydrogel (PVA/ MXene/PANI or PMP hydrogel)	PVA (polyvinyl alcohol), MXene ($Ti_3C_2T_x$), PANI (polyaniline)	Incorporation of MXene and in situ polymerization of aniline within the PVA matrix to form chemical bonds and hydrogen bonding network	High tensile strength (4.1 MPa) High fracture energy (130 kJ/m^2) High conductivity (0.22 S/m) Antibacterial (NIR-activated via MXene) Wear-resistant and flexible	Inhibits bacterial activity (in vitro and in vivo) Promotes cell proliferation and migration via ES	In vitro: Antibacterial activity, cell proliferation, and migration assays In vivo: Skin wound healing model	Accelerates skin wound healing Enhances angiogenesis and collagen deposition Demonstrates potential as a multifunctional, wear-resistant wound dressing	[45]
PANI (polyaniline), grafted onto MeGC forming Me-PANI NPs	Nanocomposite hydrogel (Me-PANI NPs@PAM hydrogel)	Polyacrylamide (PAM) MeGC (methacrylated glycol chitosan) PANI (grafted onto MeGC) Me-PANI nanoparticles (self-assembled from PANI-g-MeGC)	Grafting PANI onto MeGC to form amphiphilic copolymer Ultrasonic self-assembly into Me-PANI NPs Incorporation of Me-PANI NPs into PAM hydrogel network as crosslinkers	High swelling ratio (~1300 %) Stretchability (up to 400 %) Enhanced compressive and tensile strength Photothermal conversion under NIR (up to ~58 °C in 10 min) Water retention: 96.4 % (1 day), 69.6 % (7 days) Maintains structure and function under NIR Biocompatible (NIH 3T3 cell viability >80 %)	Non-toxic to NIH 3T3 fibroblasts Promotes fibroblast proliferation Kills *Staphylococcus aureus* and MRSA biofilms upon NIR-induced heating Effective antibacterial action is NIR-dependent (≥50 °C)	Antibacterial activity against SA and MRSA NIH 3T3 cell viability and proliferation assays NIR-induced heating and photothermal testing	Maintains a moist wound environment Strong antibacterial performance with external NIR stimulus Good mechanical and thermal properties for dynamic wound dressing applications Promising as a smart dressing for bacterial-infected skin wounds	[46]
PEDOT:PSS (poly(3,4-ethylenedioxythiophene): polystyrene sulfonate)	Electroconductive porous membrane (P5 membrane) coated with PEDOT:PSS, used as a wound patch with or without cell sheet integration	Porous polymer substrate (controlled by spin-coating speed) PEDOT:PSS conductive layer Collagen (coating for biocompatibility and bioactivity) Cell sheet (keratinocyte monolayer in some configurations)	Spin-coating to control porosity (1000–5000 rpm) Repeated PEDOT:PSS coatings (optimal at 6 times) Collagen coating for improved adhesion and biofunctionality Cell culture for sheet formation (with subsequent ES)	Tunable porosity and mechanical stiffness (Young's modulus up to 214 MPa for P5) Electrical conductivity increases with coating thickness Surface roughness enhances cell adhesion (up to 23.07 nm) Reversible resistance for monitoring cell sheet formation and detachment Effective cell sheet transfer upon −200 mV stimulation Biodegradability tunable with collagen coating	Enhanced cell proliferation, spreading, and actin organization on porous (P5) vs flat (F5) surfaces Cell viability >80 %, with ES promoting actin network formation Optimal PEDOT:PSS coating (6 ×) balances stiffness and bioactivity Reduced TNF-α (inflammation marker) and enhanced expression of CD31 (angiogenesis), K14/K10 (epithelial regeneration), and Occludin/Claudin-1 (barrier formation)	In vitro: Cell attachment/ proliferation (NIH3T3, keratinocytes), ES studies, resistance monitoring In vivo: Full-thickness excisional wound model in mice, histological analysis at days 0, 1, 3, 5, and 7	Rapid wound closure (only 4.8 % remaining wound area by day 7 under ES) Enhanced epithelial thickness, angiogenesis (CD31), and reduced inflammation (TNF-α) Effective re-epithelialization and barrier formation (Occludin/Claudin-1 expression) Porous membrane under ES outperformed flat surfaces and non-stimulated controls	[47]
PLGA/PDA/CS (Poly(lactic-co-glycolic acid)/Polydopamine/ Chitosan)	Electrospun fibrous membrane	PLGA: Base polymer PDA: Coating for adhesion and hydrophilicity	Electrospinning, followed by surface modification with PDA and CS coatings	Super-hydrophilicity (WCA ~0°) Swelling ratio: 585.1 ± 3.7 %	Promotes cell adhesion Enhances fibroblast proliferation	NIH 3T3 fibroblasts Scratch assay (fibroblast migration) CCK-8 assay, MTT assay,	Accelerated fibroblast proliferation under ES (2.0 × compared to PLGA)	[106]

(*continued on next page*)

Table 4 (*continued*)

Conductive Polymer/platform	Material Form	Composite Components	Fabrication Method	Key Functional Properties	Biological Effects	In Vivo/In Vitro Model	Healing Outcome/ Performance	Refs
		CS (Chitosan): Coating for improved conductivity and cell interaction		Wet electrical conductivity: 2.85 × 10^{-3} S/cm in DMEM Tunable mechanical properties (within skin dressing range) High protein adsorption (fibronectin) Biocompatibility (non-cytotoxic)	Improves collagen production (↑ hydroxyproline) Supports cell migration Responsive to ES	Live/dead staining Protein adsorption using FITC-tagged serum proteins	Enhanced re-epithelization (97.4 % wound closure in 12h with ES) Increased collagen production Superior cell adhesion and viability (113.9 ± 2.8 %) Electrically conductive and hydrophilic, promoting faster and more efficient healing	
DOXH-loaded PFKU membrane with 3D-printed GelMA-Bio-IL conductive hydrogel (MD-CH)	Electrospun fibrous membrane (PFKU/DOXH) 3D-printed conductive hydrogel strips on the surface (GelMA-Bio-IL)	PFKU (Polymeric base with thioketal group for ROS responsiveness) DOXH (Doxorubicin-hydrazone, drug with immunomodulatory and anti-inflammatory effect) GelMA (Gelatin methacryloyl) Bio-IL (Biocompatible ionic liquid)	Electrospinning for PFKU/DOXH membrane 3D printing + UV polymerization for conductive GelMA-Bio-IL hydrogel strips onto membrane	ROS-responsive degradation (due to thioketal linkage in PFKU) Drug release: Burst in 30 min; responsive to H_2O_2 Electrical conductivity: ~0.754 ± 0.040 S/m (hydrogel with 5 % Bio-IL) Mechanical performance: Compressive modulus: 59.26 ± 5.19 kPa Tensile modulus: Softened with hydrogel, MD ~82.05 MPa Elasticity: Maintained under 10 cycles of 10 % strain Excellent biocompatibility (>95 % cell viability) High surface area-to-volume ratio	Promotes endothelial cell migration (HUVECs) Induces M2 macrophage polarization (anti-inflammatory phenotype) Scavenges ROS Reduces pro-inflammatory cytokines: IL-6, IL-1β, TNF-α Enhances VEGF & PDGF expression (angiogenesis factors) Boosts collagen I and TGF-β1 modulation Supports tissue regeneration and scar reduction	In vitro: HUVECs (Human Umbilical Vein Endothelial Cells) RAW 264.7 macrophages (flow cytometry for M2 markers) Cytotoxicity assay, wound healing assay, ROS & cytokine quantification In vivo: Diabetic rat full-thickness skin wound model Wound size: 7 mm (initial), later larger for efficacy testing Histology: H&E, Masson trichrome, CD31, CD68, CD206 staining qRT-PCR (VEGF, PDGF, Col-I, TGF-β1)	Best healing with MD-CH (combined DOXH + conductive hydrogel) Fastest wound closure (visible by day 14) Most organized collagen deposition (↑ Col-I, ↓ scar area) Highest angiogenesis (↑ CD31, VEGF, PDGF) Highest M2 macrophage presence (CD206/CD68 ratio) Most effective ROS and inflammation suppression Comparative insights: DOXH stronger in immunomodulation Conductive hydrogel boosts cell migration and vascularization Synergistic effect in combined formulation	[48]
3ABAPANI-PLA (Electrospun blend of 3-aminobenzoic acid-polyaniline copolymer and PLA)	Electrospun nanofibrous mat (Honeycomb-like porous 3D network)	3ABAPANI (conductive, antimicrobial) PLA (biodegradable scaffold)	(from DMSO/THF polymer solution; optimized voltage, flow rate, and distance)	Electrical conductivity up to 8.1 mS/cm High porosity, honeycomb morphology Tunable hydrophobicity (contact angle ↑ with more 3ABAPANI) Mechanical strength ↑ with 3ABAPANI (up to 30 MPa) Fiber diameters:	Enhanced fibroblast proliferation Normal fibroblast morphology (pseudopodia, spread cells) >99 % cell viability (COS-1 cells) Supports adhesion and growth	COS-1 fibroblasts (Resazurin, SEM, fluorescence microscopy) *S. aureus* (BacLight assay for antimicrobial testing)	Supports cell growth and biocompatibility Significant antimicrobial activity (69 % bacterial kill vs. controls) Potential dual-function wound dressing (healing + infection control) No cytotoxicity or known side effects like silver/iodine dressings	[49]

(*continued on next page*)

Table 4 (*continued*)

Conductive Polymer/platform	Material Form	Composite Components	Fabrication Method	Key Functional Properties	Biological Effects	In Vivo/In Vitro Model	Healing Outcome/ Performance	Refs
				170 → 25 nm (with more 3ABAPANI)				
SF-pPy (Silk Fibroin with Polypyrrole coating) Conductive electrospun mesh with pPy-coated silk fibroin fibers	Electrospun fibrous mesh, with nanofiber diameters ~2300–2630 nm (high porosity, ECM-like structure)	Silk Fibroin (SF) – biocompatible natural polymer Polypyrrole (pPy) – conductive polymer (uniformly coated)	Electrospinning of SF In situ chemical polymerization of pyrrole for pPy coating	Conductivity: Supports anodic/cathodic currents ± 8 mA in NaCl (non-degrading) Young's Modulus: ↑ from 266.7 ± 17.3 MPa (SF) to 310.5 ± 37.6 MPa (SF-pPy) Chemical interactions: pPy bonds with SF (H-bonding, electrostatics) Preserved fiber structure: Coating doesn't block pore space Crystallinity: ↑ β-sheet content after pPy coating (FTIR shift in Amide I)	hFb (fibroblasts): Better adhesion & proliferation on SF-pPy at day 1 & 21 ahMSCs: Slower growth on SF-pPy vs. SF (significant differences at day 7, 14, 21) Cytoplasmic extensions and healthy morphology on both surfaces Some cytotoxicity possibly due to residual pPy synthesis byproducts	In vitro: hFb (human fibroblasts) ahMSCs (adult human mesenchymal stem cells) Assays: SEM, MTT, adhesion/proliferation studies over 21 days	Good support for cell growth and morphology pPy coating enhances mechanical strength and conductivity Slight suppression in ahMSC growth, but hFb proliferation maintained Suitable for future ES studies in regenerative applications	[50]
Polypyrrole (PPy)-coated PET fabric (Polyethylene terephthalate substrate uniformly coated with PPy)	Woven fabric form (Non-electrospun, coated textile fibers with preserved porosity)	PET (structural polymer substrate) PPy (conductive polymer layer ~100 nm grain size)	Chemical oxidative polymerization of pyrrole directly on PET fabric Uniform surface coating without blocking inter-fiber spaces	Electrical resistivity (dry/wet): 138 Ω m (dry) → 213 Ω m (wet) Retains 78 % conductivity after 24 h pulsed stimulation Thermal behavior: Melting point ~284 °C Similar crystallinity to virgin PET (~38 %) Surface morphology: PPy coating is thin, uniform, granular (<100 nm) Surface chemistry (XPS): ↑ Nitrogen content confirms PPy presence Lower Cl/N ratio than pure PPy (0.13 vs. 0.19)	Increased cell viability (MTT assay): OD ↑ under pulsed ES (0.110 vs. 0.083 at 24 h; 0.153 vs. 0.138 at 48 h) Enhanced fibroblast adhesion and viability after ES No adverse morphological effects observed under SEM	In vitro: Fibroblasts cultured on PPy-coated and virgin PET Assays: SEM imaging, MTT viability test with/ without pulsed electrical stimulation (P-ES)	ES enhanced fibroblast proliferation Viable candidate for smart wound dressings: Biocompatible Electrically responsive Mechanically stable Potentially suitable for applications where ES is used to enhance healing	[51]
PLLA/PEDOT (Poly(L-lactic acid) microfiber web coated with PEDOT conductive polymer)	Nonwoven electrospun-like microfiber fabric (Smooth, porous web; fiber diameter ~13–14 μm)	PLLA – biodegradable structural polymer PEDOT – conductive polymer coated via oxidative polymerization Trace: Cl^- (dopant) and Fe (catalyst residue)	Coating PEDOT onto pre-fabricated PLLA microfiber web EDOT concentration optimized at 0.25 mol/ L for conductivity and consistency	Surface resistivity: 49.4 → 0.4 kΩ/sq as EDOT ↑ Contact angle: ↓ from 125.3° (PLLA) to 93° (PLLA/PEDOT) → ↑ hydrophilicity Thermal stability: Comparable TGA profiles; no early degradation Glass transition (Tg) ↓	Human dermal fibroblasts showed: Good adhesion, spreading, and proliferation on both PLLA and PLLA/ PEDOT Slight increase in metabolic activity under ES Deep infiltration into	In vitro: Human cutaneous fibroblasts MTT assay, Hoechst staining, and microscopy ES tests (6 h ES + 48 h post-incubation)	Good cytocompatibility Conductive PEDOT coating enables ES, boosting cell activity Mechanical reinforcement and maintained porosity Suitable for electroactive wound healing scaffolds	[107]

(*continued on next page*)

Table 4 (*continued*)

Conductive Polymer/platform	Material Form	Composite Components	Fabrication Method	Key Functional Properties	Biological Effects	In Vivo/In Vitro Model	Healing Outcome/ Performance	Refs
				from 53.2 °C to 34.4 °C (↑ chain mobility) Tensile strength ↑ from 1.77 MPa → 3.99 MPa Young's modulus ↑ from 6.71 kPa → 15.73 kPa Elongation ↓ from 144 % → 85 % Electrical stability: Maintains electronic conductivity; 0.17 %/hr decline in wet conditions over time	the porous matrix confirmed			
CG/DA-Ppy hydrogel (Chitosan–gelatin (CG) hydrogel with dopamine-polypyrrole (DA-Ppy) conductive nanofibers and Fe^{3+} crosslinking)	Injectable/adhesive hydrogel (Uniform network with DA-Ppy nanofibers; crosslinked with Fe^{3+}; forms cohesive gel)	Gelatin (Gel) – base polymer Chitosan (Chi) – antibacterial, ROS scavenger β-CD (β-cyclodextrin) – grafted onto gelatin HCA (hydrocaffeic acid) – modified onto chitosan (Chi-C) DA-Ppy nanofibers – conductive & photothermal agent Fe^{3+} – ionic crosslinker	Chemical modification (β-CD, HCA grafting) In situ polymerization of pyrrole with dopamine (DA-Ppy) Hydrogel crosslinked with Fe^{3+} Catechol groups enable adhesion to wet tissues	Adhesion: Strong on wet pigskin; retains adhesion in flowing water Conductivity: 1.3 × 10^{-4} S/cm (CG/1.0 DA-Ppy) Photothermal effect: ↑ temperature to 59.7 °C under 808 nm NIR (1.5 W/cm^2) Swelling: High initial absorption; decreased later due to Gel dissolution Mechanical strength: G' ↑ from 1069 to 5643 Pa with Fe^{3+}; good rheology Stable DA-Ppy nanofibers (vs. free pyrrole which precipitates)	Biocompatibility: Cell viability >90 % at all concentrations (L929 fibroblasts) ISO standard (>75 %) confirms non-toxicity Cell migration: CG/DA-Ppy + ES group shows fastest scratch closure ES activates Ca^{2+} channels, boosts fibroblast movement ROS scavenging: CG hydrogel reduces intracellular ROS DA-Ppy further enhances ROS clearance Macrophage polarization: Promotes shift from M1 (CD86) → M2 (CD206) Anti-inflammatory and pro-regenerative phenotype	In vitro: L929 fibroblasts (viability, migration, ROS, cytoskeleton, staining) RAW264.7 macrophages (polarization via flow cytometry) Bacteria (*E. coli* & *S. aureus* colony counting, biofilm assay) In vivo: Rat infected wound model (full-thickness skin defect) Compared with Aquacel Ag and control groups Monitored days 0–14 (gross, histology, immuno)	Antibacterial: Chitosan: ~70–80 % inhibition DA-Ppy + NIR: ~99.9 % inhibition (photothermal sterilization) Wound healing: Fastest closure in CG/DA-Ppy + NIR group Granulation tissue thickest in CG/DA-Ppy + NIR On day 14: intact epidermis, follicles, reduced dermal gap Immunomodulation: ↑ IL-10 (anti-inflammatory), ↓ IFN-γ, IL-6, TNF-α Sustained M2 macrophage presence → promotes healing Collagen & vascularization: High Masson stain intensity (collagen) Capillary growth restored by day 14	[53]
PEDOT:PSS coated on PLA/PHBV electrospun membrane	Electrospun nanofibrous membrane	PLA, PHBV, PEDOT:PSS (10 % and 30 % v/v coatings)	Electrospinning of 20 % (w/v) PLA/PHBV (50:50) blend followed by surface coating with PEDOT:PSS	Conductivity (1.45 μS/m for 30 % PEDOT:PSS), improved wettability (reduced WCA to 83.25°), increased surface roughness, high porosity (~69–72 %), fiber diameter 0.19–4.6 μm	Non-toxic (via MTT assay), increased cell attachment, enhanced cell proliferation, over 97 % viable cells on coated membrane	In vitro studies with human skin fibroblast (HSF) cells; live/dead assay, SEM, MTT, attachment & proliferation studies	Improved cell adhesion and proliferation, favorable cell–scaffold interactions, enhanced cellular activity due to conductivity and hydrophilicity	[54]

(*continued on next page*)

Table 4 (*continued*)

Conductive Polymer/platform	Material Form	Composite Components	Fabrication Method	Key Functional Properties	Biological Effects	In Vivo/In Vitro Model	Healing Outcome/ Performance	Refs
QCSP (quaternized chitosan/ polyaniline) incorporated into PCL nanofiber matrix	Electrospun nanofibrous membrane (NFM)	Polycaprolactone (PCL) + QCSP (quaternized chitosan + polyaniline)	Electrospinning after solution blending of PCL and QCSP; QCSP synthesized separately before mixing	Nanofiber diameter: 91–175 nm Electroactivity (confirmed via CV) Antioxidant (up to 80 % DPPH scavenging) Antibacterial (>90 % for *S. aureus*, *E. coli*) Mechanical stretchability (up to 81.7 %) Swelling ability (up to 130 %) Biocompatible, hemocompatible	Reduced TNF-α expression (anti-inflammatory) Enhanced VEGF expression (angiogenesis) Supports fibroblast proliferation (L929) Exhibits hemocompatibility (hemolysis ratio <1.5 %) Good cytocompatibility (except PCL/QCSP20)	In vitro: L929 fibroblasts (cytocompatibility, proliferation) In vivo: Mouse full-thickness wound model (wound contraction, histology, cytokine analysis)	PCL/QCSP15 showed fastest wound closure (up to 43 % by day 3, full closure by day 14) Thickest granulation tissue, highest collagen deposition (hydroxyproline) Hair follicle and blood vessel formation observed Best performance among all tested groups, outperforming Tegaderm™ film	[55]
Polypyrrole (PPY) and Polyaniline (PANI) coatings on silk fibroin (SF) fibers	Electroconductive fiber mats (PPY/SF and PANI/SF) synthesized via in situ polymerization	Silk fibroin (SF) + polypyrrole (PPY) or polyaniline (PANI)	In situ oxidative polymerization using $FeCl_3$ (for PPY) and ammonium persulfate (for PANI); conjugated polymer coats silk via adsorption and hydrogen bonding	Conductivity: PPY/SF ≈ 2.2×10^{-5} S/cm, PANI/SF ≈ 1.6×10^{-4} S/cm Maintains thermal stability (TGA: stable up to 250 °C) Increased glass transition temperature (Tg): SF ≈ 72 °C, PPY/SF ≈ 93 °C, PANI/SF ≈ 98 °C Roughened surface topography (SEM) β-sheet structure partially retained (XRD)	Enhanced HaCaT keratinocyte adhesion (especially on PANI/SF) Viability: PPY/SF (47 %), PANI/SF (51 %) vs SF (29 %) Cytocompatible and supports cell proliferation	In vitro: HaCaT (human keratinocyte) cell culture on collagen-treated and untreated fiber mats	Coated fibers show enhanced adhesion and viability of keratinocytes PANI coating most effective for promoting cell adhesion Materials retain structure and conductivity post-coating, suggesting strong potential in tissue engineering and implantable devices	[56]
Graphene oxide (GO) incorporated in PVA electrospun nanofibers	Electrospun nanofibrous scaffold (PGNSs) – PVA with 0 %, 0.25 %, 0.5 %, 1.0 % GO	Poly(vinyl alcohol) (PVA) + Graphene oxide (GO)	Electrospinning of 10 % PVA in water/acetic acid with GO; post-treatment by glutaraldehyde cross-linking vapor to stabilize against water dissolution	Nanofiber diameter: 230 nm (PGNS-0) to 164 nm (PGNS-1.0) Enhanced tensile strength with GO (up to 5.17 MPa) Maintains hydrophilicity Increased protein adsorption with GO Biocompatible, non-hemolytic (<2 %) GO improves electrical properties and solution conductivity	GO content influences cytocompatibility: Low GO (0.25 %) improves cell viability and adhesion High GO (1.0 %) increases ROS and apoptosis PGNS-0.25 had highest cell density and proliferation Good adhesion of L929 cells confirmed by DAPI & SEM	In vitro: L929 fibroblast cells (MTT, adhesion, fluorescence/SEM imaging) In vivo: Full-thickness skin wound model in SD rats over 12 days	PGNS-0.25 showed best healing performance (90 % wound closure by day 9) Minimal inflammation, dense collagen & blood vessels Higher GO (0.5 %, 1.0 %) led to more inflammation and less effective repair PGNS-0.25 selected as optimal scaffold for skin regeneration	[57]
Polyaniline (PANi) blended with chitin	Electrospun aligned nanofibrous scaffold (Chi/PANi)	Chitin + Polyaniline (PANi)	Electrospinning using rotating drum collector to align fibers	Smaller fiber diameter than pure chitin ~91 % higher conductivity than random Chi/PANi Aligned structure enhances directional	Enhanced HDF (human dermal fibroblast) cell viability Aligned fibers promoted 2.1 × higher cell proliferation (vs.	In vitro: Human dermal fibroblasts (HDFs), tested via CCK-8 assay and morphology evaluation	Aligned Chi/PANi nanofibers enhanced cell survival, proliferation, and alignment Scaffold suitable for wound healing or	[58]

(*continued on next page*)

Table 4 (*continued*)

Conductive Polymer/platform	Material Form	Composite Components	Fabrication Method	Key Functional Properties	Biological Effects	In Vivo/In Vitro Model	Healing Outcome/ Performance	Refs
				cell behavior Mechanical and wettability characteristics assessed	random) after 7 days Cells displayed directional, bipolar alignment along nanofibers		tissue engineering where directional cell growth is needed	
Polypyrrole/Iodine (PPy/I) coated on PVP nanofibers and microspheres	Electrospun and electrosprayed nanofiber/ microsphere scaffolds (PVP-S1: nanofibers, S2/S3: microspheres)	Polyvinylpyrrolidone (PVP) + Polypyrrole (PPy) + Iodine (I)	Electrospinning (PVP-S1) and electrospray (PVP-S2, S3) using different solvent systems (chloroform, DMF, water mixtures); PPy/I coated via chemical polymerization	Morphology: nanofibers (135.6 nm) and microspheres (1.01–1.7 μm) Coating increases size slightly due to PPy/I Elemental analysis confirms N and I from PPy/I FTIR/XRD confirm PPy/I incorporation and amorphous nature No residual solvent detected (non-toxic)	PPy/I coating improves HaCaT cell viability and adhesion PVP alone moderately to strongly cytotoxic Cell viability increased 26.9 % (PVP-S1-PPy/I) at 24 h F-actin organization enhanced in coated scaffolds Reduced number of pyknotic (dying) nuclei in PPy/I coated samples	In vitro: Human keratinocyte cell line (HaCaT) for MTT assay, cell adhesion, cytoskeleton (F-actin) analysis, and wound closure (scratch) assay	PVP-S1-PPy/I scaffold significantly promotes in vitro wound closure (62.57 % faster than control) Enhances keratinocyte proliferation, migration, and cytoskeletal integrity Potential to accelerate re-epithelialization and ECM remodeling in wound healing	[59]
Polypyrrole (PPy) blended into a natural polymer matrix (Chitosan, Collagen, PEO)	Electrospun crosslinked nanofibrous scaffold (PPCC10)	Polypyrrole (PPy) + Chitosan (Cs) + Collagen (Col) + Polyethylene oxide (PEO)	Electrospinning of blended polymer solution (varying PPy %) followed by vapor-phase glutaraldehyde crosslinking	Fiber diameter reduced by increasing PPy content Electrical conductivity: up to 164.27×10^{-3} S/m (PPCC15) Mechanical strength (PPCC10): E = 1.09 MPa, σ = 4.6 MPa Biodegradability: ~26 % weight loss in 21 days Homogeneous, bead-free fiber morphology at optimal PPy concentrations Crosslinking enhanced scaffold stability in aqueous environments	PPCC10 showed best cell viability (295 % on Day 3, 310 % on Day 5) PPy provides mechanical stimulation, electrical cues, and improved cell interconnectivity Smaller fiber diameter increased porosity, aiding adhesion and growth Chitosan and collagen support early cell attachment; PPy enhances later proliferation	In vitro: Fibroblast cell line (MTT assay, SEM imaging, morphology, proliferation, migration) over Days 1, 3, and 5	PPCC10 scaffold most effective in promoting cell adhesion, proliferation, and migration Electrically conductive, biocompatible, and biodegradable Strong potential for electrically active tissues (nerve, cardiac, muscle) Scaffold mimics ECM and enhances both biological and physicochemical integration	[60]
Carboxylic acid-functionalized polyaniline (CPSA-PAni) blended with PLCL	Electrospun nanofibrous scaffold with random fiber distribution	CPSA-PAni + poly(L-lactide-co-ε-caprolactone) (PLCL)	Electrospinning from HFIP solution of PLCL and CPSA-PAni at various ratios (15 % and 30 % PAni); PACL-1 (0 %), PACL-2 (15 %), PACL-3 (30 %)	Fiber diameters: 430 ± 116 nm (PACL-1), 423 ± 100 nm (PACL-2), 382 ± 102 nm (PACL-3) Conductivity: 0.0015 S/cm (PACL-1), 0.00765 S/cm (PACL-2), 0.0138 S/cm (PACL-3) Mechanical properties: PACL-3 has reduced strength (0.69 MPa) and elongation (207.85 %) but retains superior elasticity vs. other conductive scaffolds Stable surface presence	Enhanced metabolic activity (MTT) for human dermal fibroblasts, NIH-3T3 fibroblasts, and C2C12 muscle cells in a PAni concentration-dependent manner PACL-3 (30 % PAni) showed ~3 × cell activity vs. PACL-1 (PLCL only) Good cytoskeletal structure (F-actin staining), excellent cell morphology and	In vitro: Human dermal fibroblasts, NIH-3T3 fibroblasts, C2C12 mouse skeletal muscle cells; with and without ES	Excellent biocompatibility and metabolic activity improvement in vitro ES (20 mA) enhanced fibroblast proliferation on conductive scaffold Ideal for applications requiring elasticity and electrical responsiveness (neural, muscle, skin tissue engineering)	[108]

(*continued on next page*)

Table 4 (*continued*)

Conductive Polymer/platform	Material Form	Composite Components	Fabrication Method	Key Functional Properties	Biological Effects	In Vivo/In Vitro Model	Healing Outcome/ Performance	Refs
				of PAni confirmed via ATR-FTIR, Raman, and XPS Good thermal stability (residual PAni mass post-TGA: ~21 % in PACL-3)	spreading Electrically conductive nanofibers stimulated NIH-3T3 cells to higher metabolic activity (best at 20 mA stimulation)			
pMXene (polydopamine-modified Ti_3C_2 MXene) with bFGF	Composite scaffold using Decellularized Adipose Tissue (DAT)	DAT + pMXene nanosheets + basic fibroblast growth factor (bFGF)	Chemical exfoliation of MXene → PDA coating → bFGF loading → Integrated into DAT matrix	Conductivity: 0.14 ± 0.02 S/m (wet) Excellent water absorption & porosity Mechanical strength with elasticity Antioxidant capacity (ROS scavenging) Sustained bFGF release (60.4 %)	Enhances cell adhesion, proliferation (HUVECs, NIH-3T3) Promotes angiogenesis and tube formation Improves Schwann cell outgrowth (S100-β, GFAP) Induces macrophage polarization (M1 → M2) Strong hemocompatibility (hemolysis <5 %)	In vitro: HUVECs, NIH-3T3, Schwann cells, RAW264.7 macrophages In vivo: Diabetic full-thickness wound rat model	96.9 % wound closure in 14 days (best among groups) Enhanced collagen deposition and re-epithelialization Reduced TNF-α, IL-6; increased IL-10, Arg-1 Decreased oxidative stress (ROS) in wound tissue Neuro-immune regulation improves regeneration	[65]
Carbon Nanotubes (CNTs) integrated into BSA + Cellulose hydrogel	Injectable, adhesive, porous hydrogel	BSA (Bovine Serum Albumin), Cellulose, CNTs (variable concentration: CNT1–CNT3)	Heat-induced gelation of BSA + CNT dispersion → Lyophilization → NIR photothermal modulation	High conductivity (up to 8.77 S/m) Photothermal conversion (ΔT ≈ 43 °C with CNT3) Tunable swelling (up to 480 %) and degradation Strong adhesion (up to 10.89 kPa) Excellent rheological and mechanical stability	Low cytotoxicity, >98 % cell viability (L929, 3T3) Antibacterial (*S. aureus*, *E. coli*): 81 %–96 % reduction with NIR Antioxidant (DPPH scavenging: up to 89 %) Enhances collagen deposition, angiogenesis (CD31↑, α-SMA↑), and reduces inflammation (CD68↓)	In vitro: NIH 3T3 fibroblasts, hemolysis, FDA/PI In vivo: STZ-induced diabetic wound model in rats	Wound closure: 96 % in 15 days (B + C + CNT1+NIR group) Oxygen saturation up to 66 % and vascularity up to 74 % (via real-time photoacoustic imaging) Best granulation tissue, collagen density, and epithelialization with NIR + CNT synergy	[82]
Ag-pDA/BC (rGO)	Composite film	BC, GO/rGO, polydopamine (pDA), Ag nanoparticles	Bio-blending and multi-step fabrication: blend growth of BC and GO → dopamine coating → $AgNO_3$ impregnation and UV reduction	Conductivity, mechanical strength, thermal stability, swelling control	Antibacterial, biocompatible, electrically active	NIH3T3 fibroblast cells (in vitro), bacterial zone inhibition assays	>90 % cell viability at 24h, ~84 % bactericidal rate after 72h, promotes healing via conductivity and mild thermal effect	[83]
SIS-rGO (Reduced Graphene Oxide–Small Intestinal Submucosa)	3D porous scaffold	Decellularized porcine SIS, GO, rGO (via ascorbic acid reduction), EDC/NHS crosslinker	Decellularization → GO incorporation → Lyophilization → Crosslinking → in situ reduction (ascorbic acid)	High porosity (>97.5 %), enhanced conductivity (↑10^4 × vs GO), thermal stability, pore interconnectivity	Non-hemolytic (<0.5 %), >90 % cell viability (Vero, HaCat, HFF-1), no platelet activation	In vitro: Vero, HaCat, HFF-1 cell lines; hemolysis and platelet adhesion assays	Excellent biocompatibility, strong cell adhesion, uniform distribution, high cytocompatibility; promising for chronic wound healing and electrostimulation	[109]
Hep-PDA-rGO-PAM (Heparin–Polydopamine–Reduced	Injectable/ stretchable	Heparin, Polydopamine, rGO, PAM (Polyacrylamide)	Two-step synthesis: GO reduction by heparin & PDA → PDA coating →	High electrical conductivity (3.63 S/m), compressive/tensile	Low hemolysis (within 5 %); >97 % cell viability (3T3	In vitro: 3T3 cells, hemolysis, ROS, antibacterial assays; In	~99.7 % wound closure (Day 14) with ES; high collagen	[84]

(*continued on next page*)

Table 4 (*continued*)

Conductive Polymer/platform	Material Form	Composite Components	Fabrication Method	Key Functional Properties	Biological Effects	In Vivo/In Vitro Model	Healing Outcome/ Performance	Refs
Graphene Oxide in Polyacrylamide hydrogel)	conductive hydrogel		dispersion in PAM hydrogel matrix	strength, antioxidant (ROS scavenging), antibacterial, stretchable, pressure/ strain-sensitive	fibroblasts); ROS scavenging; antibacterial (*S. aureus* & *P. aeruginosa*)	vivo: diabetic rat full-thickness infected wound model (with and without ES)	deposition, angiogenesis (↑VEGF, PDGF, VEGFR2); reduced inflammation; hair follicle regeneration; superior to Ag+ and GO groups	
PLGA/GO (with/without ES)	Porous biodegradable film	PLGA (poly(lactic-co-glycolic acid)), graphene oxide (2 %)	Solvent blending/ casting of PLGA with GO; optimal GO loading determined (2 %)	Improved mechanical strength, surface roughness, hydrophilicity; antibacterial (vs. *S. aureus* & *E. coli*); conductive; supports ES	Enhanced cell adhesion, proliferation (Balb/c 3T3 fibroblasts); ↑VEGF & COL-1 expression; antibacterial; low cytotoxicity at 2 % GO	In vitro: Balb/c 3T3 fibroblasts; In vivo: full-thickness skin-defect model in rats (with bacterial infection and ES)	PLGA/GO + ES: highest wound healing rate (~day 12), increased vascularization (↑CD31, VEGF), collagen deposition, epithelial remodeling; synergistic effect over either alone	[85]
ICG-PGO-CaP-PVA Hydrogel	Injectable, stretchable, conductive nanocomposite hydrogel	PVA, PDA-reduced GO (PGO), amorphous CaP, ICG (Indocyanine green)	In situ CaP growth in PVA → PDA reduction of GO → PGO dispersion → ICG loading → hydrogel formation	High mechanical strength (tensile: 1.4 MPa, strain: 253 %); self-healing; conductivity (137 S/m); NIR-triggered photothermal and photodynamic response; Ca^{2+} release	Enhanced C2C12 cell spreading, viability; ROS generation; antibacterial vs. S. epidermidis and *E. coli*; immunomodulatory (M2 macrophage polarization); promotes collagen deposition and neovascularization	In vitro: C2C12 myoblasts, bacteria (ROS, viability); In vivo: full-thickness skin defect in rats (NIR-irradiated)	90 % wound closure (Day 15); superior tissue regeneration (↑collagen maturity, blood vessels, hair follicles); lowest inflammation; ~17 × improved antibacterial efficacy vs. control (S. epidermidis); synergistic effect of photothermal + photodynamic + electroactive cues	[86]
NG-based Electrotherapy Bandage	Flexible bandage device with integrated electrodes	Cu/PTFE/Cu triboelectric nanogenerator (NG) on PET + gold (Au) dressing electrodes	Layered assembly: PET substrate + Cu + sliding PTFE + Au electrodes; wrapped around chest to harvest biomechanical energy	Self-powered from breathing (0.2–2.2 V); electric field generation (~10 V/cm localized, 250 V/m for in vivo); flexible, skin-adaptive, biocompatible	Promotes fibroblast proliferation (127 % viability), alignment, and differentiation; ↑ TGF-β, EGF, VEGF; lower ROS than AC; effective cell guidance via electric field	In vivo: SD rats (linear & full-thickness wounds); In vitro: 3T3 fibroblasts (96-well plates, culture dish)	94 % closure in 48 h (vs. 30 % in controls); full closure in 72 h; significantly faster than stem cell, nanomaterial, and laser therapies; enhanced epithelialization and collagen production	[87]
BDG ZnO NR-based PZP (Piezoelectric Patch)	Flexible, multilayer piezoelectric patch	BDG ZnO nanorods (NRs), PDMS, PEDOT:PSS (base layer), Ag electrodes (for characterization only)	Spin-coating PDMS with PEDOT:PSS base → hydrothermal synthesis of BDG ZnO NRs → alignment via rubbing → multilayer stacking with spin-coated PDMS → embedded NRs (up to 9 layers)	Generates up to 1.8 V & 85 nA/cm^2 upon bending; self-powered from body motion; stable >15 days; bendable/stretchable; optimal with 95.2 % NR density	Non-toxic, promotes fibroblast proliferation (↑PCNA, Ki67), migration, differentiation (↑SM α-actin); ↑FGF-2, TGFβR, COL III/IV, laminin, involucrin, keratin 17; ↑Ca^{2+} deposition in keratinocytes	In vitro: human dermal fibroblasts, keratinocytes; In vivo: full-thickness mouse skin wound model (with PDMS, no-alignment PZP, fibrin gel, and untreated controls)	95.2 % NR patch (PZP-1X): fastest wound closure, full epithelialization, ↑neovascularization (↑CD31, SM α-actin); superior to all controls including fibrin gel; activates PI3K/Akt/ ERK/Rho signaling; accelerates inflammation,	[88]

(*continued on next page*)

Table 4 (*continued*)

Conductive Polymer/platform	Material Form	Composite Components	Fabrication Method	Key Functional Properties	Biological Effects	In Vivo/In Vitro Model	Healing Outcome/ Performance	Refs
							proliferation, remodeling phases	
Stretchable EBFC-integrated Bioelectric Plaster	Wearable, adhesive, stretchable patch	CNT-coated carbon fiber (electrodes), fructose dehydrogenase (anode), bilirubin oxidase (cathode), conductive PEDOT:PU resistor, double-network hydrogel (gellan gum + polyacrylamide), citrate buffer, fructose fuel	Enzyme immobilization on CNT-carbon fiber fabric → PEDOT:PU strip resistor (10 kΩ) → hydrogel electrolyte loading → layered assembly and skin fixation via medical adhesive tape	Ionic current generation (sustained >12 h); conformal skin fit; buffer optimization (200 mM citrate, pH 5); durable enzyme electrodes; moist healing support	Safe to skin; accelerates keratinocyte and fibroblast migration (via ionic current); maintains moist environment; no skin irritation observed	In vivo: Female ICR mouse, full-thickness skin wound (oval, ~8 × 4 mm); 3 groups (no treatment, hydrogel only, bioelectric plaster)	22–25 % improved wound width reduction vs hydrogel alone (Day 6–7); enhanced closure speed after Day 3; reduced contracture; improved epidermal regeneration; combines ES + moist healing benefits	[110]
Ag/Zn Bioelectric Dressing (BED)	Printed, flexible bioelectric patch	Polyester substrate, embedded Ag and Zn dots (2 mm and 1 mm), biocompatible binder	Printing of 99.999 % pure Ag and Zn grains onto polyester in dot arrays (~1 mm apart), non-contiguous grain reservoirs (2–10 μm), no external power source needed	Self-generates electric field (0.2–1 V, up to 13.5 V/cm); produces H_2O_2; initiates redox reactions when in contact with exudate/ saline; long-range patterned field	Accelerates keratinocyte migration via electrotaxis; ↑ H_2O_2 generation; ↑ mitochondrial membrane potential (JC-1, TMRM); ↑ glucose uptake; ↑ IGF1R phosphorylation; ↑ integrin αv expression; ↓ protein thiols (but not glutathione); effects blocked by catalase/NAC	In vitro: HaCaT keratinocytes (scratch assay, RTK array, fluorescence microscopy, ELISA); No in vivo data reported in this study	Significantly accelerated scratch closure at 6 h and 9 h vs Ag or Zn alone; enhanced mitochondrial function, electrotaxis-driven migration, and metabolic activity; first report of ES-induced integrin expression; H_2O_2 identified as key mediator	[89]
MT-MAA Hydrogel with ES	Hydrogel patch with conductive nanotubes	Methacrylic acid (MAA) hydrogel + 1 % Microtubules (MTs) from tubulin	Tubulin polymerization into MTs; embedded in MAA hydrogel matrix; optimized at 1 % MT and 2 % MAA content	Conductivity up to ~3.85×10^{-2} S/m; skin-mimicking; pH-sensitive; stable in vitro for 14 days; biodegradable; tunable mechanical modulus	↑ Aligned NIH3T3 migration & proliferation; ↑ VEGF, TGF-β, EGF secretion; ↑ angiogenesis ($CD31^+$), nerve fiber growth, MSC osteogenic differentiation; ↓ T/B cell infiltration; M1→M2 macrophage transition; antibacterial (*E. coli*, *S. aureus*)	In vitro: NIH3T3, ECs, MSCs (scratch, ELISA, tube formation, RT-PCR); In vivo: Full-thickness diabetic mouse wound model	Rapid wound closure in 7 days; ↑ epidermal regeneration (1.82 mm MET), angiogenesis (25.6 CD31+/HPF), nerve regrowth; effective bacterial clearance; enhances remodeling and growth factor deposition; superior to hydrogel or ES alone	[74]
GT-DA/CS/CNT Hydrogel	Injectable adhesive hydrogel	Gelatin-dopamine (GT-DA), chitosan (5 wt%), polydopamine-coated CNTs (CNT-PDA, 2 wt%)	EDC/NHS conjugation of dopamine to gelatin; CNTs coated with polydopamine; oxidative crosslinking using H_2O_2/HRP to form hydrogel	Conductivity: up to ~7.2×10^{-2} S/m; strong adhesion (~6.5 kPa); antioxidant (DPPH scavenging ~86.5 %); shape-recovery; photothermal antibacterial (NIR responsive); sustained drug release; hemostatic	↑ Cell viability & hemocompatibility; ↓ TGF-β (inflammation); ↑ CD31 (angiogenesis), epidermal thickness, collagen deposition, granulation tissue; antibacterial (*E. coli*, *S. aureus*); drug release (doxycycline)	In vitro: L929 fibroblasts, bacteria (zone of inhibition, LIVE/DEAD); In vivo: full-thickness infected mouse skin wound model	Rapid wound closure (14 days); ↑ collagen (hydroxyproline), thicker epidermis, granulation tissue, & angiogenesis; 100 % bacteria killing in vitro/in vivo with NIR; superior to Tegaderm™ film	[92]

(*continued on next page*)

Table 4 (*continued*)

Conductive Polymer/platform	Material Form	Composite Components	Fabrication Method	Key Functional Properties	Biological Effects	In Vivo/In Vitro Model	Healing Outcome/ Performance	Refs
PMO-CNT Hydrogel	Thermoresponsive conductive hydrogel	OEGMA, MEO2MA, CNT-OH, SDS	In situ free radical polymerization; ultrasonic dispersion of CNT-OH in OEGMA/ MEO2MA; SDS for CNT stabilization	Thermal conductivity: 0.73 W/m·K; strong cooling ability; shape-recovery; adhesive (0.33 kPa at 30 mm/ min); highly stretchable (~301 % elongation); swelling ratio up to ~2750 %; thermally responsive swelling/ shrinkage; photothermal (NIR) activity	High cell viability (>80 %) for L929 fibroblasts; supports fibroblast migration and granulation tissue formation; reduces thermal damage; biosafe and biocompatible	In vitro: L929 fibroblasts (CCK8, Live/Dead); In vivo: scald burn model on SD rats (thermal imaging, histology)	Rapid wound cooling (to 28.8 °C vs 11.9 °C icing); reduced tissue damage; re-epithelialization and fibroblast infiltration by day 7; thicker granulation tissue (1.23 mm by day 21); superior safety over icing (no hypothermia); easy removal without tissue damage	[66]
N,O-CMC/AgNps Hydrogel	Injectable, self-healing hydrogel	N,O-carboxymethyl chitosan (N,O-CMC), silver nanoparticles (AgNps), EDTA:Fe^{3+} complex	In situ formation: N,O-CMC reduces $AgNO_3$ to AgNps; metal-ligand coordination between $–COO^-$ and Fe^{3+} from EDTA-Fe^{3+} complex induces gelation	Self-healing (1 min), conductivity (75 μA @ 5 V), shear-thinning, adhesive (lap shear: 14.7 ± 0.005 kPa), injectable, stable morphology, ~25 nm AgNps, antibacterial & antibiofilm, swelling equilibrium in ~7 days	Hemocompatible (≤5 % hemolysis); cytocompatible (≥82 % viability at ≤100 mg); hemostatic (clotting time ↓ to ~4.25 min); antibacterial (*S. aureus*, MRSA, *E. coli*, *K. pneumoniae*, *P. aeruginosa*); biofilm inhibition (up to 83 %)	In vitro: L929 fibroblasts (Alamar blue), hemolysis, blood clotting, biofilm (*E. coli*, *S. aureus*, *P. aeruginosa*)	Effective in vitro hemostasis; broad-spectrum antibacterial action; reduces biofilm formation by up to 83 %; suitable for infected wound closure; injectable with stable rheological behaviour	[111]
HPDChCl-1.0 Gel	Conductive, adhesive, self-healing eutectogel	Hyaluronic acid–thiol (HA-SH), acrylamide (AM), glycerol (Gly), choline chloride (ChCl), PDES (deep eutectic solvent)	Hydrogen bonding eutectogel network formation from HA-SH and PDESChCl via polymerization (grafting degree 42.81 %); self-assembled network with dynamic H-bonds	Conductivity: 0.25 ± 0.05 S/m; self-healing (5 min macro, 12 h micro); elastic recovery after 5000 % strain; adhesive (50 ± 2 kPa to porcine skin); stretchable (77 %), matches skin modulus (0.42–1.12 MPa); high water retention, transparency (98 %)	Antibacterial: 90 % (*E. coli*, *S. aureus*); ↑ cell proliferation (128 %) and migration; ES synergistically enhances L929 migration (1.5 × vs gel alone); no toxicity; adheres to biological tissues and non-biological surfaces	In vitro: L929 fibroblasts (scratch assay, viability, ES 3 V, 1 Hz, 1 h); In vivo: deep 2nd-degree burn wound model in rats; daily 1 h ES for 18 days	Wound closure: 98.05 % (Day 14), complete healing Day 18 with ES + gel; ↑ epidermal thickness and collagen deposition; superior to ES or gel alone; stable conductivity supports continuous ES	[67]
DES-SH/PDA/TTO/PNE Hydrogel	Conductive, adhesive, self-healing hydrogel	Deep eutectic solvent (DES: choline chloride + glucose), sodium hyaluronate (SH), polydopamine (PDA), tea tree oil (TTO), Panax notoginseng extract (PNE, ginsenoside Rg1)	Physical crosslinking via hydrogen bonding and electrostatic interactions; aged at 40 °C for 12 h to form viscoelastic 3D hydrogel	Conductivity: bright LED circuit; swelling ratio: ~102 %; self-healing (macro and tissue), adhesive (94.3 g s on pigskin); stretchable, viscoelastic, shear-thinning, temperature-stable (−20–40 °C), antioxidant (DPPH, ABTS scavenging)	Hemocompatible (hemolysis rate 4.39 %); cytocompatible (HUVEC, NIH3T3, >85 % viability); promotes cell migration (HUVEC, 65 % at 48 h); bactericidal: *E. coli* & *S. aureus* (>100 % kill via contact, ~16 mm inhibition zone); anti-oxidative stress	In vitro: HUVEC, NIH3T3 (live/dead stain, scratch test); In vivo: full-thickness wound on mice, with/without ES; sensor testing on human joints, face, throat	Wound closure: 97.6 % (Day 9), 99.7 % (Day 12) with ES + hydrogel; ↑ hair follicles, vessels, collagen (58.2 % on Day 12); multifunctional: heals burns, antibacterial, antioxidant, and enables motion/vocal sensing	[68]
PAA-SA@rGO Hydrogel	Conductive, adhesive, antioxidant hydrogel	Polyacrylic acid (PAA), sodium alginate (SA), reduced graphene oxide (rGO)	Free radical polymerization forming dual network hydrogel (PAA-SA)	Conductive (restores electric field, reduces resistance to 2.067 MΩ); stretchable (3 ×	Biocompatible: >85 % fibroblast viability (live/dead, CCK-8); hemocompatible	In vitro: fibroblasts, ROS model, hemolysis; In vivo: infected buccal wound in SD rats (S.	Wound closure: 92.2 % (Day 7), full closure by Day 10 (vs. 66.5 % PAA-SA, 73 % bFGF-	[69]

(*continued on next page*)

Table 4 (*continued*)

Conductive Polymer/platform	Material Form	Composite Components	Fabrication Method	Key Functional Properties	Biological Effects	In Vivo/In Vitro Model	Healing Outcome/ Performance	Refs
			with rGO; self-supporting, wave-like structure	original length); adheres in wet/ dynamic oral conditions (≈1 N tensile); low swelling; antioxidant (↑Nrf2, HO-1); stable in buccal mucosa >24 h	(hemolysis <5 %); promotes ROS scavenging (84.5 % in 20 min); ↓ TNF-α, IL6; ↑ CD31, Col-1, SOX2, PITX1/2 (qPCR, IHC); antibacterial: *S. aureus*, *E. coli*, S. mutans (zones: 14.25 & 17 mm)	mutans); bFGF-gel and blank controls	gel, 40 % control); ↑ collagen (81.6 %); functional mucosal regeneration; restores electric field to normal levels; outperforms bFGF-gel and other recent therapies	
OSA/CMCS/AgNPs Hydrogel	Injectable, conductive, self-healing hydrogel	Oxidized sodium alginate (OSA), carboxymethyl chitosan (CMCS), AgNPs (in situ photoreduction from $AgNO_3$)	Schiff base crosslinking (imine bonds) + in situ UV reduction of Ag^+ to AgNPs (no chemical reductants)	Injectable (dual syringe, shear-thinning); self-healing (stable under strain, full recombination); conductive (0.0127 S/ cm with AgNPs); tunable gelation time (13–432 s); swelling and mechanical strength tunable via OSA oxidation; pore-rich, 2 nm AgNPs	>80 % L929 viability (0–1 mM $AgNO_3$); hemolysis: 0.5–4.2 %; enhanced proliferation under ES (600–1200 mV); antibacterial: 98.7 % (*S. aureus*), 76.6 % (*E. coli*) @ 0.5 mM Ag^+; reduces TNF-α, ↑ CD31, α-SMA	In vitro: L929 cytocompatibility, ROS, hemolysis, live/dead staining; In vivo: full-thickness wound model in rabbits (with/without ES); immunohistochemistry for TNF-α, α-SMA, CD31	Wound closure: 80 % (Day 10), almost complete by Day 14; with ES (100 mV/ mm), fastest healing, better epithelial/ follicle regeneration, collagen deposition, and angiogenesis; outperforms Tegaderm and no-dressing control	[70]
Alg-PBA/PVA/GOH hydrogel	Hydrogel	Alg-PBA, PVA, GOH	One-pot synthesis via reversible PBA-diol ester bonding and supramolecular interaction under alkaline conditions	Injectable, self-healing, conductive, pH-responsive, photothermal, motion sensing, good mechanical strength	Biocompatible (≥85 % cell viability), hemocompatible (hemolysis <3 %), low cytotoxicity under light/dark conditions, promotes fibroblast growth	In vitro: L929 fibroblast viability, hemolysis assay In vivo: Mouse full-thickness skin wound model (*S. aureus* infection), real-time impedance monitoring	Rapid wound closure (≈97 % by day 9), real-time infection detection, effective photothermal bacterial killing (>99.99 %), collagen regeneration, restored skin appendages (hair follicles, sebaceous glands), minimal inflammation	[71]
Gel-MA/Chi-C/G-PPy/His-1 hydrogel	Hydrogel	Gel-MA, Chitosan-catechol (Chi-C), Gelatin-g-polypyrrole (G-Ppy), His-1	Crosslinking of Gel-MA with Chi-C and G-Ppy, followed by His-1 incorporation	Conductive, adhesive, porous, biodegradable, swelling capacity, angiogenic, anti-inflammatory	Good cytocompatibility, supports endothelial cell migration and angiogenesis, encourages M2 macrophage polarization	In vitro: L929 cytotoxicity test, tube formation, scratch assay In vivo: Diabetic wound healing model in mice	Faster wound healing, minimal scarring, enhanced collagen deposition, angiogenesis, inflammation suppression, restored skin structure	[72]
PBAE-TA/HA-SH/Geln-Van/Lac/ ADSCs hydrogel (Sequential IPN)	Hydrogel	PBAE-TA, HA-SH, Geln-Van (gelatin-vanillin), Lac (lactate oxidase), ADSCs (adipose-derived stem cells)	Sequential IPN formation via Schiff-base reaction and enzymatic crosslinking; encapsulation of ADSCs	Conductive, hypoxia-inducing, fast-gelling, injectable, cell-adhesive, programmable oxygen consumption	Maintains high ADSC viability (>85 %), upregulates key pro-angiogenic and anti-inflammatory genes (HIF-1α, VEGF, ANG-1, Cx43, TGF-β1/3)	In vitro: ADSC biocompatibility and gene expression assays In vivo: Humanized diabetic rat skin wound model (subcutaneous and excisional wound studies)	95 % wound closure by day 21, enhanced angiogenesis, collagen remodeling, hair follicle regeneration, reduced inflammation	[73]
PAAm-DN/PNIPAm-DN hydrogel patch with Ag-TA nanoparticles (mucus + suction-cup system)	Hydrogel patch	PAAm-DN, PNIPAm-DN, Ag-tannin (Ag-TA) nanoparticles, gelatin, tannic acid, VEGF	Two-step synthesis: Ag-TA nanoparticles grafted onto gelatin (mucus) + free radical	NIR-responsive, self-healing, strong adhesion (via mucus and suction-cup	Excellent biocompatibility (HUVECs), broad-spectrum	In vitro: Cell viability (HUVECs), antimicrobial assays, motion and temperature sensing	Significantly accelerated healing (best in patch + VEGF + NIR group),	[75]

(*continued on next page*)

Table 4 (*continued*)

Conductive Polymer/platform	Material Form	Composite Components	Fabrication Method	Key Functional Properties	Biological Effects	In Vivo/In Vitro Model	Healing Outcome/ Performance	Refs
			polymerization of PAAm and PNIPAm for DN hydrogel; template perfusion for forming the heterogeneous patch	mechanism), photothermal conversion, programmable drug release, motion and temperature sensing, reusable	antimicrobial activity (*E. coli*, *S. aureus*, C. albicans), ROS scavenging, reduced inflammation (↓IL-6)	In vivo: Rat model of infected full-thickness skin wound	enhanced collagen deposition, neovascularization (↑CD31, α-SMA), decreased inflammation, partial skin regeneration with hair follicles	
SFMA@IL conductive hydrogel	Injectable hydrogel	Silk fibroin methacrylate (SFMA), ionic liquid (IL), phenylboronic acid groups	Synthesis of SFMA via reaction of silk fibroin with GMA; IL synthesized via alkylation; hydrogel formed by UV-initiated free radical polymerization	Injectable, rapid gelation (<10 s), photocrosslinkable, conductive (0.2152 S/m), ROS scavenging, anti-swelling, anti-inflammatory, mechanically robust	Biocompatible (PC12 cells), anti-inflammatory (↓TNF-α), anti-apoptotic (↑Bcl2, ↓Bax), promotes neurogenesis, supports signal transmission (via gene upregulation: Ache2, Atf1, Ntrk1, Calca-1)	In vitro: PC12 cell viability, RNA sequencing, ROS scavenging In vivo: Rat spinal cord complete transection model, cortical SSEPs, tissue regeneration assessment	Enhanced axon regrowth, suppressed glial scar formation, ~45 % tissue preservation, partial restoration of sensory signals (SSEPs), upregulation of genes supporting neuroregeneration and signal conduction	[76]
PPCA hydrogel with AgPPy nanotubes	Hydrogel	Poly(acrylic acid) (PAA), polyethyleneimine (PEI), cobalt ions (Co^{2+}), Ag-decorated polypyrrole nanotubes (AgPPy)	Soft-template synthesis of AgPPy using LCA nanotubes, followed by in situ polymerization with PAA, PEI, Co^{2+}; rapid gelation catalyzed by Ag nanoparticles (<10 s)	Rapid gelation, high conductivity (≈0.048 S/m), stretchable, compressible, antibacterial, moisture-retentive, adhesive to tissue (≈15.88 kPa tensile), porous structure	Good cytocompatibility (3T3 fibroblasts), low cytotoxicity, enhanced cell proliferation and adhesion, strong antibacterial activity (*E. coli*, *S. aureus*)	In vitro: Fibroblast viability and bacterial inhibition In vivo: Diabetic mouse full-thickness skin wound model	Accelerated wound closure (~97 % by day 14), enhanced angiogenesis (↑capillaries), re-epithelialization, hair follicle regeneration, reduced inflammation	[77]
PQCD-A@Cur hydrogel (PANI-based with AMNP@Cur)	Injectable hydrogel	Polyaniline-grafted quaternary chitosan (PQCS), oxidized dextran (OD), AMNP@Cur nanoparticles (1,8-dihydroxynaphthalene-based), curcumin	Two-step synthesis of PQCS and OD; Schiff base formation between amino (PQCS) and aldehyde (OD) groups; Curcumin loaded onto AMNP via π-π stacking; hydrogel formed by dynamic covalent and non-covalent interactions	Injectable, conductive (2.53 mS/cm), self-healing, photothermal conversion (up to 48.6 °C), NIR-controlled curcumin release, antioxidant, antibacterial, shear-thinning, rheologically robust	Scavenges ROS, promotes cell viability and migration (RSC, L929), enhances angiogenesis (HUVEC tube formation), induces macrophage polarization (↑CD206, ↓CD86), modulates cytokines (↓IL-6, ↓TNF-α, ↑IL-10), supports neurogenesis and remyelination	In vitro: Antioxidant assay (DCFH-DA), migration (scratch assay), angiogenesis (tube formation), inflammation (immunofluorescence for CD86, CD206) In vivo: Rat models of peripheral nerve injury and STZ-induced diabetic infected wounds	Improved sensory and motor function, restored nerve myelination (↑MBP, ↑Tuj-1), revascularization (↑CD31, ↑VEGF), collagen deposition, reduced inflammation, balanced immune microenvironment, enhanced cutaneous innervation, regulation of neuro-immune pathways (↑SOX10, MBP; ↓IL12B, CXCL17)	[79]
OSD/CMC/Fe/PA hydrogel	Injectable, self-healing hydrogel	Oxidized sodium alginate-grafted dopamine (OSD), carboxymethyl chitosan (CMC), Fe^{3+} ions, polydopamine-coated poly(thiophene-3-acetic acid) (PA)	EDC/NHS coupling of dopamine to oxidized sodium alginate; coating of PTAA with polydopamine; Fe^{3+} coordination and Schiff base formation with CMC and OSD	Self-healing, conductive (up to 7.2×10^{-4} S/m), adhesive, antioxidant, photothermal (ΔT up to 25 °C), antibacterial, hemostatic, biodegradable	Reduces TNF-α (inflammation), increases VEGF (angiogenesis), scavenges ROS (DPPH, $\cdot O_2^-$), promotes granulation tissue formation, epithelial regeneration, vascularization; good	In vitro: DPPH & NBT antioxidant assays, L929 cell viability, hemolysis, rheology/self-healing tests, photothermal response, antibacterial (MRSA, *E. coli*) In vivo: MRSA-infected full-thickness skin wound model in mice; histology	97.02 % wound closure in 14 days (with NIR); enhanced granulation tissue and skin appendage regeneration, reduced inflammation (↓TNF-α), improved angiogenesis (↑VEGF), >99 % bacterial	[80]

(*continued on next page*)

Table 4 (*continued*)

Conductive Polymer/platform	Material Form	Composite Components	Fabrication Method	Key Functional Properties	Biological Effects	In Vivo/In Vitro Model	Healing Outcome/ Performance	Refs
					cytocompatibility and hemocompatibility	(H&E, VEGF, TNF-α), wound closure tracking, granulation thickness, hair follicle analysis	clearance (MRSA, *E. coli*)	
PC Hydrogel (PPB/CDL/rGO@PDA/ Met)	Injectable, adhesive, self-healing hydrogel	CS-DA-LAG (catechol-modified chitosan with L-arginine), PEGS-PBA-BA, polydopamine-coated reduced graphene oxide (rGO@PDA), metformin	Schiff base and phenylboronate ester dynamic covalent bonding between CS-DA-LAG and PEGS-PBA-BA; PDA coating on GO to form rGO@PDA; incorporation of metformin for dual-responsive drug release	Self-healing, pH/ glucose-responsive drug release, antibacterial, antioxidant, hemostatic, adhesive, conductive ($\sim 10^{-1}$ S/ m), injectable, stretchable, degradable	Reduces inflammation (↓IL-6), promotes angiogenesis (↑CD31, ↑α-SMA), collagen deposition, ROS scavenging, hemostasis, enhanced cell viability and proliferation (HUVEC), antibacterial (*E. coli*, MRSA >99 %), enhanced wound adhesion	In vitro: antioxidant (DPPH, ROS), mechanical tests, rheology, drug release, cytocompatibility (HUVEC), antibacterial (*E. coli*, MRSA) In vivo: diabetic foot wound model in rats, blood clotting index, liver bleeding, histology (H&E, Masson), immunofluorescence (IL-6, CD31, α-SMA)	≥98 % wound closure in 21 days, enhanced re-epithelialization, granulation tissue, angiogenesis and follicle regeneration; reduced inflammation, superior to commercial dressings; synergistic enhancement by metformin and rGO@PDA	[81]
M-H-A-A TENGs wound healing system	Conductive hydrogel integrated with aqueous-aqueous TENGs	Dextran (DEX), polyethylene glycol (PEG), potassium carbonate/polyacrylic acid/calcium chloride (K_2CO_3/PAA/$CaCl_2$) conductive hydrogel, minocycline	16 pairs of DEX-PEG aqueous two-phase system (ATPS) droplets serially connected to form TENGs; conductive hydrogel synthesized and loaded with minocycline	High current output (790 nA, 5.4 V), self-healing, adhesive, stretchable, conductive, biocompatible, stable in humidity and temperature, biodegradable	Promotes fibroblast proliferation and migration, enhances collagen deposition, angiogenesis (↑CD31, ↑VEGF), reduces inflammation (↓TNF-α, ↓IL-6), antibacterial efficacy (especially against *S. aureus*), improved drug penetration	In vitro: fibroblast (3T3) proliferation, migration, Live/Dead staining, antibacterial tests (*E. coli*, *S. aureus*), scratch assay In vivo: infected full-thickness wound model in rats with *S. aureus*, histology (H&E, Masson), immunofluorescence (TNF-α, IL-6, CD31, VEGF)	Complete wound closure by day 10; highest collagen deposition, angiogenesis, and granulation tissue; lowest inflammation; wound size reduction to 20.3 % by day 5 and complete by day 10, outperforming controls and S-S TENGs systems	[91]
Ag NPs/CPH hydrogel wound dressing	Conductive, antibacterial, and porous hydrogel sheet	Polyvinyl alcohol (PVA), gelatin, polyaniline (PANI), phosphoric acid (PA), silver nanoparticles (Ag NPs)	Freeze–thaw process with optimized PVA (5 wt%), gelatin (1.5 wt %), aniline (600 μL), PA (600 μL); immersion loading of Ag NPs	Stretchable, compressible, porous structure, high water absorption (up to 180 % swelling), tunable conductivity (up to 0.069 S/cm), stable, moldable, antimicrobial	Antibacterial activity (*E. coli*, *S. aureus*), low cytotoxicity (HaCat, LO2, 293T), enhanced collagen deposition, inflammation reduction, blood vessel formation	In vitro: bacterial cultures, HaCat/LO2/ 293T cytotoxicity tests; In vivo: full-thickness infected wound model in mice (*S. aureus*)	Near-complete wound closure by day 14, reduced inflammation, increased collagen and vascularization, non-adhesive, effective for severe wound infections	[93]
PDES electroactive eutectogel (PAAAQ hydrogel)	Electroactive, adhesive, injectable, antibacterial hydrogel	Quaternized chitosan (QCS), acrylamide (AAm), acrylic acid (AAc), 2-acrylamido-2-methylpropanesulfonic acid (AMPS), α-ketoglutaric acid, deep eutectic solvent (DES)	One-pot photopolymerization under 365 nm UV light; varying donor–acceptor ratios to form DES-based eutectogel	High conductivity (>1 S/m), ionic piezoelectricity (up to 0.12 V), fast gelation (~20 s), high swelling (800–1100 %), excellent adhesiveness (40–75 kPa to skin), universal adhesion, stretchable, compressible, fatigue-resistant, biosensing, anti-protein fouling	Reduces inflammation (↓CD86, ↑CD206), promotes angiogenesis (↑α-SMA, ↑vWF), collagen remodeling (↑type III/I ratio), cell proliferation (↑Ki-67), ROS reduction (↓DHE), strong antibacterial efficacy (*E. coli*, *S. aureus*), fibroblast migration, blood compatibility	In vitro: L929 and HUVEC cell viability, migration assay, hemocompatibility, ROS, protein adsorption, antimicrobial (*S. aureus*, *E. coli*) In vivo: Full-thickness infected rat wound model, liver hemorrhage hemostasis model, histology (H&E, Masson, Sirius Red), immunofluorescence (CD86, CD206, α-SMA, vWF, DHE, Ki-67)	Nearly complete infected wound healing by day 12; enhanced collagen III/ I ratio, improved skin elasticity, angiogenesis, and reduced inflammation and oxidative stress; superior hemostatic performance and biosensing functionality	[94]

(*continued on next page*)

Table 4 (*continued*)

Conductive Polymer/platform	Material Form	Composite Components	Fabrication Method	Key Functional Properties	Biological Effects	In Vivo/In Vitro Model	Healing Outcome/ Performance	Refs
HPEM Scaffold (HCHO/PGE/ MXene@PDA)	Injectable, adhesive, conductive, biodegradable hydrogel scaffold	Hyaluronic acid aldehyde (HCHO), PEI–glycerol triacrylate polymer (PGE), MXene@PDA ($Ti_3C_2T_x$ nanosheets), Schiff-base linkages	Schiff-base reaction between amino (PGE), aldehyde (HCHO), and ketocarbonyl (MXene@PDA); injectable hydrogel formed via dynamic covalent bonds	High conductivity (2.89 ± 0.025 S/m) Strong self-healing (G′ recovery: 99.1 %) Tissue adhesive (~1400 Pa normal stress) Porous morphology (SEM), thermal stability Antibacterial (*E. coli*, *S. aureus*, MRSA >99 %) Hemostatic (rapid liver bleeding cessation in 60 s, tail bleeding time reduced) Promotes collagen deposition, granulation, angiogenesis	Biocompatibility: L929 cells >99 % viability at 25 μg/mL Low LDH leakage, negligible organ toxicity (in vivo Ti distribution cleared by day 7) Promotes fibroblast and endothelial cell proliferation Upregulates wound-healing genes: α-SMA, COL III, VEGF Anti-inflammatory (↓ IL-6, F4/80, Ly6G)	In vitro: L929 and NIH-3T3 fibroblasts, HUVECs (viability, LIVE/DEAD, Alamar Blue, qRT-PCR) In vivo: MRSA-infected full-thickness wound model in mice; liver hemorrhage model; tail bleeding model; histology (H&E, Masson, Ki-67), immunofluorescence (α-SMA, CD31), IL-6, F4/80, Ly6G	~96 % wound closure by day 14 (vs. ~60 % in controls) Significantly reduced MRSA load and inflammation Thickest granulation tissue (~120 μm), high collagen deposition Strongest Ki-67, α-SMA, CD31 expression Outperformed gauze (3M), blank, and HPE controls in all healing indicators	[95]
QCS/OD/SDI/PANI/PS/Plasma (QOSP) hydrogel	Charged, conductive, self-powered hydrogel dressing	Quaternized chitosan (QCS), oxidized dextran (OD), sulfadiazine (SDI), polyaniline nanowires (PANI), polystyrene (PS), plasma-injected charge	Schiff base reaction between QCS and OD; SDI enhances cross-linking; PANI and PS are incorporated for conductivity and structure; charge injection via plasma treatment establishes a stable internal electrofield	Self-powered conductive network High dielectric breakdown strength (8.7 kV/mm) Improved conductivity (3.33×10^{-5} S/m) Thermal stability (310 °C) Self-healing and adhesive Porous (≈71 μm pores) Responsive to pH and temperature Electro-dielectric stimulation without external input	Antibacterial (*S. aureus* and *P. aeruginosa*, enhanced at acidic pH) Biocompatible (Live/ Dead, hemolysis <5 %) Promotes Th1 immune polarization (↑CXCR3, ↑T-bet, ↓GATA3) Suppresses fibrosis (↓TGF-β, ↓α-SMA) and inflammation (↓iNOS) Modulates proteomic pathways: ↓TLR4, ↓coagulation cascade, ↓JAK/STAT, ↓necroptosis	In vitro: NIH/3T3 cytocompatibility, Jurkat polarization, bacterial inhibition (SA, PA), CCK-8, hemolysis In vivo: Second-degree infected burn model in mice; H&E, Masson, immunostaining (TGF-β, α-SMA, iNOS, CXCR3, GATA3, CD31); qPCR; proteomics; western blot	Rapid wound contraction (85 % by day 10) Thickest granulation tissue (699 μm) Controlled collagen deposition (Masson stain) Reduced angiogenesis (CD31), inflammation, and scarring Outperformed QO, QOS, and blank control Enabled integration with sensors (ECG, EEG, EMG); responsive to muscle and nerve signals	[96]
COGFe5 Hydrogel (Catechol–Fe^{3+}/ Imine Cross-linked)	Self-healing, injectable, adhesive, electroactive hydrogel	Quaternized chitosan (QCS), oxidized sodium alginate (OSA), gelatin, gallic acid (GA), poly (gallic acid) (pGA), Fe^{3+} ions	Dual dynamic cross-linking via imine bond formation and Fe^{3+}–catechol coordination	High porosity (~90 μm), excellent adhesion (to skin and tissue), photothermal conversion (36.1 %), antioxidant and UV shielding, conductivity (~10^{-3} S/m), strong mechanical strength (176 kPa)	Hemocompatibility (hemolysis <5 %), cytocompatibility with L929 and NIH 3T3 cells, promotes cell migration, antioxidant activity, ROS scavenging	In vitro: cytotoxicity, hemolysis, ROS assay, cell migration; In vivo: full-thickness infected wound model in rats (*S. aureus*), liver and tail hemostasis models	Accelerated wound closure (~72 % at day 3 vs. ~46 % control), enhanced neovascularization (↑CD31), collagen deposition (↑TGF-β), hemostasis in <50s, infection control with NIR-triggered photothermal therapy	[97]
H-NPs-12 Hydrogel (Ag-Lignin@PAHC)	Injectable, adhesive, self-healing, conductive hydrogel	PAHC (4-carboxyphenylboronic acid-grafted hydroxypropyl cellulose), Ag-Lignin nanoparticles, borate ester bonds	Dynamic covalent crosslinking (borate ester bonds, hydrogen bonding); in situ reduction of Ag^+ by lignin	Electrical conductivity (0.85 mS/cm), antioxidant (DPPH scavenging >92 %), tissue adhesion (up to 8.76 kPa), shear-thinning and injectable, porous network (pore size ~8 μm), self-healing	Excellent biocompatibility (cell viability >90 %, hemolysis <1.4 %), hemostatic (blood loss ~332 mg in liver injury), antibacterial (100 % against *E. coli*, *S. aureus*, C. albicans, MRSA)	In vitro: antioxidant, antibacterial, cytotoxicity, hemostasis; In vivo: MRSA-infected full-thickness wound model in rats, liver bleeding model	Accelerated wound healing (complete closure by day 15), ↑collagen deposition (26.4 %), ↑angiogenesis (CD31), ↓inflammation, M2 macrophage polarization (↑CD206/ CD68 ratio)	[98]

reaction conditions, pH, temperature, and concentration, limiting their robustness in non-lab settings. Moving forward, these methods would benefit from streamlined, one-pot synthesis approaches that maintain multifunctionality without introducing excessive complexity.

An important dimension to analyze is how fabrication methods affect material compatibility and final architecture. For example, electrospinning allows for tight control over fiber alignment, porosity, and diameter, which are crucial for mimicking native ECM and enhancing cell migration. When followed by surface functionalization (PDA, collagen, or polypyrrole coatings), it allows precise control over wettability, adhesion, and conductivity. Similarly, methods that use layered or hybrid assembly (hydrogel-on-membrane systems, triboelectric generators, or CNT-electrode integration) demonstrate a clear intent to replicate skin's hierarchical structure while delivering electrical cues or drug payloads. However, certain methods like electrospray + in situ polymerization may struggle with achieving uniform dispersion of conductive elements, especially when working with nanoparticles that agglomerate or poorly interface with hydrophilic matrices. Additionally, fabrication methods like enzyme-assisted crosslinking (HRP/H_2O_2) or photo-initiated polymerization offer spatial-temporal control but must consider enzyme activity loss, UV damage to cells or drugs, and oxygen inhibition during curing. From a translational viewpoint, fabrication methods must align with clinical constraints, such as sterility, patient safety, degradation profile, and cost. While in situ chemical reductions and metal nanoparticle loadings (Ag^+ to AgNPs) enhance antimicrobial properties, they raise concerns around cytotoxicity, uncontrolled ion release, and regulatory hurdles, especially if non-biodegradable or not clearly traceable in vivo. Similarly, multi-step chemical syntheses (PDA-coated MXenes with growth factor loading) offer high-performance composites but would require stringent toxicological validation. Conversely, processes like freeze–thaw gelation, UV-polymerization, and printable eutectogels are more regulatory-friendly, using known GRAS (Generally Recognized as Safe) materials and mild fabrication conditions. An ideal fabrication method would use aqueous processing, room-temperature conditions, and known biopolymers with minimal use of organic solvents, heavy metals, or uncharacterized nanomaterials.

The fabrication methods used for conductive wound healing platforms reflect a diverse and evolving toolbox that balances between precision engineering and clinical feasibility. Among these, electrospinning stands out for its versatility and scalability. It allows for the creation of nanofibrous scaffolds that closely mimic the extracellular matrix (ECM), promoting cell migration and nutrient exchange. When combined with post-processing steps like surface coating (PPy, PDA) or crosslinking (glutaraldehyde, UV), electrospun fibers can be endowed with conductivity, drug-loading capacity, or antimicrobial properties, making them excellent candidates for chronic wound applications. Additionally, 3D printing coupled with UV-crosslinking has emerged as a key method for spatially defined hydrogel structuring, enabling the integration of conductive paths, drug reservoirs, or even living cells. Methods like spin-coating and freeze–thaw gelation also offer simplicity and reproducibility, especially when used to prepare PEDOT:PSS films or PVA/gelatin-based conductive sheets, supporting their transition to scalable manufacturing. In contrast, solvothermal synthesis, ultrasonic self-assembly, and multi-step chemical reductions though powerful in generating nanoscale precision or high-functionality composites (AgNP-decorated PPy or BiOCl-PPy nanosheets) are often labor-intensive, sensitive to process parameters, and difficult to standardize, posing barriers to clinical scalability. A particularly promising trend in fabrication is the incorporation of dynamic covalent chemistries and biocompatible crosslinking strategies that enable materials to be injectable, self-healing, and tissue-adhesive. Techniques utilizing Schiff-base bonding, metal coordination (Fe^{3+}), borate ester networks, or phenylboronic acid interactions allow hydrogels to maintain structural integrity under mechanical stress while also adhering strongly to wet tissue an essential feature for irregular or exudative wounds. Many systems are synthesized via one-pot or mild aqueous processing, making them both green and clinically friendly, especially when combined with natural polymers like chitosan, gelatin, or HA-SH. Moreover, fabrication methods involving layer-by-layer assembly, electrospray, or enzyme-catalyzed crosslinking (HRP/H_2O_2) offer tailored functionality and bioactivity but come with technical constraints like enzyme degradation, time-consuming layering, or solvent incompatibility. Ultimately, the most translationally relevant methods will likely combine scalable structural formation techniques (electrospinning, 3D printing) with modular chemical strategies that allow for the incorporation of responsive, conductive, and therapeutic elements all synthesized under conditions that ensure reproducibility, sterility, and regulatory compliance. Further information on fabrication methods can be found in Fig. 17.

8.3. Key functional properties and biological effects

The breadth of key functional properties across these platforms reflects deliberate efforts to engineer multifunctional, biomimetic wound dressings that go well beyond simple scaffolds. A central theme is high electrical conductivity, which is critical for bioelectric signal delivery, stimulation-induced healing, and supporting endogenous electrophysiological processes. Reported conductivity values span from 10^{-4} to over 8 S/m, indicating significant progress, especially with PEDOT:PSS, PPy, rGO, and MXene-based systems. However, conductivity must be balanced with mechanical integrity, as soft, flexible materials are necessary for conformal skin contact, yet must also withstand handling, body movement, and exudate. Many platforms achieve tensile strengths exceeding 1 MPa and elongations beyond 200 %, with self-healing and stretchability integrated via dynamic bonds or double-network hydrogel structures. Responsiveness to NIR light, pH, ROS, strain, or temperature is another notable advancement, enabling smart platforms that adapt to wound environments. For instance, photothermal conversion for bacterial eradication and triggered drug release under NIR irradiation (~50–67 °C) is leveraged effectively in several systems. The incorporation of antioxidant properties (DPPH/ABTS scavenging), adhesiveness, and programmable swelling/degradation adds to their clinical realism, supporting both acute and chronic wound management. From a biological standpoint, the majority of platforms excel in antibacterial, antioxidant, and anti-inflammatory activity, crucial for preventing infection and controlling chronic inflammation in non-healing wounds. Many systems especially those incorporating silver nanoparticles, photothermal agents, or chitosan derivatives achieve >90 % bacterial reduction against common pathogens like *E. coli*, *S. aureus*, and even MRSA. Beyond microbial defense, an increasing number of platforms are designed to modulate the immune response, notably by inducing M1-to-M2 macrophage polarization, which is essential for transitioning from inflammation to tissue repair. This is paired with significant promotion of angiogenesis (↑VEGF, CD31) and collagen deposition, as evidenced by enhanced fibroblast proliferation, migration, and extracellular matrix remodeling. Systems responsive to ES demonstrate accelerated wound closure through improved calcium channel activation, actin cytoskeletal reorganization, and gene expression (TGF-β, EGF, PDGF). Notably, several advanced hydrogels and scaffolds maintain >90 % viability in L929 or 3T3 fibroblasts, affirming their cytocompatibility even when embedded with conductive or metallic agents. Integration with stem cells, Schwann cells, or ADSCs further elevates their regenerative potential, positioning these platforms not just as dressings, but as bioelectronic therapeutics capable of actively guiding tissue regeneration.

The current generation of wound healing platforms showcases impressive innovation in multi-functional integration, with several systems combining conductive scaffolding, ES, drug delivery, and immunomodulation in a single construct. For example, hydrogels capable of NIR-triggered antibiotic release, self-powered ES via triboelectric or biofuel mechanisms, or ROS-activated degradation mark a major leap forward. Others integrate piezoresponsive or

thermoresponsive behavior, enabling feedback-controlled behavior under physiological stimuli. Platforms that support real-time tissue monitoring, such as impedance-based cell growth detection or responsive drug release based on wound pH or oxidative status, point toward smart dressings with biosensing and therapeutic feedback loops. Importantly, materials like MXenes, ionic liquids, deep eutectic solvents, and catechol-functionalized biopolymers bring new levels of versatility to hydrogel systems. Still, despite the rapid evolution in functionality, the challenge remains in combining all these traits into simplified, clinically scalable architectures. Most systems still rely on multi-step syntheses or require complex instrumentation, which can limit mass production, increase cost, and complicate regulatory approval. The next innovation step lies in the modular assembly of synergistic components, ideally through one-pot synthesis, to enable user-friendly, disposable, or reusable wound interfaces. While the preclinical data and functional metrics are encouraging, the pathway toward clinical translation remains fragmented and underdeveloped. Critical gaps include long-term biosafety, standardized performance metrics (especially for conductivity and mechanical testing under wet conditions), and limited validation in large-animal or human models. Additionally, many highly conductive materials such as MXenes, high-load AgNPs, or PPy composites pose concerns around chronic toxicity, non-degradability, or systemic accumulation, especially in immunocompromised patients. There is also a need for customization of platforms for different wound types, such as diabetic ulcers, burns, surgical incisions, or pressure sores each of which has unique pathophysiological features. Regulatory agencies will scrutinize these materials not only for efficacy but also for stability, shelf-life, sterilization methods, and degradation byproducts. To bridge this gap, future platforms should focus on compliance with ISO and FDA guidelines, incorporation of biodegradable, GRAS-listed components, and development of ready-to-use, shelf-stable formats like sprayable gels, adhesive films, or wearable hydrogel patches. Additionally, digital integration, with mobile-connected biosensors for wound pH or electrical impedance tracking could enable remote monitoring and personalized wound therapy, a transformative direction for chronic care. Ultimately, the most impactful innovation will come not just from better materials, but from simplifying high-performance systems into clinically feasible solutions.

8.4. In vivo and in vitro models

The selection of in vitro and in vivo models across these studies reflects a deliberate strategy to balance mechanistic insight with biological relevance, yet also highlights gaps in standardization and translational readiness. In vitro models typically rely on fibroblast (NIH-3T3, L929, HDF), keratinocyte (HaCaT), endothelial (HUVEC), and macrophage (RAW264.7) cell lines, providing valuable data on cytocompatibility, adhesion, proliferation, migration, ROS scavenging, and inflammatory modulation. The frequent use of MTT, CCK-8, scratch assays, live/dead staining, and immunocytochemistry allows robust screening of bioactivity and cytotoxicity, while macrophage polarization assays and cytokine profiling deepen our understanding of immunomodulatory capacity. Furthermore, many platforms integrate ES, photothermal activation, and drug release studies to mimic wound microenvironments. However, there is often a lack of standardized exposure conditions (ES voltage/frequency, NIR parameters), which complicates direct comparison across studies. Most importantly, while 2D culture assays are accessible and informative, they fall short of replicating the complex immune, vascular, and ECM interactions of chronic or infected wounds, limiting their predictive power.

In vivo, the field has made strides by employing relevant full-thickness skin wound models, frequently using rat and mouse systems, often complicated with diabetes (STZ-induced) or bacterial infection (*S. aureus*, MRSA) to better reflect clinical wound challenges. Many studies go beyond simple wound closure tracking, incorporating histology (H&E, Masson's trichrome, Sirius Red), immunohistochemistry (CD31 for angiogenesis, CD86/CD206 for macrophage phenotype, α-SMA for fibrosis), and qRT-PCR (VEGF, TGF-β, IL-6) for molecular-level insight. Still, the heterogeneity of animal models, wound sizes, infection load, and treatment duration introduces variability. Several studies also explore burn wounds, buccal mucosal defects, and spinal cord injuries, reflecting an exciting push toward platform versatility but only a minority employ large-animal models, limiting direct extrapolation to human skin behavior. Furthermore, biodegradation kinetics, systemic toxicity, and long-term immunogenicity remain underexplored. For successful clinical translation, future research must incorporate standardized, reproducible wound models with clinically meaningful endpoints, and ideally include longitudinal data, larger species validation, and comparative benchmarks, to build a comprehensive preclinical dossier that aligns with regulatory and therapeutic expectations.

8.5. The impact on wound healing

Across the spectrum of materials evaluated, one of the most consistent outcomes is accelerated wound closure, often exceeding 90–97 % within 10–15 days in full-thickness wound models. Many platforms demonstrate not only faster closure but also improved tissue quality, characterized by increased collagen deposition, granulation tissue thickness, and neovascularization (CD31, VEGF expression). These improvements are typically linked to synergistic combinations of conductive scaffolds, ES, PTT, and responsive drug delivery. Particularly, hydrogels and electrospun membranes incorporating rGO, PEDOT:PSS, PPy, or MXene, along with therapeutic agents (VEGF, DOXH), outperform standard dressings like Tegaderm™ by promoting angiogenesis, re-epithelialization, and scar reduction. This integrative approach reflects a deeper understanding of the healing cascade, targeting multiple phases inflammation, proliferation, and remodeling simultaneously. A key advancement is the growing functional use of electrical conductivity, not just as a material trait, but as a therapeutic mechanism. Numerous studies report significantly enhanced fibroblast proliferation, actin organization, and faster re-epithelialization when scaffolds are combined with controlled ES. For example, platforms such as PLGA/GO with ES or PEDOT:PSS-coated scaffolds led to faster healing, improved barrier formation (Occludin/Claudin-1), and better tissue alignment. Notably, self-powered systems like TENGs and bioelectric patches eliminate the need for external power sources, utilizing body motion or respiration to deliver localized electrical cues. These approaches not only improve practicality but also begin to mimic the natural wound electric field, restoring bioelectric gradients that guide cell migration and regeneration. These findings validate conductivity as more than a passive property it's a powerful bioelectronic signaling cue when integrated properly. Beyond mechanical support and bioelectric regulation, conductive platforms are increasingly designed to offer infection control and inflammation management, especially for chronic and diabetic wounds. A large proportion of systems demonstrate >90 % bacterial clearance, with photothermal agents (CNTs, PPy/I, MXene) reaching up to 99.9 % efficacy under NIR light. Antioxidant capacity (via ROS scavenging or thioketal-based degradation) also reduces oxidative stress, thereby promoting cellular proliferation. Immunomodulatory effects are particularly promising, with multiple studies showing increased M2 macrophage polarization, suppression of pro-inflammatory cytokines (TNF-α, IL-6), and elevated anti-inflammatory markers (IL-10, Arg-1). These outcomes support not just rapid closure, but higher-quality healing with reduced scarring and chronicity, making these materials highly suitable for wounds complicated by infection, immune dysregulation, or aging.

What distinguishes the top-performing platforms is not only speed but the functional and structural quality of the regenerated skin. Studies report full epidermal reconstitution, hair follicle regeneration, capillary network formation, and ECM organization, verified via histology and immunofluorescence (α-SMA, collagen I/III, Ki-67). Several platforms,

especially those combining biophysical stimuli (ES, PTT, ROS signaling) with bioactive cues (growth factors, stem cells, or neurotrophic factors) support nerve reinnervation, sweat gland regeneration, and improved dermal thickness, reaching near-complete skin restoration. This level of outcome suggests an evolution from passive dressings to active regenerative matrices, capable of reprogramming immune response, guiding angiogenesis, and reestablishing sensory function, key metrics for durable healing, especially in full-thickness and chronic wounds. An emerging hallmark of these platforms is the synergy of multi-modal therapies. For instance, materials that combine electrical conductivity with photothermal response and smart drug release often outperform single-function platforms. The DOXH + conductive hydrogel, or CNTs + NIR + VEGF-loaded platforms, show additive or even synergistic benefits across all healing dimensions, faster closure, enhanced tissue organization, and reduced infection. Some materials even demonstrate smart responsiveness, with real-time sensing of inflammation, bacterial presence, or pH changes, enabling precision therapy. Moreover, platforms with biosignal recording capabilities (ECG, EMG, SSEPs) or those integrating into motion-sensitive systems open the door to closed-loop bioelectronic medicine, where healing is both monitored and adjusted in real time. These next-generation designs are particularly exciting for digital wound care management and remote therapeutic platforms. Despite the remarkable healing outcomes observed in vivo, translational barriers remain. Most studies use small animal models (mice or rats), with limited long-term tracking of immune responses, biodegradation, or systemic toxicity. While materials often show high biocompatibility and cytocompatibility, more rigorous studies on sterilization, storage, large-scale reproducibility, and chronic use safety are needed. The variability in wound sizes, treatment durations, and evaluation endpoints also limits comparative benchmarking. Moreover, manufacturing scalability for platforms that require multi-step synthesis, complex doping, or photothermal agent loading remains a hurdle. For clinical translation, the most viable candidates will be those offering easy fabrication, shelf stability, user-friendly application (sprays, patches, injectables), and regulatory-aligned material composition. Nonetheless, the healing performances reported here demonstrate that conductive wound platforms are not only viable but are nearing readiness for first-in-human clinical evaluation, particularly in high-risk populations such as diabetic foot ulcer or burn patients.

9. Critical comparison of conductive polymer systems

9.1. General discussion

The PP-CDLut-AMY MN system demonstrates excellent mechanical strength, with a tip deactivation force of 2.18 N, well above the 0.06 N minimum required for skin penetration ensuring effective and safe application. Although electrical conductivity is not reported, it is likely negligible, as it plays no role in the intended biomedical functions. The MN exhibits outstanding biocompatibility, as confirmed by high cell viability (>80 %), minimal hemolysis (<0.5 %), no observed toxicity in major organs, and normal weight gain in treated animals. Its application scope is broad, offering combined antioxidant, photothermal antibacterial, and biofilm-degrading capabilities, making it a highly effective and safe dressing for infected chronic wounds, particularly those involving *S. aureus* biofilms [38]. The A30 and AA-A30 hydrogels exhibit exceptional multifunctional performance for biomedical applications, particularly in wound healing and anti-adhesion therapy. The hydrogels show moderate electrical conductivity, as evidenced by their ability to induce depolarization of PC12 cells, indicating suitability for use in electroactive wound healing and neural interfaces. Their mechanical strength is excellent, with tunable compressive modulus and non-linear stress-strain behavior similar to human skin, offering resistance to deformation and maintaining structure during application. Both A30 and AA-A30 hydrogels demonstrate high biocompatibility, supported by >190 % L929 and HUVEC cell viability, minimal organ toxicity, and no adverse tissue response in vivo. In terms of application scope, the hydrogels possess robust wound healing capabilities, enhancing angiogenesis, reducing inflammation, and accelerating skin regeneration, while the AA-A30 variant provides strong anti-adhesion functionality in surgical settings by modulating the fibrinolytic system (↑tPA, ↓PAI-1), forming a physical barrier, and resisting postoperative adhesion formation [39].

The PDA@AgNPs-PPyGel-Fe hydrogels exhibit a multifunctional profile ideal for advanced wound care applications. The hydrogels show excellent electrical conductivity, ranging from 24 to 36 mS/cm, significantly surpassing the native conductivity of skin (1×10^{-4} to 2.6 mS/cm), and are capable of powering an LED, confirming their bioelectronic potential. They also possess high mechanical strength, with compressive stress resistance up to 55 kPa and 60 % deformation, while remaining soft and flexible properties enhanced by Fe^{3+} cross-linking and the incorporation of PDA@AgNPs. The hydrogels display exceptional biocompatibility, with <5 % hemolysis, >80 % L929 cell viability over 72 h, and normal cell morphology, as well as demonstrated blood coagulation activity (BCI <30 %). Their application scope is extensive: they offer robust antioxidant activity (100 % DPPH and $ABTS^{+}$ radical scavenging at high PDA@AgNP content), strong broad-spectrum antibacterial effects against *E. coli* and *S. aureus* (>90 % kill rate), self-healing capability within 30 min, and stable rheological behavior under physiological conditions. These properties make them highly suitable for electroactive wound dressings, infection control, moist wound healing, and potential biosensing or wearable electronic interfaces [40].

The GC/BP bioactive film, composed of CS, GE, BH, and PPy, demonstrated strong multifunctionality, including photothermal, conductive, antioxidant, and antibacterial properties, while maintaining excellent biocompatibility. At 5 % PPy, the film reached a safe peak temperature of ~47 °C under irradiation, showing photothermal stability and a conversion efficiency of 21.07 %. Mechanically, BH enhanced tensile strength and elasticity, while PPy improved flexibility. The film showed amorphous structure, uniform integration of components, and strong hydrogen bonding compatibility. Optical tests revealed good transparency modulation by BH and strong light absorption by PPy. Breathable, hydrophilic, and thermally stable, the film's conductivity rose to 0.3119 μS/cm with PPy. BH demonstrated a fast release profile fitting first-order kinetics, beneficial for early-stage antimicrobial action. The film exhibited prolonged antioxidant activity, with >92 % DPPH scavenging after 48 h, and excellent blood compatibility (hemolysis <5 %) and cytocompatibility (>80 % L929 cell viability). Antibacterial assays revealed >97 % inhibition of *S. aureus* and enhanced *E. coli* killing under NIR light due to PPY's photothermal effect. In vivo, the GC/BP + NIR film promoted wound healing (93.2 % closure in 9 days), significantly reduced inflammation (low TNF-α), increased fibrous tissue and vascular regeneration (CD31 expression), and showed no systemic toxicity, suggesting high potential as a multifunctional wound dressing [41]. The PPy-BiOCl intercalated nanosheets demonstrate a highly effective multifunctional platform for wound healing and infection control through synergistic PTT and PDT. The nanosheets exhibit moderate electrical conductivity, enhanced by the conductive PPy intercalation, supporting photocurrent generation and ROS production under NIR light. Mechanically, they maintain robust nanosheet morphology and thermal stability (~275–500 °C), with a tightly confined, layered structure allowing effective energy transfer. Biocompatibility is excellent, with >98 % BMSC cell viability, <1 % hemolysis, and no organ toxicity observed in vivo. In terms of application, the platform offers strong antibacterial performance (99.25 % for *S. aureus*, 99.23 % for *E. coli*), photothermal conversion (up to 50 °C in 10 min), and in vivo wound healing enhancement showing over 90 % wound closure in 14 days with significant collagen regeneration and reduced inflammation [42]. Therefore, PPy-incorporated platforms for wound healing exhibit a wide range of functional properties suitable for biomedical applications. Their electrical conductivity spans from

0.3119 μS/cm (as seen in GC/BP films) to 36 mS/cm (in PDA@AgNPs-PPyGel-Fe hydrogels), enabling both mild electroactivity and high conductivity for bioelectronic interfaces. Mechanical strength is consistently excellent across systems, with tensile strength reaching up to 8.05 mPa, compressive strength up to 55 kPa, and elongation at break up to 99.6 %, ensuring flexibility and durability for skin-like wound dressings. All platforms demonstrate outstanding biocompatibility, with cell viability ranging from >80 % to >190 %, hemolysis rates below 5 %, and no observed organ toxicity in vivo.

The PAM-SHA-PANI (PSP) hydrogel platform demonstrates excellent multifunctional properties for wound healing applications. It exhibits notable electrical conductivity at 1.05 mS/cm in swollen state and 1.20 mS/cm when dry, ensuring sustained electroactivity in physiological conditions. Its mechanical strength is significantly enhanced, with tensile strength and elongation at break increased by 300 % and 115 %, respectively, compared to control, and remains stable under dynamic conditions. The platform also shows superior biocompatibility, maintaining >98.2 % cell viability in fibroblast cultures and exhibiting no cytotoxic effects. In terms of application, the hydrogel is selectively effective against Gram-positive bacteria, inhibits biofilm formation, and shows substantial in vivo efficacy in wound healing enhancing epithelialization, collagen remodeling, and angiogenesis. Notably, it performs synergistically with ES to further accelerate healing, making it a strong candidate for chronic wound management [44]. The Me-PANI NPs@PAM hydrogel is a multifunctional wound dressing platform with strong mechanical resilience, excellent photothermal antibacterial effects, and reliable biocompatibility. It incorporates amphiphilic PANI-g-MeGC copolymers that self-assemble into nanoparticles and are embedded into a polyacrylamide (PAM) matrix. The resulting hydrogel displays robust mechanical properties, with compressive toughness and up to 400 % stretchability, ideal for dynamic body areas. It exhibits high photothermal efficiency, achieving surface temperatures >50 °C under NIR irradiation, effectively killing *S. aureus* and MRSA biofilms within 10 min. The hydrogel also maintains a high swelling ratio (~1300 %) and excellent water retention (70 % after 7 days), supporting a moist wound environment. Importantly, it shows strong biocompatibility, with >80 % cell viability even after NIR exposure, indicating no thermal cytotoxicity [46]. PANI-based hydrogels for wound healing exhibit a versatile range of performance characteristics. Their electrical conductivity ranges from 1.05 to 1.20 mS/cm (as seen in the PSP hydrogel), enabling electroactive wound environments, while photothermal systems like Me-PANI NPs@PAM achieve antibacterial action through NIR-triggered heating rather than conductivity. Mechanically, these hydrogels are highly resilient, with tensile strength improved by up to 300 % and stretchability reaching 400 %, making them suitable for dynamic body areas. Both systems show excellent biocompatibility, maintaining >80–98 % cell viability even under elevated temperatures (>50 °C). Antibacterial activity is strong and mechanism-dependent: PSP is selectively bactericidal to Gram-positive bacteria and inhibits biofilms, while Me-PANI NPs@PAM effectively eliminates *S. aureus* and MRSA biofilms via photothermal effects. Additionally, both hydrogels support a moist wound environment, with swelling ratios around 1300 % and water retention of ~70 % over 7 days. Collectively, these features make PANI-based platforms highly effective for advanced wound care, particularly in infected or chronic wound settings.

The PEDOT:PSS-coated porous (P5) membrane platform demonstrates a synergistic combination of mechanical and ES for enhanced wound healing. Structurally, the membrane features a 3D microporous surface formed via high-speed spin-coating, which increases surface roughness and stiffness (Young's modulus up to 214 MPa). Conductivity is enhanced through multiple PEDOT:PSS coatings, with optimal performance at 6 coatings, balancing surface conductivity, biocompatibility, and mechanical cues. Electrically stimulated P5 membranes support superior keratinocyte adhesion, proliferation, and tight junction formation, leading to robust cell sheet formation and detachment. In vivo, these membranes significantly accelerate wound closure (down to 4.8 % residual wound at day 7) and promote epithelial regeneration, angiogenesis (CD31↑), and reduced inflammation (TNF-α↓). They also enhance epidermal maturation (K10↑, K14↑) and barrier integrity (Occludin↑, Claudin-1↑), outperforming flat controls. These results highlight the P5 membrane's strong potential for clinical wound dressing, particularly in regenerative skin applications requiring electrostimulation [47].

9.2. Critical comparison

CP systems developed for wound healing applications exhibit a diverse range of functionalities, with each material excelling in specific performance criteria. Among these, PDA@AgNPs-PPyGel-Fe hydrogels stand out for their exceptional electrical conductivity (24–36 mS/cm), surpassing skin's natural conductivity and supporting bioelectronic applications such as LED powering and ES, while also offering excellent mechanical resilience (compressive stress resistance up to 55 kPa), self-healing, and broad-spectrum antibacterial and antioxidant activity making them the most versatile multifunctional dressing. In contrast, the P5 membrane system, coated with PEDOT:PSS, excels in promoting rapid wound healing and tissue regeneration through combined mechanical (Young's modulus of 214 MPa) and ES, achieving the fastest wound closure (residual wound area reduced to 4.8 % by day 7) and enhanced skin barrier integrity. For applications prioritizing flexibility and dynamic movement, the Me-PANI NPs@PAM hydrogel provides excellent photothermal antibacterial effects, especially against MRSA biofilms, and mechanical adaptability with 400 % stretchability, high swelling ratio (~1300 %), and sustained water retention ideal for moist wound healing in mobile body regions. A30 and AA-A30 hydrogels demonstrate superior biocompatibility (cell viability >190 %) and wound healing performance, particularly in promoting angiogenesis and minimizing post-surgical adhesion through fibrinolytic modulation, making them highly suitable for surgical or chronic wound scenarios. The GC/BP film, incorporating PPy and berberine, offers a balanced profile of photothermal antibacterial action, antioxidant activity, and moderate conductivity, supporting both early-stage infection control and long-term healing with 93.2 % wound closure in 9 days. The PPy-BiOCl nanosheets provide unique dual-mode photodynamic and photothermal therapy with strong antibacterial effects (~99 % bacterial kill) and over 90 % wound closure in 14 days, benefiting from moderate conductivity and high ROS generation. The PSP (PANI) hydrogel is also effective in electroactive wound environments, with good conductivity (1.05–1.2 mS/cm), enhanced tensile strength (+300 %), and synergistic performance with ES, though its antibacterial action is more selective for Gram-positive strains. Finally, while the PP-CDLut-AMY microneedle system lacks electrical conductivity, it offers outstanding mechanical performance (tip force of 2.18 N), biocompatibility, and antimicrobial functionality through biofilm degradation and antioxidant activity, targeting infected chronic wounds effectively. Overall, the optimal polymer system depends on application context: PDA@AgNPs-PPyGel-Fe for multifunctional bioelectronics and infection control; P5 for accelerated healing and stimulation-based regeneration; Me-PANI for dynamic, infected wounds; and A30/AA-A30 for surgical wound healing and anti-adhesion therapy, highlighting the need for tailored material selection based on clinical requirements. Table 5 further summarizes these aspects of conductive polymers in wound healing acceleration.

10. Mechanistic insights: how conductive platforms modulate cellular behavior

Direct membrane depolarization and ion channel activation is one of the most immediate cellular responses to conductive substrates. CPs such as PPy and PEDOT:PSS, either through passive electron mobility or under applied ES, have been shown to alter the resting membrane potential of cells like fibroblasts and keratinocytes. this localized depolarization can activate voltage-gated calcium channels (VGCCs), leading

to an influx of Ca^{2+} ions an essential second messenger in cell signaling. elevated intracellular calcium concentrations influence key pathways that govern cytoskeletal rearrangement, focal adhesion turnover, and ultimately, directed cell migration and proliferation. specifically, calcium influx activates calmodulin-dependent kinases (CaMKs) and downstream transcriptional regulators such as NFAT, promoting the expression of genes critical to wound closure and tissue regeneration. these early electrochemical events are pivotal in enhancing cell responsiveness and guiding their alignment and movement across the wound bed, thereby accelerating the re-epithelialization process.

Ion transport and charge density effects also play a central role in the interaction between conductive materials and cellular systems. materials like PDA/PPy composites exhibit both high surface charge density and ionic conductivity, contributing to the formation of electrochemical gradients at the interface between the scaffold and the adhered cells. these gradients influence membrane-localized processes, notably the clustering of integrins transmembrane receptors that mediate cell adhesion and mechanotransduction. the engagement and clustering of integrins activate FAK and downstream pathways such as RhoA/ROCK and ERK/MAPK, leading to enhanced cell spreading, migration, and polarity. in addition, PDA (polydopamine) surfaces are rich in catechol groups, which can mimic mussel-inspired adhesion and promote protein adsorption. these functional groups can engage integrin ligands or interact with extracellular matrix components such as fibronectin and vitronectin, thereby reinforcing cell–material interactions and contributing to ECM remodeling. this synergy between electrical and biochemical cues at the material interface supports an environment conducive to regenerative healing.

Growth factor receptor sensitization and signal amplification offers another mechanistic layer through which conductive platforms modulate cellular behavior. conductive materials have been shown to enhance the sensitivity and activation of membrane-bound growth factor receptors particularly VEGFR, EGFR, and PDGFR by promoting receptor clustering and localized phosphorylation. under sub-threshold electric fields (as low as a few millivolts per millimeter), cell membranes may experience rearrangement of lipid rafts and increased fluidity, facilitating the redistribution of receptor proteins and co-localization with their ligands. in platforms like PLGA/PDA/CS membranes, the PDA coating plays a crucial role in mediating non-covalent adsorption of bioactive proteins, such as fibronectin or laminin, which further potentiates receptor activation and downstream signaling through canonical pathways like PI3K/Akt and MAPK/ERK. these pathways are intimately linked to angiogenesis, cell survival, and proliferation key elements of effective wound healing. this receptor sensitization allows

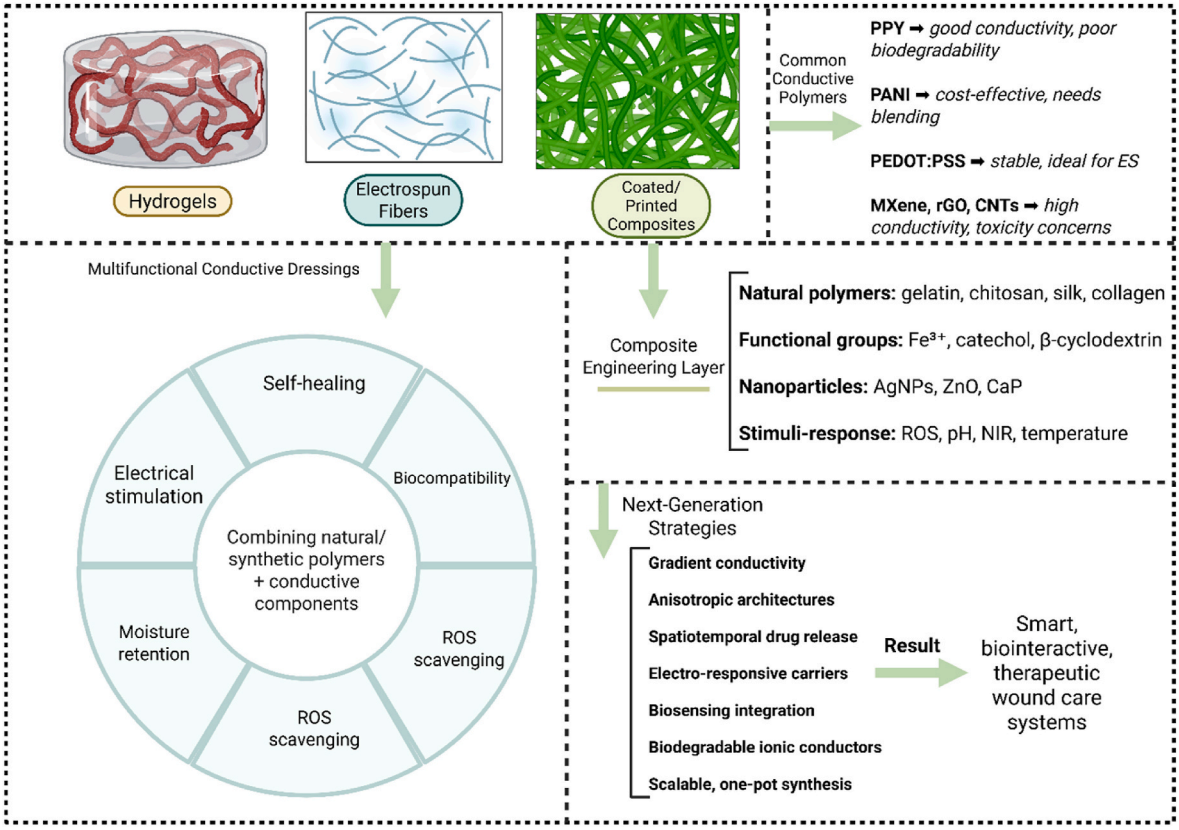

Fig. 16. Schematic representation of the evolution, composition, and design strategies of conductive polymer-based platforms for wound healing applications. The figure illustrates the primary material forms used in conductive wound dressings namely hydrogels, electrospun nanofibers, and coated/printed composites each offering unique advantages such as conformability, high surface area, and mechanical robustness. These materials serve as foundational scaffolds that are increasingly engineered into multifunctional hybrid platforms through the incorporation of conductive polymers ([PPy, PANI, PEDOT:PSS) and nanofillers (MXenes, CNTs, rGO). The selection of conductive components is governed by desired attributes such as electrical conductivity, processability, biocompatibility, and in vivo safety, with each material presenting a distinct trade-off between performance and biodegradability. Central to next-generation design is the integration of natural biopolymers (gelatin, chitosan, silk fibroin, collagen) functionalized with moieties like catechol or Fe^{3+} ions to confer properties such as tissue adhesion, self-healing, injectability, and ROS scavenging. Simultaneously, inorganic elements like AgNPs or ZnO are added for antimicrobial action, while the inclusion of stimuli-responsive elements (ROS-, pH-, or temperature-sensitive domains) allows for on-demand drug release or behavior modulation. Toward clinical translation, advanced design approaches are emerging that involve gradient conductivity for directional cell migration, anisotropic topographies for guided regeneration, biosensing for real-time feedback, and electroactive drug carriers for precise control. These combined strategies represent a shift from passive coverage materials to dynamic, biointeractive systems capable of real-time monitoring, targeted therapy, and active participation in tissue regeneration underscoring the convergence of materials science, bioelectronics, and regenerative medicine in the development of future wound healing platforms.

cells to respond more robustly to both scaffold-embedded and endogenous growth cues, offering a powerful method of amplifying therapeutic outcomes without supraphysiological stimulation.

Gene expression modulation represents a more sustained and systemic cellular response to the biophysical and biochemical cues delivered by conductive scaffolds. transcriptomic and proteomic analyses of cells cultured on conductive platforms reveal upregulation of genes associated with angiogenesis (VEGF, HIF-1α), extracellular matrix production (collagen type I, fibronectin), and anti-inflammatory responses (IL-10, MRC1). this suggests that conductive materials not only influence immediate membrane events but also initiate intracellular signaling cascades that reprogram gene expression patterns. the exact mechanisms are still being elucidated, but they likely involve both transcriptional and epigenetic changes. for instance, ionic signaling triggered by conductive materials may influence chromatin accessibility via histone acetylation or methylation states, thereby enhancing the transcription of genes involved in regeneration. furthermore, mechanical cues imparted by scaffold architecture and stiffness often modulated by CP composition may activate YAP/TAZ and other mechanosensitive transcription factors that synergize with electrical stimuli. taken together, these findings underscore that conductive wound healing platforms function as more than passive supports; they act as dynamic bioelectronic interfaces that engage and regulate cellular machinery at multiple levels, from membrane polarization to genomic reprogramming.

11. Challenges and future directions in conductive polymer-based wound healing

One major gap in the field of CPs for wound healing lies in the lack of comprehensive understanding of their long-term biocompatibility and degradation behavior in vivo. Although CPs like PPy, PANI, and PEDOT have shown promising short-term benefits in promoting cell proliferation, migration, and angiogenesis, the consequences of their prolonged presence within biological environments remain poorly characterized. Potential concerns such as chronic inflammation, immune responses, or toxicity due to degradation byproducts have not been sufficiently investigated. Without robust longitudinal studies, the safety profile of CP-based dressings, particularly for chronic or complex wound types requiring extended application periods, remains uncertain. Addressing these issues is critical to moving from proof-of-concept to widespread clinical adoption. Another significant challenge is the scalability and

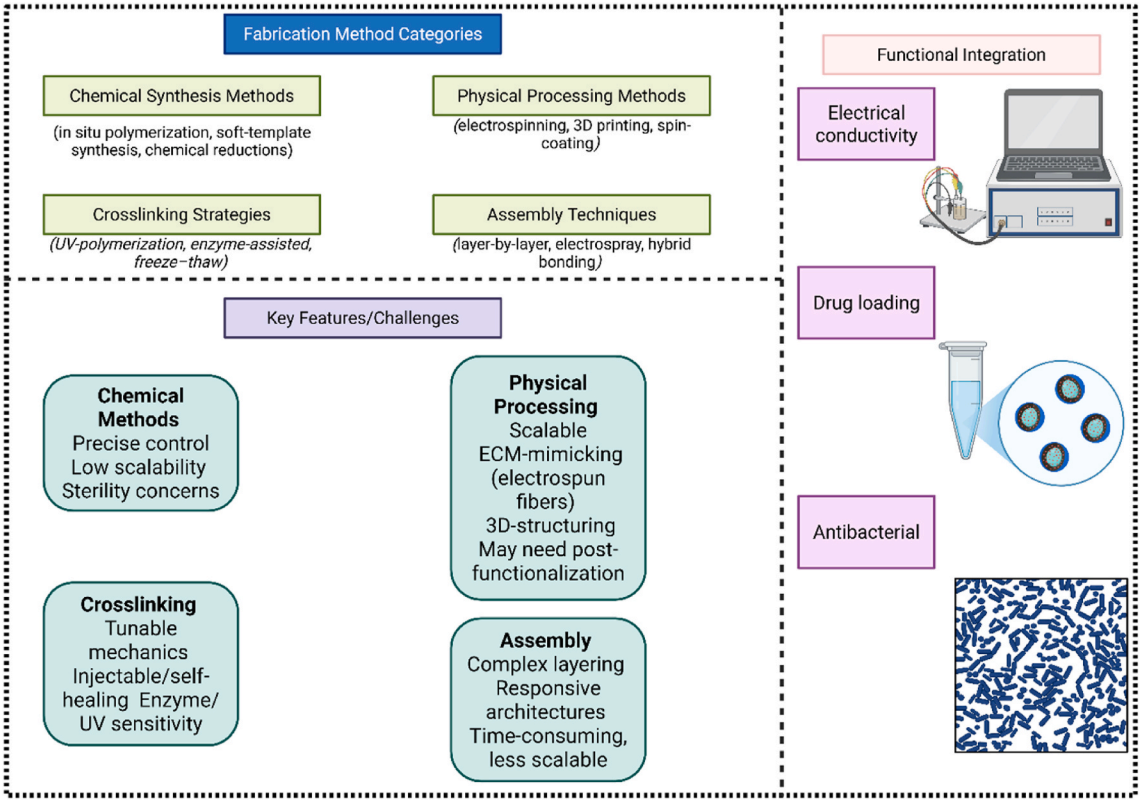

Fig. 17. Comprehensive schematic of fabrication strategies for conductive polymer-based wound healing platforms, highlighting their methodological categories, functional integration, and translational potential. The figure organizes fabrication approaches into four major categories: (1) chemical synthesis methods such as in situ polymerization, nanoparticle templating, and soft-template synthesis, which enable precise material customization but often lack scalability and sterility robustness; (2) physical processing methods like electrospinning, spin-coating, and 3D printing, which offer excellent scalability, tunable architectures, and compatibility with bioactive loading, particularly for mimicking ECM and integrating into wearable formats; (3) crosslinking strategies including UV-induced polymerization, freeze–thaw cycles, and enzyme-catalyzed crosslinking (HRP/H_2O_2), which are essential for forming stable, injectable, and often self-healing hydrogels with tailored degradation and adhesion properties; and (4) assembly techniques such as layer-by-layer deposition, hybrid coating, and electrospray-assisted polymerization, which allow the construction of multi-functional, hierarchical platforms capable of delivering electrical, mechanical, or biochemical cues. Each fabrication class connects via directional arrows to a central cluster of integrated functionalities, including electrical conductivity, drug release capacity, ROS/pH/NIR responsiveness, mechanical adaptability, and biological activity (angiogenesis, antimicrobial function). These features are critical for next-generation smart dressings. The final layer of the figure stratifies methods based on clinical translation readiness highlighting scalable, industry-aligned processes (electrospinning, UV-crosslinking, freeze–thaw) versus more complex, less scalable strategies (multi-step chemical reductions, enzyme-based systems) that may offer functional advantages but face regulatory and production barriers. The overall layout underscores the need for future fabrication to balance multifunctionality, biointegration, and manufacturing simplicity favoring one-pot, aqueous, room-temperature synthesis routes using GRAS components. This convergence of engineering precision with translational pragmatism defines the current and future landscape of fabrication in bioelectronic wound healing platforms.

Table 5
A critical comparison of different conductive polymer systems for wound healing.

Platform	Electrical Conductivity	Mechanical Strength	Biocompatibility	Application Scope	Refs
α-Amylase and polydopamine@polypyrrole-based hydrogel microneedles	–	2.18 N per needle (≫ 0.06 N required)	Excellent (low cytotoxicity, hemolysis <0.5 %, no organ damage)	Wound healing, biofilm decomposition, photothermal therapy, antioxidant delivery	[38]
Polypyrrole-modified gelatin-based hydrogel	Moderate (induces PC12 depolarization; suitable for electroactive cell regulation)	High; skin-mimetic non-linear compression behavior; stable rheology even with PEG-NHS	Excellent; >190 % cell viability, no organ toxicity, strong cytocompatibility and histocompatibility	Broad: wound healing, angiogenesis, inflammation control, tissue adhesion prevention, neural interfacing	[39]
PDA@AgNPs-PPyGel-Fe Hydrogel	High (24–36 mS/cm), suitable for bioelectronic wound dressings	Strong yet flexible (up to 55 kPa, 60 % strain); soft and skin-compatible	Excellent (<5 % hemolysis, >80 % cell viability, low BCI, non-toxic morphology)	Multifunctional: wound healing, antioxidant, antibacterial, self-healing, bioelectronics	[40]
GC/BP film	0.3119 μS/cm (enhanced by PPY)	TS: ~4.3–8.05 mPa; EAB: up to 99.6 %	Hemolysis <5 %; L929 viability >80 %; no organ toxicity	Antibacterial (NIR-enhanced), antioxidant, drug delivery, photothermal wound healing	[41]
PPy-BiOCl intercalated nanosheets	Moderate; supports photocurrent & ROS generation under NIR	Stable nanosheet structure; thermal stability up to 500 °C	>98 % BMSC viability; <1 % hemolysis; no organ toxicity	NIR-triggered PDT/PTT, antibacterial (99 %+), wound healing, collagen regeneration	[42]
PAM-SHA-PANI (PSP) Hydrogel	1.05 mS/cm (swollen), 1.20 mS/cm (dry)	300 % increase in tensile strength and 115 % higher elongation at break vs control; stable under strain up to 179 % and frequency range of 0.1–100 Hz	High cell viability (>98.2 % with L929 fibroblasts); non-cytotoxic; excellent cell compatibility (live/dead staining)	Bactericidal to Gram-positive bacteria; inhibits biofilm formation; promotes wound closure, collagen deposition, angiogenesis; synergizes with ES	[44]
Me-PANI NPs@PAM Hydrogel	–	Compressive recovery and tensile strain up to 400 %; enhanced strength with increasing NPs (up to 10 mg/mL)	>80 % NIH3T3 viability with or without NIR; no cytotoxicity; thermally safe	Photothermal antibacterial (*S. aureus*, MRSA), anti-biofilm, water-retentive wound dressing; suitable for NIR-responsive infection control	[46]
PEDOT:PSS-Coated P5 Membrane	High (increases with coating, optimal at 6 ×)	Young's modulus up to 214 MPa, roughness up to 23 nm; optimal coating: 6 × for performance balance	Promotes keratinocyte adhesion, viability (>90 %), and sheet formation; non-toxic under ES	Wound healing via cell sheet engineering, ES-assisted epithelialization, angiogenesis, barrier formation, and inflammation reduction	[47]

reproducibility of CP-based wound dressings. Many innovative strategies involve intricate fabrication techniques, such as electrospinning, in-situ polymerization, or nanocomposite integration, which are often labor-intensive and difficult to standardize on a commercial scale. Variations in batch quality can impact mechanical properties, conductivity, and biocompatibility, leading to inconsistent clinical outcomes. Moreover, the cost associated with producing these advanced materials is still relatively high compared to conventional wound care products. To bridge this gap, there is a need for streamlined, cost-effective manufacturing processes that ensure consistent quality, reproducibility, and scalability without compromising the functional advantages of CPs. An additional research gap concerns the limited integration of real-time monitoring and adaptive response capabilities into conductive wound healing systems. While prototypes combining CPs with sensors and stimuli-responsive elements (such as pH-sensitive or photothermal-triggered drug release systems) have demonstrated potential, most devices are still in early stages of development and lack the sophistication required for dynamic, personalized wound management. Current systems often function independently rather than interactively adjusting treatment protocols based on the evolving wound environment. Future research must focus on developing fully integrated smart wound dressings that not only detect physiological changes like infection or pH shifts but also autonomously modulate therapeutic responses (adjusting ES or drug delivery accordingly). The interaction between CPs and complex wound environments, especially those involving bacterial biofilms, diabetic wounds, or ischemic tissues, also remains insufficiently explored. While CPs inherently possess some antibacterial and antioxidant properties, the extent of their effectiveness in hostile wound environments characterized by persistent infection, oxidative stress, and impaired angiogenesis is unclear. Furthermore, the mechanisms through which ES delivered via CP-based platforms might synergistically enhance antimicrobial activity or modulate immune responses are not fully understood. Investigating these interactions at a cellular and molecular level would provide critical insights necessary for optimizing CP-based therapies for challenging wound types. Finally, there is a translational gap between promising laboratory results and clinical application. Despite numerous successful preclinical studies, few CP-based wound healing products have advanced to clinical trials, let alone received regulatory approval. This gap is partly due to regulatory uncertainties regarding novel bioelectronic materials, as well as the absence of standardized testing protocols that evaluate both electrical performance and biological safety in a unified manner. Furthermore, there is a need for multidisciplinary collaborations among material scientists, bioengineers, clinicians, and regulatory experts to design studies that address real-world clinical needs while satisfying regulatory demands. Without such concerted efforts, the remarkable therapeutic potential of CPs risks remaining confined to academic research.

While CPs such as PPy, PANI, and PEDOT have demonstrated immense potential in smart wound healing applications due to their electrical conductivity, antibacterial properties, and ability to promote tissue regeneration, their long-term biocompatibility and degradation behavior warrant careful consideration. Many CP-based dressings incorporate biodegradable substrates like poly(L-lactide) (PLLA), which, although effective as structural matrices, produce byproducts such as lactic acid that can lower local pH and potentially trigger inflammatory responses if not adequately managed. Additionally, the slow degradation of certain polymeric scaffolds may misalign with the dynamic phases of wound healing, thereby impeding optimal tissue remodeling. Consequently, integrating degradation studies and assessing the bioactivity of degradation byproducts are essential steps in developing CP-based systems that are both safe and effective for long-term clinical use. Future research must not only focus on enhancing the functional performance of these materials but also on tuning degradation kinetics and ensuring that byproducts do not adversely affect wound healing

outcomes.

Standard rat models of wound healing, such as those used to evaluate materials like PPy/PDA/PLLA nanofibers, CG/DA-Ppy hydrogels, and MnCoO@PDA/CPH scaffolds, have proven useful in demonstrating proof-of-concept efficacy for novel wound healing therapies, particularly in terms of biocompatibility, conductivity, and antibacterial activity. However, these models fall short of replicating the intricate and multifactorial pathology of human chronic wounds. One of the primary limitations is the inability of rodent models to fully mimic the immunological dysregulation seen in chronic human conditions like diabetic foot ulcers, where persistent inflammation, impaired angiogenesis, and disrupted macrophage polarization (M1/M2 balance) are central features. Moreover, human chronic wounds often host polymicrobial communities organized into biofilms, which confer significant resistance to treatments a complexity not faithfully reproduced in most rodent models that typically involve mono-infections or acute bacterial challenges. Rats also possess loose skin and a high capacity for wound contraction due to the panniculus carnosus muscle, a trait not present in humans, which leads to healing mechanisms that rely less on re-epithelialization and granulation tissue formation. As a result, while rat models are effective for early-stage screening of materials and mechanisms such as photothermal effects, ES-driven tissue regeneration, and antibacterial efficacy they are limited in their ability to predict therapeutic outcomes in human clinical scenarios. Translational challenges include discrepancies in immune response dynamics, tissue architecture, wound chronicity, and the physiological impact of comorbidities like diabetes, vascular disease, and aging. To bridge this gap, future studies should incorporate more representative models, such as diabetic pigs or humanized mouse models with biofilm-infected wounds, to better simulate the chronicity, microbial burden, and immune dysfunction characteristic of human pathology.

12. Conclusion and perspectives

The incorporation of CPs into wound healing systems marks a major advancement in regenerative medicine. CPs, like PPy, PANI, and PEDOT, leverage their unique electroactive characteristics to accurately replicate the body's natural electrical environment, thus facilitating crucial cellular processes such as migration, growth, and differentiation. When combined with nanofibers, hydrogels, scaffolds, and membranes, these polymers offer various benefits, enhancing electrical conductivity while also providing antibacterial, antioxidant, and hemostatic features. Additionally, their ability to develop composites using both natural and synthetic biomaterials significantly improves their mechanical strength, biocompatibility, and response to physiological stimuli. This multifunctionality allows for the management of various wound types, such as diabetic ulcers, infected wounds, and burns, which are often aggravated by inflammation, bacterial colonization, and inadequate vascularization. Additionally, the integration of CPs into smart dressing systems like self-powering triboelectric devices, photothermal activated patches, and pH/glucose-sensitive hydrogels highlights their potential in creating adaptive, personalized treatment platforms. These advanced systems offer real-time observation, controlled drug administration, and accurate ES independently of external power sources, addressing the rising demand for non-invasive, self-managing treatments. The combination of materials science, nanotechnology, and bioelectronics in these applications suggests that CPs will play a crucial role in the next generation of wound care technologies. Continuous multidisciplinary studies, along with translational clinical research, are essential to maximize their therapeutic capabilities and promote the integration of these novel systems from the lab into routine medical practice.

The effective use of CPs in wound healing is advancing rapidly, presenting promising opportunities for personalized, efficient, and minimally invasive therapies. In clinical settings, these materials are being explored for developing smart wound dressings capable of delivering localized ES to enhance cellular processes, such as fibroblast growth, angiogenesis, and collagen production crucial factors in accelerating tissue repair. Hydrogels and nanofibrous scaffolds made from CPs have proven to be especially effective in treating chronic wounds, including diabetic foot ulcers and pressure sores, where traditional treatments often fail because of persistent inflammation, poor vascularization, and microbial infections. Their natural antibacterial and antioxidant properties reduce the need for systemic antibiotics, thus lowering the risk of antibiotic resistance. Additionally, their incorporation with wearable bioelectronic devices, such as TENGs and piezoelectric patches, enables self-sufficient, real-time monitoring and treatment of wounds, which is especially beneficial in outpatient and remote care settings. CP-based photothermal and pH-responsive systems enable precise, on-demand drug release, making them appropriate for evolving wound environments that require flexible responses. These advanced technologies not only shorten recovery time but also reduce scarring and improve patient comfort and compliance. While most clinical applications still exist in preclinical or experimental stages, a few prototypes have shown considerable translational potential, aiding the process towards gaining regulatory approval and integration into standard wound care practices. As their efficacy and safety gain validation through clinical trials, CPs are expected to revolutionize wound treatment approaches in both hospital and home-care environments.

The stages of wound healing most significantly affected by CPs and platforms are the proliferation and remodeling (maturation) phases. Conductive materials consistently enhance fibroblast proliferation, angiogenesis (new blood vessel formation), granulation tissue formation, and re-epithelialization. This is evidenced by frequent reporting of enhanced cell migration, angiogenesis, collagen deposition, and reduced inflammation across the platforms evaluated. These materials also show strong effects on tissue remodeling and wound closure. Remodeling involves organized collagen reformation and tensile strength improvement, areas where platforms like hydrogels, nanofibers, and patches have shown accelerated recovery.

Despite the growing promise of CPs in wound healing, the path to clinical adoption is hampered by significant regulatory complexities. CP-based materials often combine multiple functional modalities ES, antimicrobial activity, drug delivery which complicate their classification under regulatory frameworks such as those of the FDA or EMA. These multifunctional products may fall under combination device-drug classifications, requiring comprehensive data on safety, efficacy, and biocompatibility across different functional mechanisms. Moreover, the long-term biosafety of conductive additives, their potential degradation products, and the stability of CPs in physiological environments remain partially understood. These gaps necessitate robust preclinical toxicology studies and standardized testing protocols to ensure regulatory compliance. In addition, the lack of harmonized guidelines for electroactive biomaterials creates uncertainty for developers and impedes translation from bench to bedside. Another key translational hurdle lies in bridging the efficacy of CP-based interventions observed in rodent models with human clinical applications. Rodent wound healing mechanisms differ from human physiology particularly in terms of skin structure, immune response, and re-epithelialization pathways which limits the predictive value of current preclinical studies. To address this, future research must emphasize large animal models or ex vivo human skin models that more closely mimic clinical conditions. Furthermore, scalability and reproducibility of CP-based dressings and scaffolds are major challenges for industrial translation. Many of the promising formulations discussed such as hydrogel composites, microneedle patches, and electrospun nanofibers rely on complex synthesis methods that are difficult to standardize or scale without compromising material properties or performance. For CP-based systems to reach commercial and clinical viability, manufacturing methods must be optimized for consistency, cost-effectiveness, and regulatory quality control. Addressing these challenges will be critical to transforming innovative lab-scale prototypes into reliable, scalable therapeutic products suitable for widespread clinical use.

The electrical field generated by conductive polymer-based membranes like PPy/PDA/PLLA and PLGA/PDA/CS does not act via a singular mechanism but rather initiates a cascade of interconnected molecular and cellular responses. Specifically, the electric conductivity and charge density of these materials modulate cellular behavior in part through direct depolarization of the cell membrane, which alters the local transmembrane potential. This depolarization can activate voltage-gated ion channels, such as calcium channels, thereby increasing intracellular calcium levels a critical secondary messenger involved in cell proliferation, migration, and differentiation. Additionally, the electrical field can facilitate receptor phosphorylation on growth factor receptors (VEGFR and EGFR), likely through conformational changes that enhance receptor-ligand interactions or by indirectly triggering intracellular signaling cascades such as PI3K/Akt and MAPK. This is further supported by studies where electrically stimulated fibroblasts exhibit upregulation of TGF-β1 and ERK/NF-κB pathway activation, leading to myofibroblast differentiation and enhanced extracellular matrix production. Thus, the conductive properties of the polymer scaffold serve not merely as passive electrical conduits but as active biointerfaces capable of orchestrating complex cellular responses through electrochemical signaling. Moreover, gene expression profiling of cells cultured on conductive substrates such as PLGA/PDA/CS and PPy/PDA/PLLA membranes has revealed upregulation of genes associated with wound repair, including those involved in angiogenesis (VEGF), collagen synthesis (COL1A1), and inflammation modulation (IL-10). The conductivity level, often in the range of 10^{-3} to 10^{-2} S/cm for skin-like scaffolds, appears to be critical; insufficient conductivity fails to trigger cellular responses, whereas optimal conductivity enhances wound closure and vascularization. The role of charge density also emerges as significant, as it influences protein adsorption and cell adhesion, both prerequisites for mechanotransduction and gene expression changes. In PLGA/PDA/CS, for instance, the improved hydrophilicity and ion-exchange capacity due to PDA-mediated surface modification further amplify the membrane's bioactivity under low-voltage ES. Additionally, the spatial distribution of electric fields across these substrates fosters directional cell migration (galvanotaxis), particularly important in re-epithelialization. Thus, the conductive scaffolds function as electrochemical stimulants that synergistically engage direct electrical effects, biochemical signaling, and gene regulation to orchestrate enhanced wound healing. Future mechanistic studies combining single-cell transcriptomics and ion channel mapping will be essential to fully elucidate these pathways.

CRediT authorship contribution statement

Yanhua Jiang: Writing – review & editing, Writing – original draft. **Yongjian Zhou:** Writing – review & editing, Writing – original draft. **Yu Tian:** Writing – review & editing, Writing – original draft. **Noushin Nabavi:** Writing – review & editing. **Milad Ashrafizadeh:** Writing – review & editing. **João Conde:** Writing – review & editing, Writing – original draft, Conceptualization. **Zhe Li:** Writing – review & editing, Writing – original draft, Conceptualization. **Liang Guo:** Writing – review & editing, Writing – original draft, Conceptualization.

Declaration of competing interest

The authors do not have any possible conflicts of interest.

Acknowledgement

We developed the figures using Biorender.com. Moreover, AI was used for improving English language.

Data availability

No data was used for the research described in the article.

References

[1] M. Rodrigues, et al., Wound healing: a cellular perspective, Physiol. Rev. 99 (1) (2019) 665–706.
[2] O.A. Peña, P. Martin, Cellular and molecular mechanisms of skin wound healing, Nat. Rev. Mol. Cell Biol. 25 (8) (2024) 599–616.
[3] R. Dong, B. Guo, Smart wound dressings for wound healing, Nano Today 41 (2021) 101290.
[4] M. Talikowska, X. Fu, G. Lisak, Application of conducting polymers to wound care and skin tissue engineering: a review, Biosens. Bioelectron. 135 (2019) 50–63.
[5] G.K. Menon, New insights into skin structure: scratching the surface, Adv. Drug Deliv. Rev. 54 (2002) S3–S17.
[6] D. Mijaljica, et al., The heterogeneity and complexity of skin surface lipids in human skin health and disease, Prog. Lipid Res. 93 (2024) 101264.
[7] H. Sorg, C.G.G. Sorg, Skin wound healing: of players, patterns, and processes, Eur. Surg. Res. 64 (2) (2022) 141–157.
[8] B.H.J. Gowda, et al., Nanoparticle-based therapeutic approaches for wound healing: a review of the state-of-the-art, Mater. Today Chem. 27 (2023) 101319.
[9] S. Bacci, Cellular Mechanisms and Therapies in Wound Healing: Looking Toward the Future, MDPI, 2021, p. 1611.
[10] K. Szułdrzyński, et al., Plasma fibrin clot properties as determinants of bleeding time in human subjects: association with histidine-rich glycoprotein, Dis. Markers 2020 (1) (2020) 7190828.
[11] F.L. Macrae, et al., A fibrin biofilm covers blood clots and protects from microbial invasion, J. Clin. Investig. 128 (8) (2018) 3356–3368.
[12] D. Scully, et al., Optimising platelet secretomes to deliver robust tissue-specific regeneration, J. Tissue Eng. Regen. Med. 14 (1) (2020) 82–98.
[13] Y. Adib, A. Bensussan, L. Michel, Cutaneous wound healing: a review about innate immune response and current therapeutic applications, Mediat. Inflamm. 2022 (1) (2022) 5344085.
[14] S. Ellis, E.J. Lin, D. Tartar, Immunology of wound healing, Curr. Dermatol. Rep. 7 (2018) 350–358.
[15] L. Chen, L.A. DiPietro, Toll-like receptor function in acute wounds, Adv. Wound Care 6 (10) (2017) 344–355.
[16] Q. Huang, et al., Metal-organic framework-based dressings: application and opportunities in wound healing, Mater. Today Chem. 40 (2024) 102235.
[17] M. Kumar, et al., Biopolymer based nanoparticles and their therapeutic potential in wound healing – a review, Int. J. Biol. Macromol. 267 (2024) 131335.
[18] T. Sangnim, et al., Nanomaterials in the wound healing process: new insights and advancements, Pharmaceutics 16 (3) (2024) 300.
[19] Y. Cai, et al., Harnessing strategies for enhancing diabetic wound healing from the perspective of spatial inflammation patterns, Bioact. Mater. 28 (2023) 243–254.
[20] L. He, et al., Photothermal antibacterial materials to promote wound healing, J. Contr. Release 363 (2023) 180–200.
[21] F. Jonidi Shariatzadeh, et al., Enhancing wound healing and minimizing scarring: a comprehensive review of nanofiber technology in wound dressings, Prog. Mater. Sci. 147 (2025) 101350.
[22] K. Las Heras, et al., Modulating the immune system towards a functional chronic wound healing: a biomaterials and nanomedicine perspective, Adv. Drug Deliv. Rev. 210 (2024) 115342.
[23] K. Anderson, R.L. Hamm, Factors that impair wound healing, J. Am. Col. Clin. Wound Spec. 4 (4) (2012) 84–91.
[24] H. Sorg, et al., Skin wound healing: an update on the current knowledge and concepts, Eur. Surg. Res. 58 (1–2) (2017) 81–94.
[25] P. Beldon, Basic science of wound healing, Surgery 28 (9) (2010) 409–412.
[26] G.S. Ashcroft, S.J. Mills, J.J. Ashworth, Ageing and wound healing, Biogerontology 3 (2002) 337–345.
[27] M. Arnold, A. Barbul, Nutrition and wound healing, Plast. Reconstr. Surg. 117 (7S) (2006) 42S–58S.
[28] G. Han, R. Ceilley, Chronic wound healing: a review of current management and treatments, Adv. Ther. 34 (2017) 599–610.
[29] A.K. Tsirogianni, N.M. Moutsopoulos, H.M. Moutsopoulos, Wound healing: immunological aspects, Injury 37 (1) (2006) S5–S12.
[30] W. Alam, J. Hasson, M. Reed, Clinical approach to chronic wound management in older adults, J. Am. Geriatr. Soc. 69 (8) (2021) 2327–2334.
[31] V. Falanga, et al., Chronic wounds, Nat. Rev. Dis. Primers 8 (1) (2022) 50.
[32] K. Raziyeva, et al., Immunology of acute and chronic wound healing, Biomolecules 11 (5) (2021) 700.
[33] X. Ding, et al., Challenges and innovations in treating chronic and acute wound infections: from basic science to clinical practice, Burns Trauma 10 (2022).
[34] L. Zhou, et al., Rational design of intelligent and multifunctional dressing to promote acute/chronic wound healing, ACS Appl. Bio Mater. 5 (9) (2022) 4055–4085.
[35] F. Xiong, et al., Three-layer core-shell structure of polypyrrole/polydopamine/poly(l-lactide) nanofibers for wound healing application, Int. J. Biol. Macromol. 222 (Pt B) (2022) 1948–1962.
[36] M. Muchová, et al., One-step fabrication of chitosan/dialdehyde cellulose/polypyrrole composite nanofibers with antibacterial, antioxidant, and immunomodulatory effects, Int. J. Biol. Macromol. 308 (Pt 1) (2025) 142105.
[37] Q. Tang, et al., Flexible, breathable, and self-powered patch assembled of electrospun polymer triboelectric layers and polypyrrole-coated electrode for infected chronic wound healing, ACS Appl. Mater. Interfaces 15 (14) (2023) 17641–17652.

[38] Q. Guo, et al., α-Amylase and polydopamine@polypyrrole-based hydrogel microneedles promote wound healing by eliminating bacterial infection, Int. J. Biol. Macromol. 281 (Pt 4) (2024) 136604.
[39] Q. Han, et al., Polypyrrole-modified gelatin-based hydrogel: a dressing for intestinal perforation treatment with enhanced wound healing and anti-adhesion properties, Int. J. Biol. Macromol. 309 (Pt 1) (2025) 142738.
[40] S. Wang, et al., Functionalization of an electroactive self-healing polypyrrole-grafted gelatin-based hydrogel by incorporating a Polydopamine@AgNP nanocomposite, ACS Appl. Bio Mater. 4 (7) (2021) 5797–5808.
[41] Y. Chen, et al., A gelatin-chitosan-based film containing berberine hydrochloride/polypyrrole that promotes infectious wound healing through antibacterial and antioxidant properties, and electrical conductivity, Int. J. Biol. Macromol. (2025) 141228.
[42] Y. Fan, et al., Space-confined synthesis of thin polypyrrole nanosheets in layered bismuth oxychloride for a photoresponse antibacterial within the near-infrared window and accelerated wound healing, ACS Appl. Mater. Interfaces 14 (32) (2022) 36966–36979.
[43] R. Liu, et al., Flexible and antibacterial conductive hydrogels based on silk Fibroin/Polyaniline/AgNPs for motion sensing and wound healing promotion under electrical stimulation, J. Mater. Chem. B 12 (40) (2024) 10346–10356.
[44] C. Wu, et al., Intrinsic antibacterial and conductive hydrogels based on the distinct bactericidal effect of polyaniline for infected chronic wound healing, ACS Appl. Mater. Interfaces 13 (44) (2021) 52308–52320.
[45] S. Liu, et al., Flexible, high-strength and multifunctional polyvinyl alcohol/MXene/polyaniline hydrogel enhancing skin wound healing, Biomater. Sci. 10 (13) (2022) 3585–3596.
[46] Q. Pang, et al., A polyaniline nanoparticles crosslinked hydrogel with excellent photothermal antibacterial and mechanical properties for wound dressing, Macromol. Biosci. 22 (3) (2022) e2100386.
[47] Y. Jang, D. Lee, J. Oh, Fast autograft generation using transferable 3D keratinocyte cell sheet on PEDOT:PSS composite PDMS membrane for enhancing wound healing, Small 21 (8) (2025) e2406529.
[48] W. Cao, et al., A nanofibrous membrane loaded with doxycycline and printed with conductive hydrogel strips promotes diabetic wound healing in vivo, Acta Biomater. 152 (2022) 60–73.
[49] M. Gizdavic-Nikolaidis, et al., Electrospun functionalized polyaniline copolymer-based nanofibers with potential application in tissue engineering, Macromol. Biosci. 10 (12) (2010) 1424–1431.
[50] S. Aznar-Cervantes, et al., Fabrication of conductive electrospun silk fibroin scaffolds by coating with polypyrrole for biomedical applications, Bioelectrochemistry 85 (2012) 36–43.
[51] Y. Wang, M. Rouabhia, Z. Zhang, PPy-coated PET fabrics and electric pulse-stimulated fibroblasts, J. Mater. Chem. B 1 (31) (2013) 3789–3796.
[52] X. Niu, et al., An electrically conductive 3D scaffold based on a nonwoven web of poly(l-lactic acid) and conductive poly(3,4-ethylenedioxythiophene), J. Biomed. Mater. Res. 103 (8) (2015) 2635–2644.
[53] Q. Peng, et al., Nanofiber-reinforced chitosan/gelatine hydrogel with photothermal, antioxidant and conductive capabilities promotes healing of infected wounds, Int. J. Biol. Macromol. 279 (2024) 134625.
[54] H.C. Chang, et al., Conductive PEDOT:PSS coated polylactide (PLA) and poly(3-hydroxybutyrate-co-3-hydroxyvalerate) (PHBV) electrospun membranes: fabrication and characterization, Mater. Sci. Eng. C 61 (2016) 396–410.
[55] J. He, et al., Anti-oxidant electroactive and antibacterial nanofibrous wound dressings based on poly(ε-caprolactone)/quaternized chitosan-graft-polyaniline for full-thickness skin wound healing, Chem. Eng. J. 385 (2020) 123464.
[56] D. Gh, et al., Fabrication and characterization of conductive conjugated polymer-coated antheraea mylitta silk fibroin fibers for biomedical applications, Macromol. Biosci. 17 (7) (2017) 1600443.
[57] Q. Zhang, et al., Graphene oxide-modified electrospun polyvinyl alcohol nanofibrous scaffolds with potential as skin wound dressings, RSC Adv. 7 (46) (2017) 28826–28836.
[58] B.K. Gu, S.J. Park, C.H. Kim, Beneficial effect of aligned nanofiber scaffolds with electrical conductivity for the directional guide of cells, J. Biomater. Sci. Polym. Ed. 29 (7–9) (2018) 1053–1065.
[59] R. Román-Doval, et al., Enhancing electrospun scaffolds of PVP with polypyrrole/iodine for tissue engineering of skin regeneration by coating via a plasma process, J. Mater. Sci. 54 (4) (2019) 3342–3353.
[60] M. Zarei, et al., Fabrication and characterization of conductive polypyrrole/chitosan/collagen electrospun nanofiber scaffold for tissue engineering application, Int. J. Biol. Macromol. 168 (2021) 175–186.
[61] S.I. Jeong, et al., Development of electroactive and elastic nanofibers that contain polyaniline and Poly(L-lactide-co-ε-caprolactone) for the control of cell adhesion, Macromol. Biosci. 8 (7) (2008) 627–637.
[63] Y.S. Raval, et al., Hydrogen-peroxide-generating electrochemical scaffold eradicates methicillin-resistant Staphylococcus aureus biofilms, Glob. Chall. 3 (6) (2019) 1800101.
[64] S.T. Sultana, et al., Electrochemical scaffold generates localized, low concentration of hydrogen peroxide that inhibits bacterial pathogens and biofilms, Sci. Rep. 5 (2015) 14908.
[65] Z. Liu, et al., Endogenous electric field-driven neuro-immuno-regulatory scaffold for effective diabetic wound healing, Bioact. Mater. 47 (2025) 266–282.
[66] W. Shi, et al., Improved cooling performance of hydrogel wound dressings via integrating thermal conductivity and heat storage capacity for burn therapy, Biomacromolecules 23 (3) (2022) 889–902.
[67] Y. Tian, et al., Conductive hyaluronic acid/deep eutectic solvent composite hydrogel as a wound dressing for promoting skin burn healing under electrical stimulation, Adv. Healthcare Mater. 13 (17) (2024) e2304117.
[68] T. Huang, et al., Sodium hyaluronate hydrogel for wound healing and human health monitoring based on deep eutectic solvent, Int. J. Biol. Macromol. 257 (Pt 2) (2024) 128801.
[69] Q. Zhou, et al., From short circuit to completed circuit: conductive hydrogel facilitating oral wound healing, Adv. Healthcare Mater. 13 (15) (2024) e2303143.
[70] L. Zhao, et al., Electroactive injectable hydrogel based on oxidized sodium alginate and carboxymethyl chitosan for wound healing, Int. J. Biol. Macromol. 230 (2023) 123231.
[71] M. Shan, et al., Injectable conductive hydrogel with self-healing, motion monitoring, and bacteria theranostics for bioelectronic wound dressing, Adv. Healthcare Mater. 13 (11) (2024) e2303876.
[72] S. Zhu, et al., Histatin-1 loaded multifunctional, adhesive and conductive biomolecular hydrogel to treat diabetic wound, Int. J. Biol. Macromol. 209 (Pt A) (2022) 1020–1031.
[73] X. Jin, et al., Injectable hypoxia-induced conductive hydrogel to promote diabetic wound healing, ACS Appl. Mater. Interfaces 12 (51) (2020) 56681–56691.
[74] W. Fan, et al., A novel conductive microtubule hydrogel for electrical stimulation of chronic wounds based on biological electrical wires, J. Nanobiotechnol. 22 (1) (2024) 258.
[75] W. Li, et al., Multi-bioinspired functional conductive hydrogel patches for wound healing management, Adv. Sci. (Weinh.) 10 (25) (2023) e2301479.
[76] J. Ye, et al., Injectable conductive hydrogel remodeling microenvironment and mimicking neuroelectric signal transmission after spinal cord injury, J. Colloid Interface Sci. 668 (2024) 646–657.
[77] Z. Lin, et al., Antibacterial, adhesive, and conductive hydrogel for diabetic wound healing, Macromol. Biosci. 23 (2) (2023) e2200349.
[78] X. Zhao, et al., Antibacterial anti-oxidant electroactive injectable hydrogel as self-healing wound dressing with hemostasis and adhesiveness for cutaneous wound healing, Biomaterials 122 (2017) 34–47.
[79] S. Bi, et al., Versatile conductive hydrogel orchestrating neuro-immune microenvironment for rapid diabetic wound healing through peripheral nerve regeneration, Biomaterials 314 (2025) 122841.
[80] L. Qiao, et al., Antibacterial conductive self-healing hydrogel wound dressing with dual dynamic bonds promotes infected wound healing, Bioact. Mater. 30 (2023) 129–141.
[81] Y. Liang, et al., pH/Glucose dual responsive metformin release hydrogel dressings with adhesion and self-healing via dual-dynamic bonding for athletic diabetic foot wound healing, ACS Nano 16 (2) (2022) 3194–3207.
[82] K. Naik, et al., Conductive hybrid hydrogel of carbon nanotubes-protein-cellulose: in vivo treatment of diabetic wound via photothermal therapy and tracking real-time wound assessment via photoacoustic imaging, ACS Appl. Bio Mater. 8 (3) (2025) 2229–2241.
[83] L. Zhang, et al., Preparation and properties of conductive bacterial cellulose-based graphene oxide-silver nanoparticles antibacterial dressing, Carbohydr. Polym. 257 (2021) 117671.
[84] Y. Dou, et al., Multi-functional conductive hydrogels based on heparin-polydopamine complex reduced graphene oxide for epidermal sensing and chronic wound healing, J. Nanobiotechnol. 21 (1) (2023) 343.
[85] D. You, et al., Poly (lactic-co-glycolic acid)/graphene oxide composites combined with electrical stimulation in wound healing: preparation and characterization, Int. J. Nanomed. 14 (2019) 7039–7052.
[86] C. Xie, et al., Electroactive hydrogels with photothermal/photodynamic effects for effective wound healing assisted by polydopamine-modified graphene oxide, ACS Appl. Mater. Interfaces 15 (36) (2023) 42329–42340.
[87] Y. Long, et al., Effective wound healing enabled by discrete alternative electric fields from wearable nanogenerators, ACS Nano 12 (12) (2018) 12533–12540.
[88] S.H. Bhang, et al., Zinc oxide nanorod-based piezoelectric dermal patch for wound healing, Adv. Funct. Mater. 27 (1) (2017) 1603497.
[89] J. Banerjee, et al., Improvement of human keratinocyte migration by a redox active bioelectric dressing, PLoS One 9 (3) (2014) e89239.
[90] L. Wan, et al., Enhanced heterogeneous interface to construct intelligent conductive hydrogel gas sensor for individualized treatment of infected wounds, Int. J. Biol. Macromol. 258 (Pt 1) (2024) 128520.
[91] W. Wang, et al., Aqueous-aqueous triboelectric nanogenerators empowered multifunctional wound healing system with intensified current output for accelerating infected wound repair, Adv. Healthcare Mater. 13 (32) (2024) e2401676.
[92] Y. Liang, et al., Mussel-inspired, antibacterial, conductive, antioxidant, injectable composite hydrogel wound dressing to promote the regeneration of infected skin, J. Colloid Interface Sci. 556 (2019) 514–528.
[93] L. Xiao, et al., A novel conductive antibacterial nanocomposite hydrogel dressing for healing of severely infected wounds, Front. Chem. 9 (2021) 787886.
[94] S. Liu, et al., Versatile poly (deep eutectic solvents) electroactive chitosan eutectogel for infected wound healing and monitoring administration, Carbohydr. Polym. 352 (2025) 123192.
[95] L. Zhou, et al., Conductive antibacterial hemostatic multifunctional scaffolds based on Ti(3)C(2)T(x) MXene nanosheets for promoting multidrug-resistant bacteria-infected wound healing, ACS Nano 15 (2) (2021) 2468–2480.
[96] M. Liu, et al., Electret-inspired charge-injected hydrogel for scar-free healing of bacterially infected burns through bioelectrical stimulation and immune modulation, Adv. Sci. (Weinh.) 12 (13) (2025) e2411889.

[97] Q. Liu, et al., Self-healing conductive hydrogels with dynamic dual network structure accelerate infected wound healing via photothermal antimicrobial and regulating inflammatory response, ACS Appl. Mater. Interfaces 16 (24) (2024) 30776–30792.
[98] P. Deng, et al., Conductive, self-healing, adhesive, and antibacterial hydrogels based on lignin/cellulose for rapid MRSA-infected wound repairing, ACS Appl. Mater. Interfaces 13 (44) (2021) 52333–52345.
[99] C. Wu, et al., Injectable conductive and angiogenic hydrogels for chronic diabetic wound treatment, J. Contr. Release 344 (2022) 249–260.
[100] H. Liu, et al., 3D printed eutectogel dissolving microneedles patch loaded with chitosan-based nanoparticles for diabetic wound management, Int. J. Biol. Macromol. 307 (Pt 2) (2025) 142018.
[101] Y. Zhao, et al., Biomimetic nanozyme-decorated hydrogels with H(2)O(2)-Activated oxygenation for modulating immune microenvironment in diabetic wound, ACS Nano 17 (17) (2023) 16854–16869.
[102] K. Shen, et al., Nanocomposite conductive hydrogels with robust elasticity and multifunctional responsiveness for flexible sensing and wound monitoring, Mater. Horiz. 10 (6) (2023) 2096–2108.
[103] J. Jiang, et al., Flexible and temperature-responsive hydrogel dressing for real-time and remote wound healing monitoring, J. Mater. Chem. B 11 (22) (2023) 4934–4945.
[104] Y. Li, et al., Stretchable, conductive, breathable and moisture-sensitive e-skin based on CNTs/graphene/GelMA mat for wound monitoring, Biomater. Adv. 143 (2022) 213172.
[105] H. Ma, et al., 3D printed multi-coupled bioinspired skin-electronic interfaces with enhanced adhesion for monitoring and treatment, Acta Biomater. 187 (2024) 183–198.
[106] Z. Liu, et al., Electrostimulation of fibroblast proliferation by an electrospun poly (lactide-co-glycolide)/polydopamine/chitosan membrane in a humid environment, Colloids Surf. B Biointerfaces 220 (2022) 112902.
[107] X. Niu, et al., An electrically conductive 3D scaffold based on a nonwoven web of poly(L-lactic acid) and conductive poly(3,4-ethylenedioxythiophene), J. Biomed. Mater. Res. 103 (8) (2015) 2635–2644.
[108] S.I. Jeong, et al., Development of electroactive and elastic nanofibers that contain polyaniline and poly(L-lactide-co-epsilon-caprolactone) for the control of cell adhesion, Macromol. Biosci. 8 (7) (2008) 627–637.
[109] J. Cifuentes, C. Muñoz-Camargo, J.C. Cruz, Reduced graphene oxide-extracellular matrix scaffolds as a multifunctional and highly biocompatible nanocomposite for wound healing: insights into characterization and electroconductive potential, Nanomaterials 12 (16) (2022).
[110] H. Kai, et al., Accelerated wound healing on skin by electrical stimulation with a bioelectric plaster, Adv. Healthcare Mater. 6 (22) (2017).
[111] M. Pandian, et al., In-situ silver nanoparticles incorporated N, O-carboxymethyl chitosan based adhesive, self-healing, conductive, antibacterial and anti-biofilm hydrogel, Int. J. Biol. Macromol. 188 (2021) 501–511.